UTILIZATION OF GGBFS BLENDED CEMENT PASTES IN WELL CEMENTING

A THESIS SUBMITTED TO
THE GRADUATE SCHOOL OF NATURAL AND APPLIED SCIENCES
OF
MIDDLE EAST TECHNICAL UNIVERSITY

BY

BARIŞ ALP

IN PARTIAL FULFILLMENT OF THE REQUIREMENTS
FOR
THE DEGREE OF MASTER OF SCIENCE
IN
CEMENT ENGINEERING

SEPTEMBER 2012

Approval of the thesis:

UTILIZATION OF GGBFS BLENDED CEMENT PASTES IN WELL CEMENTING

submitted by **BARIŞ ALP** in partial fulfillment of the requirements for the degree of **Master of Science in Cement Engineering Department, Middle East Technical University** by,

Prof. Dr. Canan ÖZGEN _____
Dean, Graduate School of **Natural and Applied Science**

Asst. Prof. Dr. Sinan. Turhan ERDOĞAN _____
Head of Department, **Cement Engineering**

Prof. Dr. İsmail Özgür YAMAN _____
Supervisor, **Civil Engineering Dept., METU**

Prof. Dr. Serhat AKIN _____
Co-Supervisor, **Petroleum and Natural Gas Eng. Dept., METU**

Examining Committee Members:

Prof. Dr. Mustafa TOKYAY _____
Civil Engineering Dept., METU

Prof. Dr. İsmail Özgür YAMAN _____
Civil Engineering Dept., METU

Prof. Dr. Serhat AKIN _____
Petroleum and Natural Gas Eng. Dept., METU

Prof. Dr. Asuman G. TÜRKMENOĞLU _____
Geological Engineering Dept., METU

Asst. Prof. Dr. Sinan Turhan ERDOĞAN _____
Civil Engineering Dept., METU

Date: 07.09.2012

I hereby declare that all information in this document has been obtained and presented in accordance with academic rules and ethical conduct. I also declare that, as required by these rules and conduct, I have fully cited and referenced all material and results that are not original to this work.

Name, Last name: **BARIŞ ALP**

Signature :

ABSTRACT

UTILIZATION OF GGBFS BLENDED CEMENT PASTES IN WELL CEMENTING

Alp, Barış
M. Sc., Department of Cement Engineering
Supervisor: Prof. Dr. İsmail Özgür Yaman
Co-Supervisor: Prof. Dr. Serhat Akın

September 2012, 120 pages

In well cementing, the cement slurry is exposed to the conditions far different than those of ordinary Portland cement (PC) used in construction. After placement, hardened cement paste should preserve integrity and provide zonal isolation through the life of the well. American Petroleum Institute (API) Class G cement is the most common cement type used in various well conditions. Class G cement has a high degree of sulfate resistance which makes it more stable than PC when subjected to the compulsive well conditions. Ground granulated blast furnace slag (GGBFS) blended cement has a long history of use in the construction industry, but is not extensively used in well cementing applications.

This study presents an experimental program to investigate the applicability of CEM I and GGBFS blended cement pastes in the well cementing industry. Class G cement and blends of CEM I and GGBFS with the proportions (80:20), (60:40), (40:60) and (20:80) are prepared with same water/cement ratio (0.44) as restricted for Class G cement in API Specification 10A to be tested. The cement pastes are cured for ages of 1 day, 7 days and 28 days at 80 ˚C which represents the condition of medium-depth oil wells.

The presence of an adequate amount of GGBFS in the blend improves properties of the cement paste especially in the long term and at elevated temperatures. They are comparable to and under some conditions more preferable to the neat Class G cement paste. However, the physical properties of cement pastes prepared with neat Class G cement develop within the first day and negligible change is observed later. In order to get better hydration for the blended cement paste, the amount of CEM I must be kept more than GGBFS in the blend to provide sufficient alkalinity for the hydration of GGBFS. The conclusions obtained from this study indicate that GGBFS blended CEM I produces high quality well cementing material when compared to Class G cement.

Keywords: well cementing, API Class G cement, Ground Granulated Blast Furnace Slag, Slag blended Portland cement, hydrothermal conditions

ÖZ

ÖĞÜTÜLMÜŞ GRANÜLE YÜKSEK FIRIN CÜRUF KARIŞIMLI ÇİMENTO HAMURLARININ KUYU ÇİMENTOLAMADA DEĞERLENDİRİLMESİ

Alp, Barış
Yüksek Lisans, Çimento Mühendisliği Bölümü
Tez Yöneticisi: Prof. Dr. İsmail Özgür Yaman
Ortak Tez Yöneticisi: Prof. Dr. Serhat Akın

Eylül 2012, 120 sayfa

Kuyu çimentolamada, çimento karışımının maruz kaldığı koşullar, yapı sektöründe kullanılan Portland çimentosunun (PC) maruz kaldığı koşullardan oldukça farklılık gösterir. Yerleştirildikten sonra sertleşen çimento hamuru kuyunun bütünlüğünü korumalı ve bölgesel izolasyon sağlamalıdır. Amerikan Petrol Enstitüsünün (API) G sınıfı çimentosu farklı kuyu koşullarında kullanılan en yaygın türdür. G sınıfı çimentonun yüksek sülfat direncine sahip olması onu zorlayıcı kuyu koşullarında PC'den daha kararlı yapar. Öğütülmüş granüle yüksek fırın cüruf (GGBFS) karışımlı çimentolar yapı endüstrisinde uzun bir geçmişine sahipken, kuyu çimentolamada yaygın olarak kullanılmamaktadır.

Bu çalışma CEM I ve GGBFS karışımı ile hazırlanan çimento hamurlarının kuyu çimentolamadaki uygunluğunu araştıran deneysel bir program sunmaktadır. G sınıfı çimento ve (80:20), (60:40), (40:60) ve (20:80) oranları ile hazırlanan CEM I ve GGBFS karışımları G sınıfı çimentonun API Specification 10A'da belirtilen su/çimento oranına (0.44) göre hazırlanmıştır. Çimento hamurları 1 gün, 7 gün ve 28 gün süreyle orta derinlikteki petrol kuyularındaki koşulları temsil eden 80 ˚C'da küre tabi tutulmuştur.

Çimento karışımında uygun miktarda GGBFS bulunması çimento hamurunun özelliklerine uzun vadede ve yüksek sıcaklıkta katkı sağlamaktadır. Bu karışımlar G sınıfı çimento ile hazırlanan çimento hamuru ile benzer hatta bazı koşullarda daha tercih edilebilir özellik göstermektedir. Buna karşın, G sınıfı çimento ile hazırlanan çimento hamurunun fiziksel özellikleri birinci günde belirginleşmekte ve sonrasında fazla değişiklik göstermemektedir. GGBFS karışımlı çimento hamurlarında daha fazla hidratasyon elde etmek amacıyla, GGBFS hidratasyonunda gerekli alkalinitenin sağlanabilmesi için karışımdaki CEM I oranı GGBFS'den fazla olmalıdır. Bu çalışmanın sonucu; GGBFS ve CEM I karışımlı çimentonun, G sınıfı çimento ile karşılaştırıldığında yüksek kalitede bir kuyu çimentolama malzemesi olduğunu göstermektedir.

Anahtar Kelimeler: Kuyu çimentolama, API G Sınıfı çimento, öğütülmüş granüle yüksek fırın cürufu, cüruf katkılı Portland çimentosu, hidrotermal kür

To My Wife…

ACKNOWLEDGEMENTS

I would like to express great appreciation to both Prof. Dr. İsmail Özgür Yaman and Prof. Dr. Serhat Akın for their thorough supervision, guidance and continuous suggestions throughout this research and preparation of this thesis.

I appreciate the help provided by Research Center of Turkish Petroleum Corporation (TPAO). I would like to thank to both the departments of Reservoir Technology, Sedimentology and Reservoir Geology, and also express my special thanks to the department of Drilling Technology.

My sincere thanks are extended to OYAK Bolu Cement plant for supplying all the materials that I used in my thesis study.

I appreciate close assistance of the Materials of Construction Laboratory personnel in Civil Engineering Department at METU.

I am grateful to my parents for their patience, encouragement and support.

Finally, I would like to thank my wife Güldeniz for her immortal love and inimitable moral help in the hard times of my thesis study.

TABLE OF CONTENTS

LIST OF TABLES

TABLES

LIST OF FIGURES

FIGURES

NOMENCLATURE

ACI	American Concrete Institute
AFm	Alumina, ferric oxide, mono-sulfate
AFt	Alumina, ferric oxide, tri-sulfate
API	American Petroleum Institute
ASTM	American Society for Testing Materials
BFS	Blast Furnace Slag
CL	Confidence Level
C-S-H	Calcium Silicate Hydrate
DTM	Destructive Test Method
EN	European Standards
GGBFS	Ground Granulated Blast Furnace Slag
HM	Hydraulic Modulus
HSR	High Sulfate Resistance
ICDD	International Center for Diffraction Data
ICSD	Inorganic Crystal Structure Database
MSR	Medium Sulfate Resistance
OPC	Ordinary Portland Cement
PC	Portland Cement
PSD	Particle Size Distribution
RP	Recommended Practice
RPM	Revolutions Per Minute
SAI	Slag Activity Index
SEM	Scanning Electron Microscope
SRC	Sulfate Resistant Cement
TPAO	Turkish Petroleum Corporation
TS	Turkish Standards
XRD	X-Ray Diffraction
UCA	Ultrasonic Cement Analyzer

CHAPTER 1

INTRODUCTION

1.1. General

Well cementing is one of the most important operations performed on a gas or oil well. In well cementing, cement slurry is primarily used for filling up the annular space between protective pipes (casing) and the wellbore. As a second application, it can also be used for squeeze cementing to plug the wellbore and/or casing. Casing is a large diameter pipe that is assembled and inserted into a recently drilled section of a borehole and typically held into place with cement slurry.

In primary cementing, when an oil or gas well has been drilled to the desired depth, the casing string is run into the bottom of hole. Then, cement slurry is pumped through inside of the casing and then out into the annular space between casing and the surrounding wellbore, as shown Figure 1-1. In the well conditions, cement slurries are exposed to challenging environmental effects like; high temperature, high pressure and corrosive fluids.

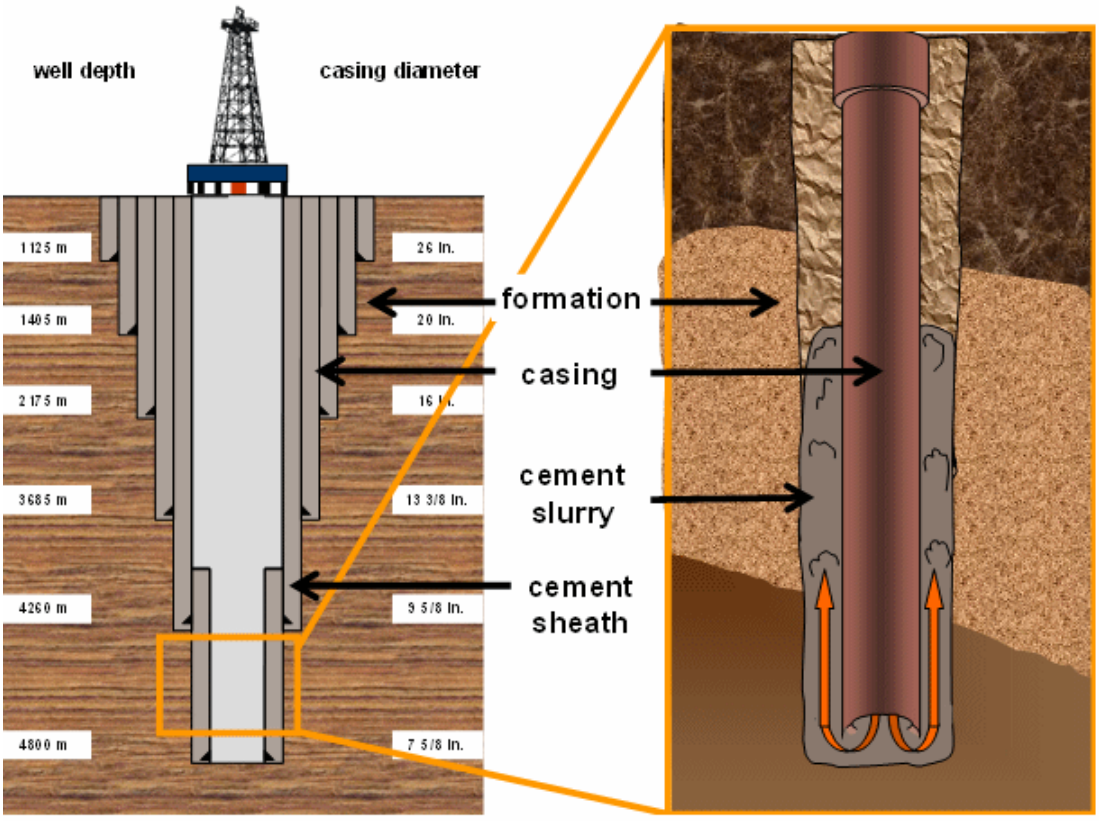

Figure 1-1 Primary cementing (World Oil, 2007)

In squeeze cementing cement slurry is forced under pressure through into a void or porous formation. Then solid particles are forced to filter out on the permeable formation surface, while the aqueous phase enters into the matrix of formation. The resulting cement slurry filter cake fills up the openings between formation and the casing as shown in Figure 1-2.

The most important task of well cementing is to restrict movement of fluids between formations, to keep casing in place, to prevent corrosion e.g. from saline and sulfated underground water. Moreover, the influx of fluids into the annular space should be avoided to prevent them migrating to other zones which also called “zonal isolation”.

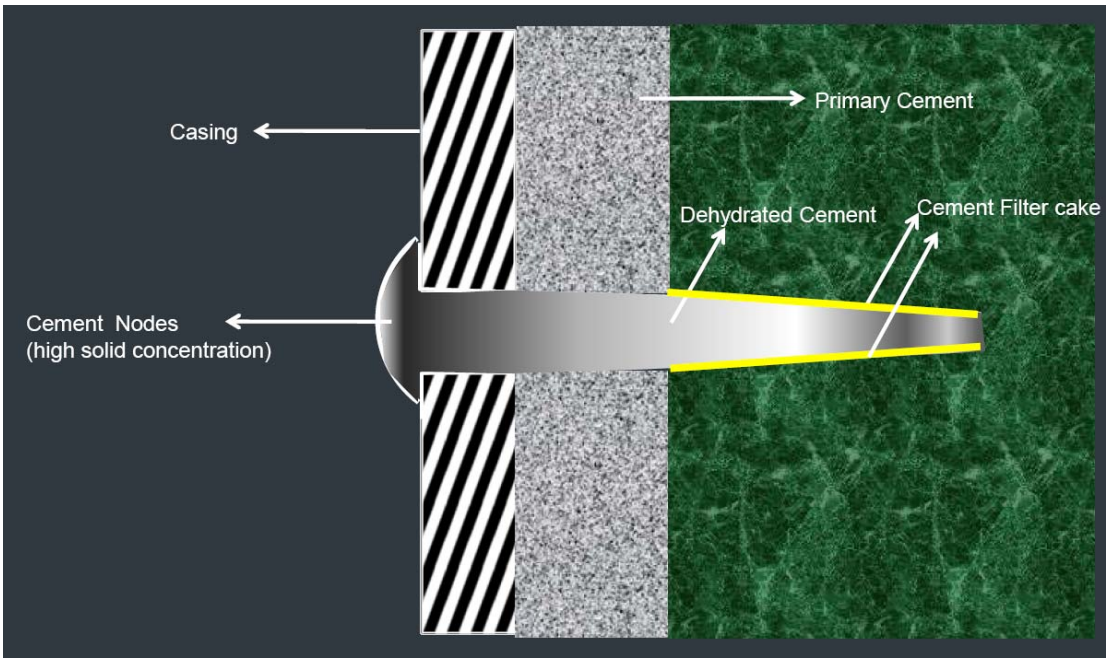

Figure 1-2 Squeeze cementing (Advanced cementing seminar, 2011)

American Petroleum Institute designates the physical and chemical properties of oil well cements. There are 8 classes of API cement types which are labeled from A to H. Among them, the most widely used one is Class G which possesses enhanced resistance against sulfate attack. It is adapted to various well conditions from surface to 2440 m, even deeper when used deeper with additives. It is more stable than other classes when subjected to high temperature and pressure. Beside the advantageous properties of API Class G cement, it is not widely available. It can be produced by the manufacturers only with API monogram and the prices are relatively higher than those of the cement types in EN 197-1.

GGBFS is a by-product of the iron industry obtained by quenching molten iron slag from a blast furnace in water or steam. It is a type of mineral additive that can be used as a supplementary cementitious material. It is mainly used for three purposes; to enhance the properties of fresh and hardened cement pastes, for environmental aspects due to utilization of industrial waste to reduce CO_2 emissions in cement manufacturing and lastly for economical reasons.

It has become industry practice that, substitution of GGBFS to CEM I provides resistance against sulfate attack. For moderate sulfate resistance (MSR) 15-25 percent of slag whereas for high sulfate resistance (HSR) 35-50 percent of slag replacement is required based on ASTM C989. Class G cement used in this study is produced with HSR grade and therefore 35-50 percent slag substitution is expected to have comparable resistance against sulfate attack. The sulfate resistance of the cement pastes is kept out of the scope of this study as the literature mentioned above.

The hydration rate of CEM I is high at early periods but slows down soon at later periods, on the contrary, GGBFS has a lower hydration rate at early periods but gradually increase at later periods. Therefore, the resulting hydration rate of GGBFS-CEM I blended cement paste will be in between CEM I and GGBFS. In addition, $Ca(OH)_2$, which is a hydration product of Portland cement, is also an activator for the hydration of slag. As a result of this, it can be used as a supplementary material of cement. According to ASTM C595, slag content in the slag-cement blend can be used up to 70 percent (in mass), while, EN 197-1 makes limitation of GGBFS in slag-cement blend up to 95 percent (in mass).

1.2. Objective

The objective of this study is to investigate the applicability of the blends of CEM I and GGBFS as oil well cement. Further to investigate whether these blends would be an alternative to the most widely used API Class G cement. For that purpose, five different cement slurries are prepared to be tested; one of them is neat API Class G cement and the remaining are the blends of GGBFS and CEM I with different proportions. The GGBFS blended cement is prepared by mixing them separately. The resulting cement slurries are tested in terms of free fluid content, compressive strength, ultrasonic cement analyzer, porosity, permeability, mercury injection, mineralogical and micro morphological analysis. (XRD and SEM). All cement slurries are tested under conditions similar to well conditions.

1.3. Scope

This thesis consists of six chapters,

Chapter 1 presents the introduction, briefly explaining major aspects of oil well cement and Portland cement and gives objective and scope of this thesis.

Chapter 2 presents the literature review to put a general background on properties of Portland cement, API cement types, slag and their hydration mechanism.

Chapter 3 presents the experimental study, briefly describing the test materials and the procedures of the analysis.

Chapter 4 presents the results and discussion, briefly gives the test results and discussion of the results.

Chapter 5 presents the main conclusion and gives the recommendations for future researchers.

Chapter 6 presents the recommendations for future studies.

CHAPTER 2

LITERATURE REVIEW

2.1. Portland Cement

Portland cement is obtained by inter-grinding industrial produced clinker with a few percent of calcium sulfate. Among the two, clinker maintains the hydraulic activity while calcium sulfate controls the setting time of cement paste.

2.1.1. Raw Materials and Manufacture

Clinker is a composition of calcium oxide (CaO), silicon oxide (SiO_2), aluminum oxide (Al_2O_3) and iron oxide (Fe_2O_3). Main components, necessary for the production of clinker, are usually available in the mixture of limestone and clay. Limestone or marly limestone is the source of CaO, while clay or marly clay is the source of SiO_2, Al_2O_3 and Fe_2O_3. These raw materials are mixed in certain proportions to obtain the required final chemical composition. Therefore, corrective ingredients are sometimes added during the production process. Pure limestone for increasing CaO content, quartz sand for increasing SiO_2 content, bauxite for increasing Al_2O_3 content and hematite or iron ore for increasing Fe_2O_3 content are typical examples on the use of corrective ingredients (Labahn, 1983). Table 2-1 shows typical composition of Portland cement.

Clinker is produced by burning properly combined raw materials up to a temperature of 1450 ºC. The first formation of liquid phase signs the starting of the clinkering also known as sintering period of clinker. After the sintering process, four major phases are formed, which are Alite (C_3S), Belite (C_2S), aluminate (C_3A) and ferrite (C_4AF). Several compounds, which are alkali sulfates, calcium oxide (CaO), magnesium oxide (MgO) and other oxides may exist as minor ingredients.

Table 2-1 Typical composition of Portland cement (Neville, 2003)

Oxide	Limit Value (wt, %)	Average (wt, %)
CaO	60-67	65
SiO_2	17-25	22
Al_2O_3	3-8	6
Fe_2O_3	1-8	3
MgO	<5	2
SO_3	<3	1
$K_2O + Na_2O$	<2	1

After the burning process if clinker is cooled slowly, some of the reactions which are already formed in the kiln would be reversed. However, if rapid cooling is provided on hot clinker, the solidification of the liquid phase is enhanced which affects the crystallization state of clinker. Rapid cooling contributes to the formation of clinker by decreasing the regression losses of C_3S to C_2S during slow cooling and thus improves the reactivity of clinker (Taylor, 1997).

2.1.2. Clinker Phases

Portland cement clinker comprises mostly four crystalline phases which are C_3S, C_2S, C_3A and C_4AF.

C_3S (alite) is the major mineral phase in Portland cement clinker with the chemical formula $3CaO{\cdot}SiO_2$; it constitutes 50-70% of clinker. C_3S is thermodynamically unstable below 1250 °C, but can be preserved in metastable state at room temperature by rapid cooling (Taylor, 1997).

C_2S (belite) is the second important mineral phase in Portland cement clinker and constitutes of about 15-20% of clinker. The chemical formula of C_2S is $2CaO{\cdot}SiO_2$ and normally present in clinker as β polymorph. At room temperature it is possible to change thermodynamically to the more stable γ polymorph, but this form does not hydrate and should be avoided in Portland cement. Therefore, β polymorph of C_2S can be stabilized at room temperature through rapid cooling (Labahn, 1983).

C_3A (tricalcium aluminate) is the most common mineral among aluminates and constitutes 5-10% of Portland cement clinker. The chemical formula of C_3A is $3CaO{\cdot}Al_2O_3$ and possesses high degree of reactivity. Its hydration is very rapid and undesirable flash setting may occur if a setting control agent (usually gypsum) is not used (Domone and Illstone, 2010).

Ferrite constitutes 10-15% of Portland cement clinker and does not have an exact chemical formula. The chemical composition may vary between $C_2(A_{0.7},F_{0.3})$ and $C_2(A_{0.3},F_{0.7})$, however, more or less the composition corresponds to tetra calcium aluminoferrite (C_4AF) (Odler, 2004; Labahn, 1983). Ferrite has little or negligible contribution to the compressive strength of the hardened cement paste. Its hydration is fast if a setting control agent (usually gypsum) is not used and gives its specific color (grey) to clinker.

Free lime (uncombined CaO) is another important component in Portland cement clinker. It may occur because of the inhomogenities of raw material or inadequate burning in the kiln. Free lime has a deleterious effect on the hardened cement paste.

Excessive amounts may cause undesirable volume expansion (also known as lime expansion), and therefore free lime content is limited up 2 percent by mass in most of the Portland cement clinker (Labahn, 1983).

Free MgO does also have a deleterious effect on hardened cement paste similar to free lime, because of its tendency to hydrate with the presence of water (Labahn, 1983). EN 197-1 limits the MgO amount to 5 percent by mass in Portland cement clinker.

Alkalis are may also present in Portland cement clinker. There are two principle alkali oxides in clinker which are sodium oxide (Na_2O) and potassium oxide (K_2O). These two alkalis are treated together and released during early periods of cement hydration. They combine with sulfates to form alkali sulfates (Taylor, 1997). Alkalis can cause expansion with certain aggregates, and some specifications limit the alkali content up to 0.6% equivalent Na_2O (Na_2O+0.66 K_2O) (ASTM C150).

In Portland cement clinker, presence of distinct components is possible. They may exist in the geochemical nature of the raw material or come from the mineral content of fuel. These possible components are; TiO_2, P_2O_5, SrO, F, MnO_3, Cr_2O_3, Cs_2O, V_2O_5, Cl, As_2O_3, CuO, PbO, CdO, BaO, Tl_2O, etc. (Taylor, 1997; Labahn, 1983; Jackson, 2004).

2.1.3. Calcium Sulfates

Calcium sulfate is added to clinker at a level between 3 and 5 percent to control the setting of Portland cement. According to EN 197-1, calcium sulfates can be gypsum (calcium sulfate dihydrate, $CaSO_4 \cdot 2H_2O$), hemihydrates (calcium sulfate hemihydrates, $CaSO_4 \cdot ½H_2O$) or anhydrite (anhydrous calcium sulfate, $CaSO_4$) or any mixture of them.

2.1.4. Pozzolans

Pozzolans are materials, which exhibit cementitious property when combined with calcium hydroxide. Pozzolans are commonly used as an additive in Portland cement to enhance long-term strength and durability. When a mixture of Portland cement and pozzolan react with water, pozzolanic reaction progresses like an acid-base reaction. Lime and alkalies released from Portland cement reacts with the oxides ($SiO_2 + A1_2O_3 + Fe_2O_3$) of the pozzolan (ACI 232).

Pozzolans can be classified into two; natural pozzolans (e.g., volcanic ashes, diatomaceous earth, etc.) and artificial pozzolans (e.g., slag, fly ash, etc.). Since the use of slag is investigated within this thesis; the following section is devoted to its properties.

2.1.5. Classification of Portland Cements

ASTM C150 defines cement types as;

I Normal

II Moderate sulfate resistance

III High-early strength

IV Low heat of hydration

V High sulfate resistance

Sulfate resistant cement is used with the presence of alkali soil or threat of sulfate salts found in ground water. This type of cement has a limitation on C_3A and C_4AF amount which affects sulfate resistance.

2.1.6. Hydration of Portland Cement

In cement chemistry, hydration is the chemical reaction between anhydrous cement grain and water. Freshly mixed paste is in liquid form and has a plastic structure. As the reaction proceeds, the hydration products gradually bond together and turn into solid called "hardened cement paste". The progress and kinetics of hydration are affected by a variety of factors (Odler, 2004):

- Composition of the cement and presence of foreign ions
- Fineness of the cement
- Water/cement (w/c) ratio
- Curing temperature
- Presence of chemical admixtures, i.e. dispersants or retarders
- Presence of mineral additives, i.e. GGBFS or pulverized fly ash

It is necessary to look for the four principle clinker phases in the hydration of Portland cement clinker. In general, the reaction of hydration can be simplified as;

clinker phases (high in energy; contain no water)	+	water	→	hydrate phases (low in energy; contain water)	+	energy (heat of hydration)	(2.1)

As shown above, the reaction of hydration is exothermic due to the high entropy energy of the clinker phases.

2.1.6.1. Hydration of Pure Clinker Phases

It is better to investigate hydration of clinker phases separately due to the complexity of hydration mechanism of Portland cement and to avoid from the influence of the foreign ions released from the hydration of other phases (Odler, 2004).

C_3S is the most important component of Portland cement clinker and generally responsible for the early strength development. The hydration products of C_3S at ambient temperatures are; amorphous C-S-H with a CaO/SiO_2 less than 3.0 and calcium hydroxide as shown in the Equation 2.2.

$$2\ C_3S + 6\ H \rightarrow C_3S_2H_3 + 3\ CH \qquad (2.2)$$

C_2S is the second important component of Portland cement and mostly responsible for the ultimate strength development. C_2S hydration is similar to C_3S, however its hydration is slower, lower heat is generated and lower amount of CH is produced. The hydration products of C_2S at ambient temperatures are; amorphous C-S-H and CH as shown in the Equation 2.3.

$$2\ C_2S + 4\ H \rightarrow C_3S_2H_3 + CH \qquad (2.3)$$

The hydration of C_3A is very fast and generates more heat compared to C_3S. In the absence of any additives, C_3A reacts with water to form gel-like material on the surface of C_3A. Later, transforms into two meta-stable intermediate hexagonal crystal phases, C_2AH_8 and C_4AH_{13} shown in Equation 2.4. Additional precipitation amounts of these crystals, converts them to cubic C_3AH_6 as shown in equation 2.5. This is the only thermodynamically stable calcium aluminate hydrate at ambient

temperatures. If the temperature is above 80 °C, C_3AH_6 can directly be form in the hydration of C_3A (Odler, 2004).

$$2\ C_3A + 21\ H \rightarrow C_4AH_{13} + C_2AH_8 \quad (2.4)$$

$$C_4AH_{13} + C_2AH_8 \rightarrow 2\ C_3AH_6 + 9\ H \quad (2.5)$$

Gypsum is usually added to the Portland cement to control the rate of reaction. In the presence of gypsum, C_3A solubility decreases and hydration slows down. C_3A reacts with gypsum in the presence of water to form AFt phases (ettringite). AFt phases then react with C_3A to form AFm phases depending on the gypsum/C_3A ratio as shown in Equations 2.6 and 2.7 (Day, 1992).

$$C_3A + 3C\bar{S}H_2 + 26H \rightarrow C_6A\bar{S}_3H_{32} \quad (2.6)$$

$$2C_3A + C_6A\bar{S}_3H_{32} + 4H \rightarrow 3C_4A\bar{S}H_{12} \quad (2.7)$$

The hydration products of ferrite are similar to C_3A. The initial hydration rate of pure C_4AF is usually faster than C_3A but then slows down soon. In the absence of gypsum, $C_2(A,F)H_8$ and/or $C_4(A,F)H_x$ is formed and then converts to more stable iron-containing hydrogarnet phase ($C_3(A,F)H_6$). In the presence of gypsum, AFt phase $C_6(A,F)\ \bar{S}_3H_{32}$ is formed as an initial hydration product (Chatterji and Jeffrey, 1962). Hydrogarnet phase is formed directly in the hydration at elevated temperatures (Negro and Steffari, 1979). After all gypsum is consumed AFt phase convert to AFm phases.

Minor ingredients in Portland cement clinker are also affecting hydration. The most significant ones are; alkalis (Na_2O and K_2O), MgO, CaO and sulfates. Alkalis are deleterious for hardened cement paste and affect strength development of cement paste. It has a positive effect on strength development at early ages, but at later ages strength retrogression occurs (Jawed and Skalny, 1978).

Free CaO and MgO are exposed to high-temperature (>1400 °C) in kiln and result in crystalline structures. The highly crystalline CaO and MgO are much less reactive with water. The delayed hydration of these minerals may cause volume instability in the hardened cement paste. The reactions are illustrated in Equations 2.8 and 2.9. The solubility of MgO in water is much less than that of CaO and therefore it is more deleterious compared to CaO (Mehta, 2006).

$$CaO + H_2O \rightarrow Ca(OH)_2 \quad (2.8)$$

$$MgO + H_2O \rightarrow Mg(OH)_2 \quad (2.9)$$

Sulfates in clinker react with CH to form additional gypsum in cement paste. Excessive amounts of gypsum contribute to the formation of AFt phases which has also deleterious effect on hardened cement paste.

2.1.6.2. Mechanism of Portland Cement Hydration

The hydration of Portland cement is more complex than the hydration of individual clinker phases. It is characterized by five stages (Odler, 2004).

Pre-induction period (first minutes)

Immediately with the contact of water, highly soluble ionic species in cement dissolves into liquid phase. Alkali sulfates dissolve in a few seconds and releases K^+, Na^+ and SO_4^{2-} ions. Calcium sulfates dissolve until super saturation and releases Ca^{2+} and additional SO_4^{-2} ions. In the pre-induction period, 2 to 10 % of C_3S is hydrated. With the hydration of C_3S, Ca^{2+} and OH^- are released and C-S-H precipitates on the cement grains. AFt phases produced and precipitated on the cement surfaces with the dissolution of C_3A and $C_4(A,F)$ in Ca^{2+} and SO_4^{-2} rich solution. Negligible amounts of C_2S hydrates at the pre-induction period.

Induction (dormant) period (first few hours)

After rapid hydration at pre-induction period, hydration slows down significantly. Ca^{2+} concentration in the liquid phase increases until it reaches to its critical supersaturation and then CH starts to precipitate. AFt phases continue to precipitate but SO_4^{-2} remains constant due to the dissolution of additional calcium sulfates. This stage is important in concrete technology because cement paste is still workable.

Acceleration stage (3-12 hours after mixing)

In this period C_3S hydration accelerates and second stage C-S-H forms and certain amounts of C_2S contributes to hydration. Crystalline CH (portlandite) precipitates and Ca^{2+} concentration in the liquid phase gradually declines. SO_4^{-2} concentration in the liquid phase also declines because of the precipitation of AFt phases. This stage determines the setting time and early strength development of cement paste.

Deceleration period

In this period hydration rate slows down gradually, and SO_4^{-2} concentration in liquid phase continues to decline. When SO_4^{-2} in liquid phase is depleted, AFt reacts with C_3A and $C_4(A,F)$ to form AFm. As a consequence of the deposition of additional hydrates, strength of hardened cement paste increases while porosity decreases.

Steady state period

In this period hydration rate is relatively slow. Hydrated C-S-H becomes denser and portlandite crystals continue to grow. The strength of hardened cement paste increases while rate of heat generation and porosity decreases. However, the duration of this period is indefinite, total hydration never attained.

Figure 2-1 illustrates the heat evolution during hydration of Portland cement with relating hydration period.

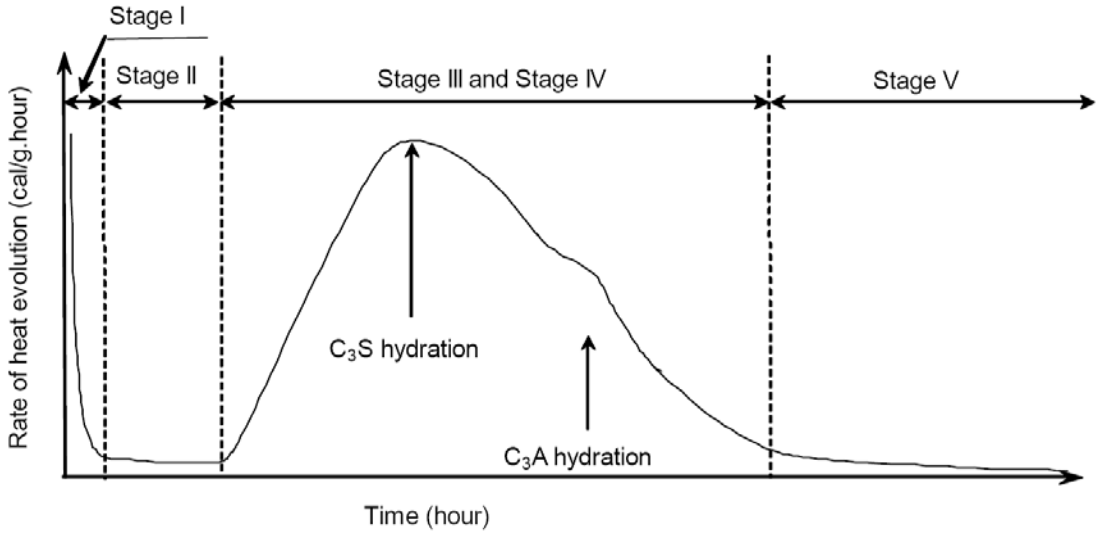

Figure 2-1 Rate of heat evolution during hydration of Portland cement (Mindess and Young, 1981)

2.1.6.3. Calcium Sulfate

The solubility of calcium sulfate depends on their form; gypsum is much lower than anhydrate, and hemihydrate has the highest solubility among them. At early and middle periods of hydration, calcium sulfate dissolves and reacts with aluminates and ferrite to form AFt or AFm phases (Nelson, 1990).

2.1.6.4. Heat of Hydration

Portland cement is a product that is formed at high temperatures and therefore possesses high-energy state. When cement hydrates, energy is liberated and turns to a low-energy state. The rates of heat liberation from hydration of the individual compounds can be used as indices of their reactivity. The data from heat of hydration studies can be used for characterizing the setting and hardening behavior of cement, or for predicting the temperature rise.

2.1.6.5. Hydration Products

2.1.6.5.1. Calcium Silicate Hydrate

Calcium silicate hydrate (C-S-H) phase is formed as a hydration product of both C_3S and β-C_2S. It is almost amorphous in structure and dashes indicate that there is not any specific chemical composition implied. On the total hydration of both C_3S and β-C_2S with stoichiometric calculations, approximate composition of the hydration product is assumed to be $C_3S_2H_3$ as shown in Equations 2.2 and 2.3. On complete hydration of Portland cement, C_3S produce 61% $C_3S_2H_3$ and 39% CH, whereas β-C_2S produce 82% $C_3S_2H_3$ and 18% CH. Therefore ultimate strength of the hydrated β-C_2S is expected to be more than C_3S (Mehta, 2006).

The chemical reactions between calcium and silicate ions in aqueous suspensions bring them together to form amorphous C-S-H gel and intermediate crystalline phases. There are 30 types of C-S-H phases, the most significant crystalline phases are; 1.4nm tobermorite, jennite, C-S-H (I) and C-S-H (II) (Taylor, 1997). Table 2-2 shows the crystal data for these phases (Taylor, 1997).

Table 2-2 Crystal structure of various C-S-H phases (Taylor, 1997)

Phase	1·4 nm tobermorite	C–S–H(I)	Jennite	C–S–H(II)
Molar ratios				
CaO	5	5	9	9
SiO_2	5·5	5	6	5
H_2O	9	6	11	11
Pseudocell parameters				
a (nm)	0·5624	0·560	0·996	0·993
b (nm)	0·3670	0·364	0·364	0·364
c (nm)	2·797	2·5	2·136	2·036
α	90·0°	90·0°	91·8°	90·0°
β	90·0°	90·0°	101·8°	106·1°
γ	90·0°	90·0°	89·6°	90·0°
Lattice type	I	I	A	A
Z	1	1	1	1
D_x (kg m^{-3})	2224	2250	2332	2350
Reference	F21,T5	T5,T22	G49,T5	G50,T5

All data are for the pseudocells and compositions stated· The true cells have doubled values of b and can be in varying degrees disordered; a and c must often be differently defined· The structure of C–S–H(I) has little more than two-dimensional order, and that of C–S–H(II) has less than full three-dimensional order.

1.4 nm tobermorite has a layer structure and 1.4 nm indicates the thickness of this layer. It is a naturally occurring mineral and can be produced from CH and hydrous silica in aqueous suspensions. After being heated to 55 °C, 1.4 nm tobermorite dehydrates and loses water and converts to 1.1 nm tobermorite (Taylor, 1997).

C-S-H (I) is the imperfect form of 1.4 nm tobermorite and can be produced from CH and hydrous silica in aqueous suspensions. Portland cement in the presence of reactive silica at elevated temperatures produces phases similar to C-S-H (I). It is

more ordered than the C-S-H gel formed in Portland cement pastes. Also, C-S-H (I) is an intermediate product of hydrothermal reactions at temperatures up to 180 °C and can be detected in pastes made from alkali-activated slag (Taylor, 1997).

Jennite can occur as a natural mineral and has a layer structure similar to 1.4 nm tobermorite. The main difference is the OH^- groups linked to the calcium atoms in the central region of the individual layers. C-S-H (II) is the imperfect form of jennite and its Ca/Si ratio is higher than that of jennite. According to Taylor from the compositional standpoint, jennite and C-S-H (II) are closer to C-S-H gel than 1.4 nm tobermorite and C-S-H(I). The conditions with high Ca/Si in suspension favor the formation of C-S-H (II) or jennite at high temperatures (Damidot and Nonat, 1994).

There are four morphological types of C-S-H gel as investigated by SEM analysis of fractured surfaces of cement paste. Type I is a fibrous material and forms at early ages of cement paste being up to 2 μm long. Type II C-S-H appears at normal early ages and forms reticular networks or honeycomb like structures. Type III is prominent in older pastes and consists of tightly packed equant grains up to 300 nm across. Type IV is observed in older ages as inner product with featureless and massive structure (Diamond, 1976).

2.1.6.5.2. Calcium Hydroxide, $Ca(OH)_2$

Calcium hydroxide (CH) crystals (also called as portlandite) are produced from hydration of mainly C_3S and β-C_2S. It constitutes 20 to 25 percent of solids by volume in the hydrated cement paste. In the available pore spaces it tends to form large hexagonal-prism crystals. The strength contribution of CH is very low or negligible compared to C-S-H and can be easily removed by the action of water. Also CH is not chemically stable. It can react with sulfates to form gypsum which is deleterious in hardened cement paste.

2.1.6.5.3. Calcium Sulfoaluminate Hydrates

Calcium sulfoaluminate hydrates (AFm and AFt) occupy 15-20 percent by volume of the hydrated paste. As mentioned earlier, in fresh cement paste gypsum reacts with alumina-bearing phase (C_3A and C_4AF) to form primarily AFt, then it eventually transforms to AFm by time. Ettringite is by far the most common AFt phase with needle-shaped prismatic crystal structures present in hydrated cement paste. Massive growth of ettringite fills the pores and cracks of hardened cement paste. Failure of hardened cement paste caused by expansion in the presence of sulfate is due to the formation of ettringite.

Monosulfate is the most common AFm phases in hydrated cement paste. It tends to occur in the later stages of hydration. It forms hexagonal-plate crystals which are less deleterious compared to ettringite. At ambient temperatures ettringite is more stable than monosulfate, and thus existence of monosulfate in the hardened cement paste make it more vulnerable to sulfate attack (Kelly, 1960).

Both ettringite and monosulfate contain small amounts of Fe^{3+} which can substitute aluminum in the crystal structure (Mehta, 2006).

2.1.6.5.4. Carboaluminate

The atmospheric CO_2 or carbonates in the cement paste react with CH to produce calcium carbonate. Calcium carbonates can also be available in the presence of finely ground limestone. Calcium carbonate is reported to react with the tricalcium aluminate to form high and low forms of the carboaluminate, $C_3A \cdot 3CaCO_3 \cdot 32H_2O$ ($C_6A\bar{C}_3H_{32}$) and $C_3A{\bullet}CaCO_3{\bullet}12H_2O$ ($C_4A\bar{C}H_{12}$) respectively. Calcium carbonates can act as a partial substitute for gypsum in sulfoaluminates (Jackson, 2004).

2.2. Oil Well Cement

In the exploration and production of oil and gas wells, there are various applications of well cementing. The most important well cementing operation is primary cementing. In primary cementing, the borehole is lined with a protective steel tube, called casing, from surface through the bottom of hole. Cement slurry is pumped and then displaced up into the annular space between the casing and the borehole wall (Bensted, 2006). The aim of primary cementing is to support and protect the casing from external pressure and corrosive underground fluids and also to prevent the movement of fluid through the cement sheath. Another important application for well cementing is squeeze cementing operation (Nelson, 1990; Mehta, 2006). In squeeze cementing, the slurry is forced to plug the voids of casing or borehole wall at a specified depth (Taylor, 1997).

The temperature that cement slurry is exposed to is proportional to the depth of borehole. As the depth of the well increases, the bottom hole temperature rises. The total pressure that cement slurry is exposed to is the sum of hydrostatic head of drilling mud and/or cement slurry in the hole and the pumping pressure of cement slurry (Bensted, 2006). Drilling mud is a fluid used to aid the drilling of boreholes into the earth.

Specifications for oil well cement are different than that of the Portland cement types applied in construction industry. API (American Petroleum Institute) designates the specifications for cement types according to the well conditions. In the well conditions, cement slurries are exposed to high temperature, high pressure and corrosive underground fluids. There are eight types of API Portland cements which are arranged from A to H. These types are defined according to the depth of wells with varying degrees of sulfate resistance. API specifications do not cover all the well conditions for cementing including extremely hot and cold well conditions. These eight types of oil well cements illustrate the chemical and physical

requirements that fulfill the most of the well conditions. API describes the cement types as below;

- Class A: Intended for use from surface to 1830 m depth, when special properties are not required. Available only in Ordinary type (similar to ASTM C150 Type I)

- Class B: Intended for use from surface to 1830 m depth, when conditions require moderate to high sulfate resistance. Available both moderate (similar to ASTM C 150, Type II) and high sulfate-resistant types.

- Class C: Intended for use from surface to 1830 m depth, when conditions require high early strength. Available in ordinary and moderate (similar to ASTM C 150, Type III) and high sulfate-resistant types.

- Class D: Intended for use from surface to 1,830 m to 3050 m depth, under conditions of moderately high temperatures and pressures. Available in both moderate and high sulfate-resistant types.

- Class E: Intended for use from surface to 1,830 m to 4270 m depth, under conditions of high temperatures and pressures. Both moderate and high sulfate-resistant types available.

- Class F: Intended for use from surface to 1,830 m to 4880 m depth, under conditions of extremely high temperatures and pressures. Available in both moderate and high sulfate-resistant types.

- Class G and H: Intended for use as a basic well cement from surface to 2,440 m depth as manufactured, or can be used with accelerators and retarders to cover a wide range of well depths and temperatures. No additions other than calcium sulfate or water, or both, shall be interground or blended with the clinker during manufacture of Class G and Class H cement. It is available only in moderate and high sulfate-resistant types.

The chemical compositions of Classes G and Class H types are similar; their principal difference is the specific surface area of the cement. Class H is coarser than Class G, and so has lower water requirement than that of the Class G.

API made restrictions on cement types to fulfill the requirements of cement slurries according to the considerable depths. These depths are based on the conditions imposed by the casing-cement specification tests (Schedule 1, 4, 5, 6, 8, 9), and should be considered as approximate values. The chemical requirements, physical requirements and typical compositions of API cement types are listed in Table 2-3, Table 2-4 and Table 2-5 respectively.

Table 2-3 Chemical requirements of API cement types (API Spec. 10A, 1995)

	Cement Class					
	A	B	C	D,E,F,	G	H
ORDINARY GRADE (O)						
Magnesium oxide (MgO), maximum, percent	6.0	NA	6.0	NA	NA	NA
Sulfur trioxide (SO_3), maximum, percent	3.5[2]	NA	4.5	NA	NA	NA
Loss on ignition, maximum, percent	3.0	NA	3.0	NA	NA	NA
Insoluble residue, maximum, percent	0.75	NA	0.75	NA	NA	NA
Tricalcium aluminate (C_3A), maximum, percent	NR	NA	15	NA	NA	NA
MODERATE SULFATE-RESIST GRADE (MSR)						
Magnesium oxide (MgO), maximum, percent	NA	6.0	6.0	6.0	6.0	6.0
Sulfur trioxide (SO_3), maximum, percent	NA	3.0	3.5	3.0	3.0	3.0
Loss on ignition, maximum, percent	NA	3.0	3.0	3.0	3.0	3.0
Insoluble residue, maximum, percent	NA	0.75	0.75	0.75	0.75	0.75
Tricalcium silicate (C_3S), maximum, percent	NA	NR	NR	NR	58[3]	58[3]
minimum, percent	NA	NR	NR	NR	48[3]	48[3]
Tricalcium aluminate (C_3A), maximum percent[3]	NA	8	8	8	8	8
Total alkali content expressed as sodium oxide (Na_2O) equivalent, maximum, percent	NA	NR	NR	NR	0.75[4]	0.75[4]
HIGH SULFATE-RESISTANT GRADE (HSR)						
Magnesium oxide (MgO), maximum, percent	NA	6.0	6.0	6.0	6.0	6.0
Sulfur trioxide (SO_3), maximum, percent	NA	3.0	3.5	3.0	3.0	3.0
Loss on ignition, maximum, percent	NA	3.0	3.0	3.0	3.0	3.0
Insoluble residue, maximum, percent	NA	0.75	0.75	0.75	0.75	0.75
Tricalcium silicate (C_3S) maximum, percent	NA	NR	NR	NR	65[3]	65[3]
minimum, percent	NA	NR	NR	NR	48[3]	48[3]
Tricalcium aluminate (C_3A), maximum, percent	NA	3[3]	3[3]	3[3]	3[3]	3[3]
Tetracalcium aluminoferrite (C_4AF) plus twice the tricalcium aluminate (C_3A), maximum, percent	NA	24[3]	24[3]	24[3]	24[3]	24[3]
Total alkali content expressed as sodium oxide (Na_2O) equivalent, maximum, percent	NA	NR	NR	NR	0.75[4]	0.75[4]

[1]Methods covering the chemical analyses of hydraulic cements are described in ASTM C114: *Standard Methods for Chemical Analysis of Hydraulic Cement.*
[2]When the tricalcium aluminate content (expressed as C_3A) of the cement is 8% or less, the maximum SO_3 content shall be 3%.
[3]The expressing of chemical limitations by means of calculated assumed compounds does not necessarily mean that the oxides are actually or entirely present as such compounds. When the ratio of the percentages of Al_2O_3 to Fe_2O_3 is 0.64 or less, the C_3A content is zero. When the Al_2O_3 to Fe_2O_3 ratio is greater than 0.64, the compounds shall be calculated as follows:

$C_3A = (2.65 \times \% Al_2O_3) - (1.69 \times \% Fe_2O_3)$

$C_4AF = 3.04 \times \% Fe_2O_3$

$C_3S = (4.07 \times \% CaO) - (7.60 \times \% SiO_2) - (6.72 \times \% Al_2O_3) - (1.43 \times \% Fe_2O_3) (2.85 \times \% SO_3)$

When the ratio of Al_2O_3 to Fe_2O_3 is less than 0.64, the C_3S shall be calculated as follows:

$C_3S = (4.07 \times \% CaO) - (7.60 \times \% SiO_2) - (4.48 \times \% A_2O_3) - (2.86 \times \% Fe_2C_3) - (2.85 \times \% SO_3)$

[4]The sodium oxide equivalent (expressed as Na_2O equivalent) shall be calculated by the formula:

Na_2O equivalent = $(0.658 \times \% K_2O) + (\% Na_2O)$

NR = No Requirement
NA = Not Available

Table 2-4 Physical requirements of API cement types (API Spec. 10A, 1995)

Well Cement Class				A	B	C	D	E	F	G	H
Mix Water, percent of the weight of cement (Table 6)				46	46	56	38	38	38	44	38
Fineness Tests (Alternative Methods) Section 5											
Turbidimeter (specified surface, minimum m^2/kg)				150	160	220	NR	NR	NR	NR	NR
Air Permeability (specified surface, minimum m^2/kg)				280	280	400	NR	NR	NR	NR	NR
(Free fluid content, maximum mL (Section 7)				NR	NR	NR	NR	NR	NR	3.5	3.5
Compressive Strength Test, Eight Hour Curing Time (Section 8)	Schedule Number, Table 7	Final Curing Temp, °F (°C)	Final Curing Pressure psi (kPa)	Minimum Compressive Strength, psi (MPa)							
	NA	100 (38)	Atmos.	250 (1.7)	200 (1.4)	300 (2.1)	NR	NR	NR	300 (2.1)	300 (2.1)
	NA	140 (60)	Atmos.	NR	NR	NR	NR	NR	NR	1500 (10.3)	1500 (10.3)
	6S	230 (110)	3000 (20700)	NR	NR	NR	500 (3.5)	NR	NR	NR	NR
	8S	290 (143)	3000 (20700)	NR	NR	NR	NR	500 (3.5)	NR	NR	NR
	9S	320 (160)	3000 (20700)	NR	NR	NR	NR	NR	500 (3.5)	NR	NR
Compressive Strength Test, Twenty-Four Hour Curing Time (Section 8)	Schedule Number, Table 7	Final Curing Temp, °F (°C)	Final Curing Pressure psi (kPa)	Minimum Compressive Strength, psi (MPa)							
	NA	100 (38)	Atmos.	1800 (12.4)	1500 (10.3)	2000 (13.8)	NR	NR	NR	NR	NR
	4S	170 (77)	3000 (20700)	NR	NR	NR	1000 (6.9)	1000 (6.9)	NR	NR	NR
	6S	230 (110)	3000 (20700)	NR	NR	NR	2000 (13.8)	NR	1000 (6.9)	NR	NR
	8S	290 (143)	3000 (20700)	NR	NR	NR	NR	2000 (13.8)	NR	NR	NR
	9S	320 (160)	3000 (20700)	NR	NR	NR	NR	NR	1000 (6.9)	NR	NR
Pressure Temperature Thickening Time Test (Section 9)	Specification Test Schedule Number Table 10	Maximum Consistency 15-30 Minute Stirring Period B_c[5]		Maximum/Minimum Thickening Time, minutes							
	4	30		90 min	90 min	90 min	90 min	NR	NR	NR	NR
	5	30		NR	NR	NR	NR	NR	NR	90 min	90 min
	5	30		NR	NR	NR	NR	NR	NR	120 max	120 max
	6	30		NR	NR	NR	100 min	100 min	100 min	NR	NR
	8	30		NR	NR	NR	NR	154 min	NR	NR	NR
	9	30		NR	NR	NR	NR	NR	190 min	NR	NR

[5]Bearden units of consistency (B_c).
B_c—Bearden units of consistency obtained on a pressurized consistometer as defined in Section 9 of API Spec 10A and calibrated as per the same section.
NR = No Requirement

Table 2-5 Typical composition and wagner fineness of API cement types (Nelson, 1983)

API Class	ASTM Type	Typical Potential Phase Composition (%)				Typical Fineness (cm^2/g)
		C_3S	β-C_2S	C_3A	C_4AF	
A	I	45	27	11	8	1600
B	II	44	31	5	13	1600
C	III	53	19	11	9	2200
D		28	49	4	12	1500
E		38	43	4	9	1500
G	(II)	50	30	5	12	1800
H	(II)	50	30	5	12	1600

2.2.1. Hydration of Portland Cement at Elevated Temperatures

At elevated temperatures, hydration rate of C_3S increases at early ages, on the other hand, hydration rate of C_2S increases both at early and later ages (months later) especially at high temperatures (Odler, 2004). Therefore, the overall hydration rate of Portland cement increases at elevated temperatures.

C-S-H gel is thermodynamically stable up to 110 °C; at higher temperatures C-S-H gel metamorphose to more stable structures. Hydration at high temperatures leads to the formation of highly crystalline silicate hydrates with more Ca/Si ratio. It takes free lime, which is already available due to C_3S and C_2S hydration, and converts to the phases called mainly "alpha dicalcium silicate hydrate" (α-C_2SH) and / or Jaffeite ($C_3SH_{1.5}$) (Andrew et al, 2008). α-C_2SH is highly crystalline and much denser than C-S-H gel. Conversion of C-S-H to α-C_2SH occurs with an associated volume reduction and therefore, is deleterious to the hardened cement paste. As a result, compressive strength and permeability of the hardened cement paste is adversely affected by the formation of α-C_2SH (Taylor, 1997; Nelson, 1990).

The strength retrogression of cement paste at high temperatures can be prevented by reducing Ca/Si ratio in the cement paste. It can be reduced to 1.0 with addition of 35-40 percent silica by weight of cement (Nelson, 1990). In the presence of finely ground silica, pozzolanic reaction takes place and C-S-H gel tend to form 1.1 nm tobermorite, ($C_5S_6H_5$) (Odler, 2004). At temperatures above 150 °C, tobermorite converts to mainly xonotlite (C_6S_6H) and gyrolite ($C_6S_3H_2$). At 250 °C truscotite begins to appear and both xonotlite and truscottie are stable up to 400 °C (Nelson, 1990).

Among pozzolans α-quartz is the most effective pozzolanic material due to its high silica content and is frequently used in thermal wells to prevent strength retrogression (Nelson, 1990).

The structure of sulfoaluminate phases are more temperature dependent. After 70 °C ettringite is no longer thermodynamically stable and decomposes to monosulptates (Kalousek, 1941; Klemm and Adams, 1990). In contrast to AFt phases, monosulptate is not deleterious for the hardened cement paste (Day, 1992). Figure 2-2 demonstrates the distribution of sulfate phases at various temperatures (Kalousek, 1965). Boiling at 100 °C for 11 days yields total destruction of monosulphates and decomposes to gypsum (Day, 1992). Further hydration over 100 °C, C_3A and $C_2(A,F)$ turns to hydrogarnet phase (Odler, 2004).

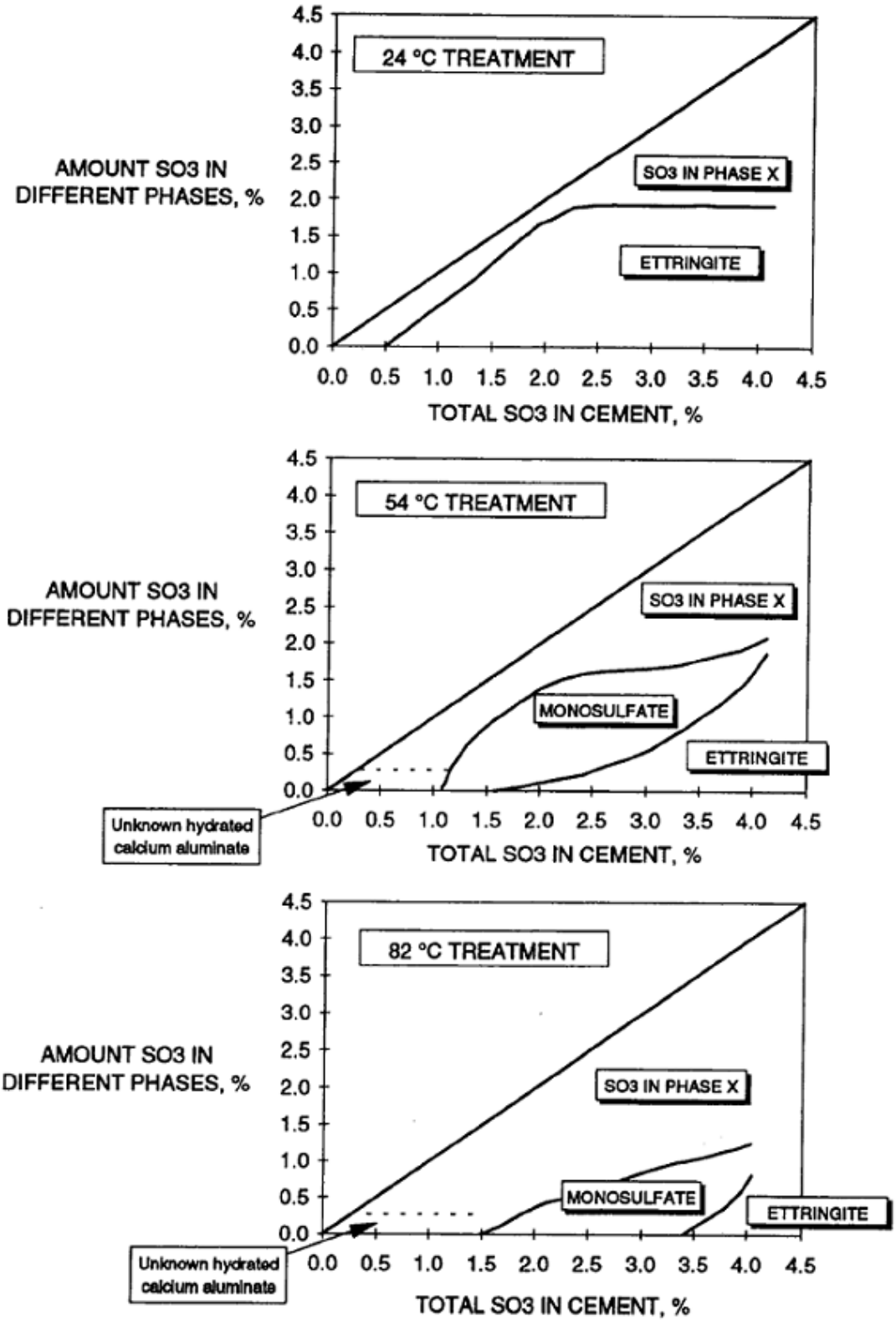

Figure 2-2 Effect of curing temperature on sulfoaluminate phases (Day, 1992)

2.3. Blast Furnace Slag

2.3.1. Raw Materials and Manufacture

The American Society of Testing and Materials (ASTM) Designation C125 recognizes blast-furnace slag as *"the nonmetallic product consisting essentially of silicates and alumino-silicates of lime and other bases, which is developed simultaneously with iron in a blast furnace."*

In nature, iron ore is found in an impure state, oxidized and with a mixture of oxides of silica, alumina and other metals. The chemical reaction occurs by the burning of coke with the ore, limestone and/or dolomite in the furnace between the temperatures of 1300^{o}C and 1600^{o}C. The preheated air blown into furnace and carbon of coke reacts with oxygen to produce heat and carbon monoxide. Carbon monoxide takes oxygen from iron oxide to form carbon dioxide, and therefore, iron oxide is reduced to form metallic iron (Lee, 1974).

The remaining fluxing stone is calcined in the furnace by heat and decomposes to calcium oxide and magnesium oxide. These oxides combine with the silicon and alumina from the iron ore to form what is called slag. Another function of fluxing lime is to react with sulfur which comes from coke and keeps the content of iron at a very low level (Lee, 1974).

2.3.2. Slag Types

There are three forms of blast-furnace slag (BFS) which are; air-cooled, granulated and expanded (or foamed) as illustrated in Figure 2-3.

Figure 2-3 Left to right, air-cooled BFS, expanded BFS and GGBFS (NSA 2012)

2.3.2.1. Air-Cooled Blast-Furnace Slag

Air-cooled blast-furnace slag is specially defined in ASTM C125 as *"The material resulting from solidification of molten blast-furnace slag under atmospheric conditions. Subsequent cooling may be accelerated by application of water to the solidified surface"*. In this type of slag, crystalline structures form similar to natural igneous rock. Crystals can form with a varying range from microscopic sizes to 3 mm. It is widely used as concrete aggregate, road stone and railway ballast (Lee, 1974).

2.3.2.2. Expanded or Foamed Blast-Furnace Slag

Expanded blast-furnace slag is specially defined in ASTM specification C125 as *"The lightweight cellular material obtained by the controlled processing of molten blast furnace slag with water, or with water, or with water and other agents such as steam or compressed air or both"*. Most expanded slag is used as lightweight aggregate in concrete.

2.3.2.3. Ground Granulated Blast-Furnace Slag

Granulated blast-furnace slag (GGBFS) is specially defined in ASTM specification C125 as *"The glassy, granular material formed when molten blast-furnace slag is*

rapidly chilled, as by immersion in water". Due to the rapid chilling and solidification of molten slag, it gains more hydraulic (cementitious) property. To enhance its hydraulic binding property, it is ground to powder and blended with alkaline activating agent such as alkalis, lime or Portland cement (Lee, 1974).

BFS can be used in three general ways in cement and concrete industry as; a) raw material for manufacturing Portland cement clinker, b) mineral additive to produce slag blended cements, c) mineral additive in concrete production.

The first method found for evaluating blast furnace slag by the cement industry is to use it as a raw material in clinker production. The manufacturing process is similar to that used conventional raw material; limestone and clay. The slag and limestone are ground and mixed in the proper ratios and then burned in the rotary kiln. The resulting clinker is similar to that of prepared with limestone and clay. The color of the clinker is brownish because of the high magnesia content of slag (ACI 233).

GGBFS itself has hydraulic setting property and can be utilized as a substitute for Portland cement to produce blended cement. According to ASTM C595, its content in the slag blended cement can be up to 70 percent (by mass), whereas, EN 197-1 makes limitation of GGBFS in slag-cement blend up to 95 percent by mass (CEM III/C). GGBFS is the maximum amount of mineral additive that is allowed to use it in the cement blends according to EN 197-1.

Most of GGBFS blended cement is produced by inter-grinding of slag and clinker together but also there is toleration for separate grinding. Slag is harder to grind than clinker and as a result, inter-grinding of GGBFS cement leaves the slag grains coarser than that of the clinker in cement. Separate grinding of GGBFS cement has the advantage of grinding GGBFS and clinker on their optimum fineness (ACI 233).

2.3.3. Pozzolanic Reaction

ASTM C219 designates a pozzolan as; *"A siliceous or siliceous and aluminous material, which in itself possesses little or no cementitious value, but will, in finely divided form and in the presence of moisture, chemically react with calcium hydroxide at ordinary temperatures to form compounds possessing cementitious properties"* The pozolanic reaction is the chemical reaction that occurs between cement and pozzolans.

As mentioned earlier, during cement hydration CH is liberated as a result of the hydration of calcium silicates. CH does not contribute to the strength of the hardened cement paste but decrease the chemical resistance of cement paste. In the presence of a pozzolan, silica reacts with free CH to form more stable cementitious compounds (called secondary C-S-H). Figure 2-4 shows the effect of pozzolan on CH content in cement paste by time.

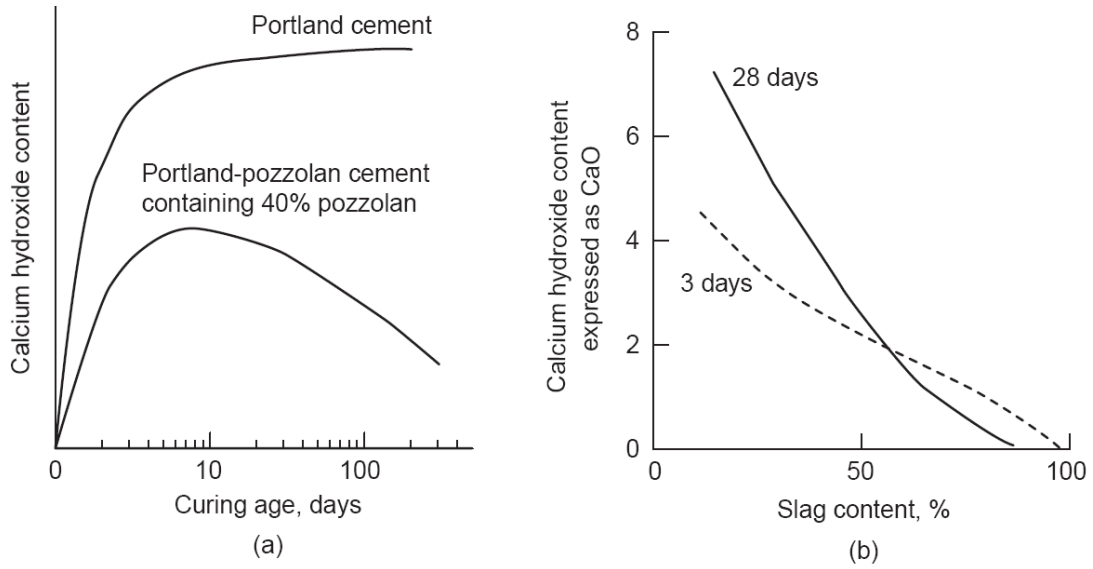

Figure 2-4 a) Effects of curing age on the calcium hydroxide content of a cement-sand mortar made with a Portland-pozzolan cement. b) Effects of curing age and proportion of slag on the lime content of the portland-slag cement paste (Lea, 1971).

2.3.4. Characteristics of GGBFS

2.3.4.1. Slag Chemistry

There are various broad range of slag types with their chemical composition. Their chemical composition depends on the ore, coke type and consumption, limestone flux, burning efficiency and the kind of iron being made. The major constituents of slag are oxides of lime, silica, alumina and magnesia. The minor constituents are sulfur, TiO_2, alkalis (Na_2O and K_2O) and, etc. Table 2-6 shows the chemical composition of blast furnace slag from different countries (Erdoğan, 1997).

Table 2-6 Chemical composition of various BFS types (Erdoğan, 1997)

Compound	Turkey	U.S. and Canada	Australia	South Africa
CaO	34-41	29-50	39-44	30-40
SiO_2	34-36	30-40	33-37	30-36
Al_2O_3	13-19	7-18	15-18	9-16
Fe_2O_3	0.3-2.5	0.1-1.5	0-0.7	-
MgO	3.5-7	0-19	1-3	8-21
MnO	1-2.5	0.2-1.5	0.1.5	-
S	1-2	0-2	0.6-0.8	1-1.6
SO_3	-	-	-	-

Figure 2-5 shows the ternary diagram of CaO-SiO_2-Al_2O_3 for the composition of BFS and Portland cement. As can be seen in the ternary diagram, the composition of BFS and Portland cement are found to be in the similar fields. As can be seen in the diagram, Portland cement is in the C_3S field whereas BFS is in the C_2S field (Pal et al, 2003).

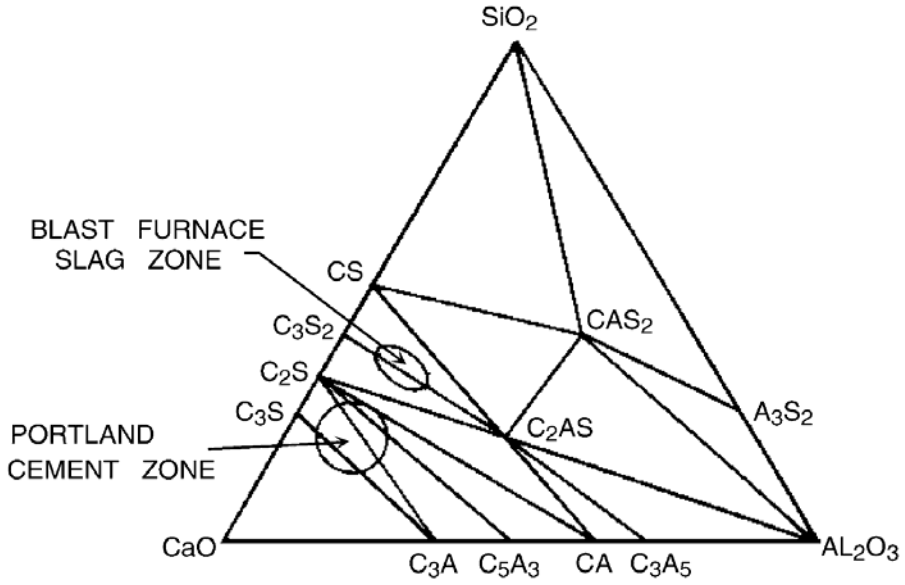

Figure 2-5 Ternary diagram of $CaO\text{-}SiO_2\text{-}Al_2O_3$ for indicating composition of PC and BFS (Lea, 1971; Bakker, 1983)

2.3.4.2. Crystalline Structure

The crystalline structures inside slag are made up of the compounds of oxides of calcium and magnesium with silica and alumina. GGBFS has more glassy and crystalline structure than air cooled slag because of the rapid cooling of molten slag (Lee, 1974).

According to Lee (1974), the main mineral constituent of the slag is melilite which is the continuous series of solid phase of akermanite ($2CaO{\cdot}MgO{\cdot}2SiO_2$) and gehlenite ($2CaO{\cdot}Al_2O_3{\cdot}2SiO_2$). In slag if lime to alumina ratio is low anorthite ($CaO{\cdot}Al_2O_3{\cdot}2SiO_2$) will form, however if lime to alumina ratio is high orthosilicate also known as belite (C_2S) will form. There are four main polymorphs of belite crystals which are α, ά, β and γ. If rapid cooling is provided β polymorph will occur which is more desirable for hydraulic reactivity. Magnesium oxide in the slag may react with the other oxides to form the minerals of merwinite ($3CaO{\cdot}MgO{\cdot}2SiO_2$) or monticellite ($CaO{\cdot}MgO{\cdot}SiO_2$). Also some minor components like fortresite ($2MgO{\cdot}SO_4$), enstatire ($MgO{\cdot}SO_4$) or spinel ($MgO{\cdot}Al_2O_3$) may occur (Lee, 1974).

The mineralogical compounds from quaternary system CaO-SiO_2-Al_2O_3-MgO that can be found after crystallization of blast-furnace slag can be seen in Table 2-7.

Table 2-7 Possible crystalline minerals of BFS (Smolcyzk, 1980; Galibert, 1984)

Main components		Minor components		Seldom observed	
Melilite	solid solution of	Dicalcium silicate	C_2S	Anorthite	CAS_2
Gehlenite	C_2AS	(α, α', β, γ)		Forsterite	M_2S
Akermanite	C_2MS_2	Monticellite	CMS	Enstatite	MS
Merwinite	C_3MS_2	Rankinite	C_3S_2	Perowskite	CT
Diopside	CMS_2	Pseudo-Wollastonite	CS	Spinelle	MA
Other Pyroxenes		Oldhamite	CaS		

§: Notation in cement chemistry is used, i.e. C = CaO, S = SiO_2, A = Al_2O_3, F = Fe_2O_3, $\overline{S}$ = SO_3 etc., see Appendix B.

2.3.4.3. Slag Activity Index

According to ASTM C 989 GGBFS is classified into three grades depending on their respective mortar strengths when blended with Portland cement with an equal mass. The three grades based on their slag activity index (SAI) are: Grade 80, Grade 100 and Grade 120 as shown in Table 2-8.

Table 2-8 Slag activity index requirements (ASTM C989)

Age and grade	SAI, minimum percent	
	Average of last five consecutive samples	Any individual sample
7-day index		
Grade 80	–	–
Grade 100	75	70
Grade 120	95	90
28-day index		
Grade 80	75	70
Grade 100	95	90
Grade 120	115	110

2.3.4.4. Hydraulic Reactivity

According to ACI 226, the factors influencing the GGBFS reactivity are: a) chemical composition of GGBFS; b) alkali concentration of the reacting system; c) glass content of the GGBFS; d) fineness of the GGBFS; and e) temperature during the early phases of hydration process. For GGBFS, hydraulic modulus (HM) is used to make relevance between its chemical composition and potential of hydraulic reactivity. Many attempts have been made to determine the HM of slag. The simplest and most widely used module is given in Equation 2.10 (Taylor, 1997):

$$(CaO + MgO + Al_2O_3) / SiO_2 \geq 1 \qquad (2.10)$$

HM according to EN 197-1 is;

$$(CaO + MgO) / SiO_2 \geq 1 \qquad (2.11)$$

Another more specific module is defined by Cheron and Lardinois (1968)

$$1.85 \geq (CaO + 1.4\ MgO + 0.56\ Al_2O_3) / SiO_2 \geq 1.65 \qquad (2.12)$$

Table 2-9 presents the formulas proposed for assesment of hydraulicity of GGBFS. Generally low values of HM correspond to low hydraulic reactivity but there is not a certain relation between them. In order to make more accurate relationship, whole chemical composition of GGBFS must be taken into account including minor elements. On the other hand, the effect of crystallinity degree on HM of GGBFS makes it more complicated to evaluate HM (Micheline and Micheline 2004).

Table 2-9 Formulas proposed for assessment of hydraulicity of GGBFS (Pal et al, 2003)

Serial number	Formula	Requirement for good performance	Preference
1	CaO/SiO_2	1.3–1.4	1
2	$(CaO+MgO)/SiO_2$	>1.4	1
3	$(CaO+MgO)/(SiO_2+Al_2O_3)$	1.0–1.3	1
4	$(CaO+0.56\ Al_2O_3+1.4\ MgO)/SiO_2$	≥ 1.65	2
5	$(CaO+MgO+Al_2O_3)/SiO_2$	≥ 1.0	3

According to literature, the effect of Al_2O_3 on the SAI of GGBFS is more complex. Smolczyk states that, if Al_2O_3 content is above 13%, it tends to increase early strengths and decreases late strengths (Smolczyk, 1978). The influence of Al_2O_3 on strength development of a hardened cement paste is illustrated with given hydraulic modulus as shown in Figure 2-6. In addition, it has been found that MgO amount up to 11% is equivalent to CaO in slag and it is efficient up to 18 %. Minor components also effect the reactivity of slag, MnO has always negative effect on slag, whereas P_2O_5 and alkalis are more complex (Smolczyk, 1978).

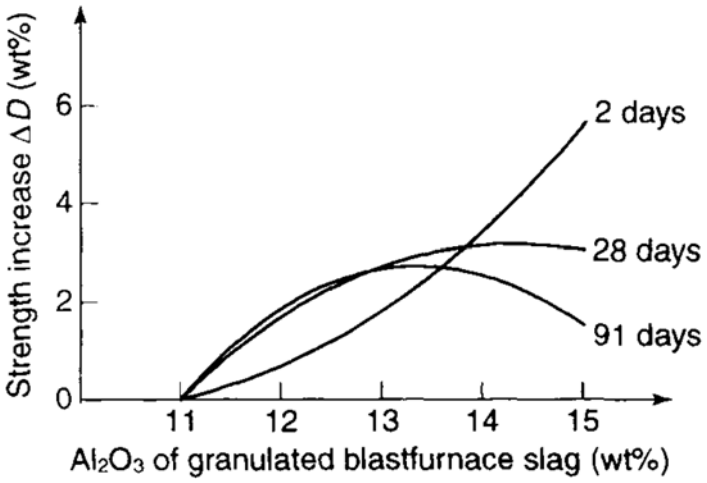

Figure 2-6 Influence of Al_2O_3 on the strength development for a hydraulic modulus (C+M)/S = 1.4 (Satarin, 1974)

2.3.4.5. Physical Properties of Slag

In the molten slag, air bubbles might be trapped inside the slag before it becomes solid. This is caused due to the pressure in the furnace, and also cooling conditions and solidification affects the quantity and amount of these bubbles (Lee, 1974). Therefore, crystal structure, density and porosity of the slag are affected by the cooling conditions.

The specific gravity of the slag is approximately 2.90 with its bulk density varying in the range of 1200–1300 kg/m3. The color of GGBFS varies from dark to off-white but generally off-white color (Pal et al, 2003).

2.3.4.5.1. Fineness

Fineness is generally evaluated by specific surface area and is calculated by Blaine Air Permeability Method (ASTM C204). Fineness affects the reactivity of slag and increased fineness improves early strength development of slag (Lumley et al, 1996). According to Swamy, an increase in the fineness of slag two to three times that of normal PC contributes in a variety of engineering properties such as bleeding, time of setting, heat evolution, better strength development and excellent durability (Swamy, 1998). Therefore, the fineness of GGBFS must be kept higher than that of cement for better performance. As shown in Figure 2-7, it is clarified that fineness of GGBFS improves strength of cement mortars at all ages.

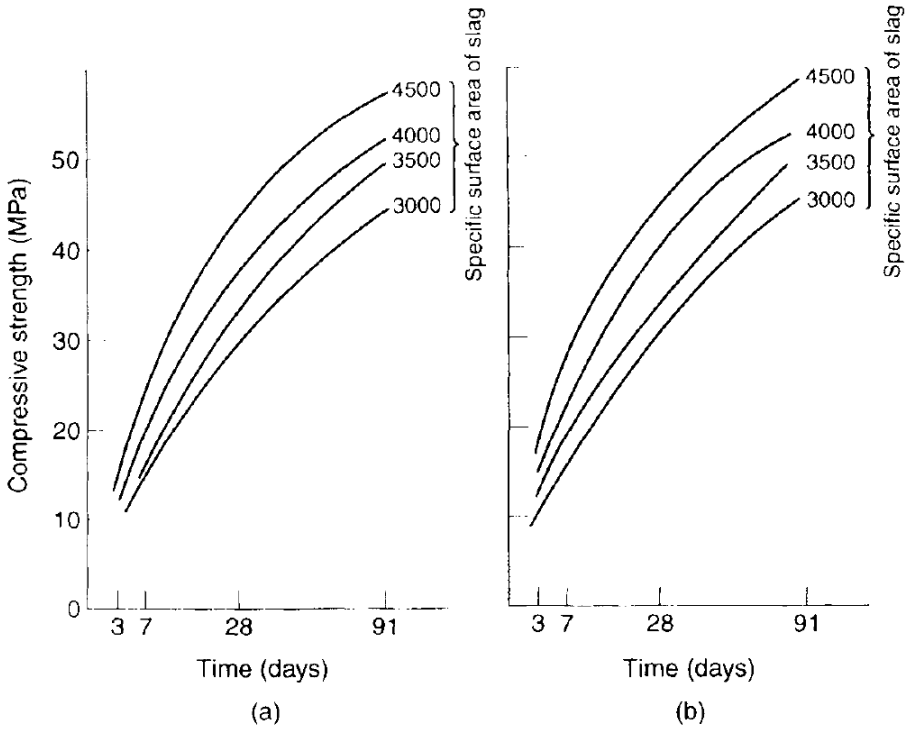

Figure 2-7 Compressive strength of mortars: cements CEM III/B with 75 percent slag of specific surface areas (a) 3000 and (b) 4000 cm^2/g (Schröder, 1968).

2.3.4.5.2. Glass Content

The temperature which the furnace is tapped is the most important variable affecting degree of vitrification, while rate of quenching influences glass content (Schwiete and Dolbor, 1963). The glass content of slag is one of the most significant variables on hydraulic reactivity; however, there is not an exact relationship between strength development and glass content (Pal et al, 2003). Slag samples with glass content as low as 30 to 65 percent have still enough hydraulic property and there is not a certain required lowest amount of glass content for slag activity. Therefore, most of the international standards evaluate slag activity by direct strength performance tests rather than minimum glass content criteria (Swamy and Bouikni, 1990). On the other hand, by the influence of empirical studies, to guarantee hydraulic activity the glass content of slag is better kept in excess of 90% (Pal et al, 2003). Figure 2-8 demonstrates the effect of glass content on the strength development of GGBFS.

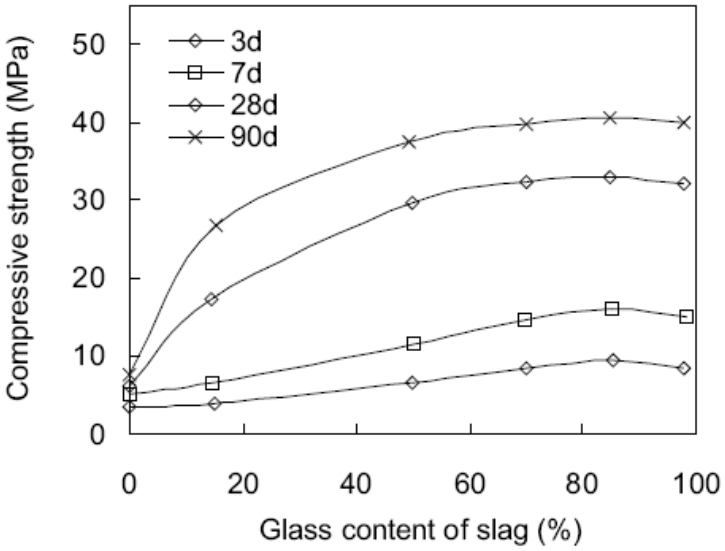

Figure 2-8 Effect of glass content of slag in compressive strength development of the mortars (Frigione, 1986)

2.3.4.6. GGBFS in Oil Well Cement

GGBFS blended cement has a long history of use in the construction industry, but is not used extensively in oil well cementing applications. As mentioned earlier, GGBFS is a pozzolanic and hydraulic material which reacts with lime to form additional C-S-H. If GGBFS is used in oil well cementing, pore sizes in the set-cement matrix become smaller and capillary porosity would be lower. The capillary porosity can be reduced by 25-30% if 75% of Portland cement is substituted with the GGBFS. Also GGBFS blended cements generally have more resistance to chemical attack than Portland cement alone (Nelson, 2006).

The major benefits are;

- Improved resistance against sulfate attack
- Less alkalis and chloride diffusion through cement matrix.
- Lower permeability of set-cement.
- Increased durability at elevated temperatures

In addition, GGBFS and GGBFS blended cements are used in the following well cementing applications (Nelson, 2006).

- Squeeze cementing and microfine cements
- Salt-saturated cement slurries
- CO_2 resistant cements
- Foamed cement
- Improvement of construction grade cements in well cementing

2.3.5. Hydration of Slag Blended Cement

2.3.5.1. Hydration of Slag

As mentioned earlier, in the ternary diagram of CaO-SiO_2-Al_2O_3 GGBFS is in the C_2S field while Portland cement is in the C_3S field. (Figure 2-5). Therefore, the hydration products of GGBFS and GGBFS blended cements are found to be similar (Smolczyk, 1978).

In the presence of water GGBFS set like Portland cement but it is much slower than that of Portland cement. Therefore, activators must be used to enhance hydraulic property of GGBFS. Alkali salts like, sodium hydroxide, sodium carbonate, sodium silicate, sodium sulfate, calcium sulfate, lime, or even Portland cement (supply of lime) can be used as an activator (Micheline and Micheline, 2004). In all cases, C-S-H is formed with incorporation of aluminum, magnesium, iron or sulfate.

2.3.5.2. Hydration of Slag in the Presence of Portland Cement

The hydration of GGBFS blended cement is more complex than that of Portland cement. In the presence of Portland cement hydration of GGBFS depend on the dissolution of the glassy slag by the hydroxyl ions released by the hydration of

Portland cement and alkali content. GGBFS first reacts with alkalis and then $Ca(OH)_2$ (from cement hydration) to produce additional C-S-H (ACI 233). Approximately one mole of slag with an uncertain stoichiometry consumes about 2.6 moles of $Ca(OH)_2$ (Richardson et al, 2002).

In the hydration of slag cement, hydration rims are formed around the slag particles (Kondo and Oshawa, 1968). C-S-H can accommodate magnesium and aluminum partially within its micro or nanostructure (Taylor, 1997). Hydrotalcite forms also by partial accommodation of magnesium and aluminum within the micro or nanostructure of C-S-H (Harrison et al, 1987) and sulfates possibly uptaken by AFm phases (Gollop and Taylor, 1996). The stoichiometry of slag blended cement hydration is approximately defined as follows (Taylor, 1997):

- Magnesium from slag forms hydrotalcite-type phase with an assumption of Mg/Al ratio 2.5
- SiO_2 from slag forms additional C-S-H phase with an assumption of Ca/Si ratio 1.55 and Al/Ca ratio 0.09
- Remaining Al_2O_3 found in AFm phase and probably contains the sulfur released from slag.
- All CaO released from slag is not enough to account for in the C-S-H and AFm phases and therefore Ca/Si ratio of C-S-H formed lower than that of Portland cement.

2.3.5.3. Hydration Products

2.3.5.3.1. Calcium-Silicate-Hydrate

The resulting C-S-H formed in the hydration of slag blended cement has lower Ca/Si ratio than that of Portland cement (Odler, 2000). Moreover, Al/Ca ratio of the C-S-H increases with the Si/Ca ratio (Richardson et al, 2002). With the contribution of

pozzolanic reactivity, GGBFS replacement in the paste increases amount of C-S-H which are more foil-like and less fibrillar in structure (Chen, 2006).

2.3.5.3.2. Calcium Hyroxide

The calcium hydroxide (CH) is a hydration product of C_3S and C_2S and is partially consumed by the hydration of slag. In the initial period of hydration there would be comparable amounts of CH within the hydration product of both Portland cement and slag cement. In the latter hydration periods, CH amount decreases with the hydration of slag in the pastes as seen in Table 2-10.

Table 2-10 Free lime content in slag blended cement pastes by wt % (Hinrichs and Odler, 1989)

Slag in cement (%)	0	25	50	70
1d	8.0	8.5	5.5	1.9
2d	15.8	12	7.8	2.8
7d	18.4	12.0	7.3	2.5
28d	18.8	11.3	6.0	2.0
365d	20.1	11.1	5.5	1.3

Specific surface area of cements: 500 m^2/kg

2.3.5.3.3. Hydrogarnet Phases

Hydrogarnet phases have a range of compositions and C_3AH_6 is the most common phase in cement hydration. Al^{3+} may be partially or wholly replaced by Fe^{3+} while Si^{4+} can be replaced with $4H^+$ and thus gives C_3AH_6. Hydrogarnet formed in presence of gypsum is almost free from Fe^{3+} (Taylor, 1997). In the hydration of ferrite with the absence of gypsum, $C_2(A, F)H_8$ and/or $C_4(A, F)H_x$ are formed as the initial products and then eventually transforms into iron containing hydrogarnet

phase, $C_3(A,F)H_6$ (Chatterji and Jeffrey, 1962). At elevated temperatures aluminate and ferrite hydration directly yields hydrogarnet (Negro and Stafferi, 1979). Higher amounts of aluminum content in the slag enhance hydrogarnet formation in slag cement hydration. Also, katoite, another hydrogarnet type, is a less documented hydration product of slag cement (Richardson and Groves, 1992).

2.3.5.3.4. Brucite and Hydrotalcite

The hydration of crystalline MgO (periclase) to magnesium hydroxide (brucite) is a slow and expansive reaction. Hydrotalcite-type phases are structurally related to brucite; that some of the Mg^{2+} ions in brucite are replaced by tripositive ions (typically Al^{3+} or Fe^{3+}) and become positively charged. The charge of structure is balanced by anions and interlayer sites are occupied by H_2O molecules. Hydrotalcite phases occur as minor products on hydration of Portland cements. Hydration products similar to hydrotalcite phases are commonly formed with hydration of slag blended cements. Hydrotalcite can also occur as a natural mineral with the composition of $[Mg_{0.75}Al_{0.25}(OH)_2]$ $(CO_3)_{0.125}(H_2O)_{0.5}$ (Taylor, 1997).

2.3.5.4. Microstructure of Slag Blended Cement Pastes

The microstructure of slag blended cement paste is similar to that of Portland cement except for its denser structure and lower porosity. The porosity of pastes are comparable at early ages, however decreases with the contribution of slag hydration at later ages (Siddique and Khan, 2011). The pore sizes in hardened slag cement paste become finer and also more discontinuous and thin walled (Feldman, 1986). Therefore, higher contents of GGBFS replacements are reported to enhance the durability of hardened cement paste (Siddique and Khan, 2011).

Figure 2-9 illustrates hydrated microstructure of glassy slag and Portland cement blend. During early hydration, slag surface is first covered with the hydration products of Portland cement. Then in the dormant period when the liquid phase reaches CH saturation, slag grains are attacked by Ca^{++} ions and produce "inner hydrated layer". After the dissolution of Ca^{2+} and Al^{3+} ions from slag, skeleton of hydrated layer remains in slag. Due to the less immobility of Mg^{2+}, skeleton hydrate layers contain more amounts than inner products and anhydrous slag (Tanaka and Totani, 1983).

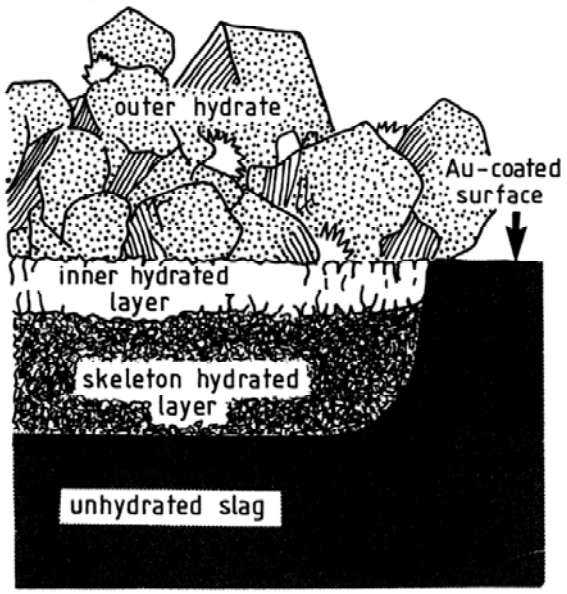

Figure 2-9 Distribution of hydration products of slag in the hydrating blended cement paste (Tanaka and Totani, 1983).

2.3.5.5. Sulfate Resistance of GGBFS Blended Cement

It is widely accepted that, substitution of Portland cement with GGBFS provide more resistance against sulfate attack. According to ASTM C989 for moderate sulfate resistance, 15-25 % slag replacement and for high sulfate resistance 35-50 % slag replacement is required. The substitution of GGBFS with Portland cement improves sulfate resistance in three ways (ACI 233);

a) GGBFS does not contain C_3A and therefore reduces overall proportion of C_3A amount in cement blend.
b) GGBFS reacts with $Ca(OH)_2$ to form additional C-S-H, thus there is a reduction in the available $Ca(OH)_2$ to form of calcium sulfoaluminate.
c) GGBFS reduces permeability in cement paste which is dependent on sulfate resistance.

Sulfate resistance depends on not only C_3A amount of cement, but also the Al_2O_3 amount of the GGBFS. If slag with high-alumina (17.7%) content is used in the blends between the GGBFS amount of 20-50 percent, sulfate resistance decreases. On the other hand, if GGBFS with low-alumina (11%) content is used, sulfate resistance increases independently from the C_3A amount of cement (Locher, 1966). The hydration products of alumina in the slag are not clear enough, but C-S-H takes some of the alumina where it is less open to sulfate attack.

CHAPTER 3

EXPERIMENTAL STUDY

3.1. Materials

The materials used in this study are; Portland cement (CEM I 42.5 R), API Class G oil well cement and GGBFS. Both of these materials are obtained from Bolu Cement plant. Chemical analysis, mineralogical composition and physical properties of these materials are presented in the following tables respectively; Table 3-1, Table 3-2, and Table 3-3.

Table 3-1 Chemical composition of materials

	Materials		
Components	**CEM I 42.5 R**	**Class G**	**GGBFS**
CaO	64.25	63.52	32.46
SiO_2	18.56	18.69	39.42
Al_2O_3	4.57	4.35	13.84
Fe_2O_3	3.58	5.19	1.62
MgO	2.21	1.43	8.34
SO_3	2.99	2.94	0.15
Na_2O	0.26	0.31	0.66
K_2O	0.51	0.54	0.92
Cl-	0.02	0.02	0.01
TiO_2	-	-	1.02
Mn_2O_3	-	-	0.77
LOI	3.58	2.60	0.07
Free CaO	2.60	1.79	-

Table 3-2 Mineralogical composition of the Portland cement and Class G cement clinker

	Materials	
Minerals	**CEM I**	**Class G**
C_3S	65.64	64.23
C_2S	3.71	5.15
C_3A	6.05	2.75
C_4AF	10.9	15.8

Table 3-3 Physical properties of Portland cement and Class G cement

Physical Properties	**Materials**	
	CEM I	**Class G**
Specific Gravity	3.20	3.21
Water Demand,% for neat cement	30.2	-
Moisture, %	-	-
Initial setting time, hr	02:05	03:00
Soundness, mm	1.0	1.0
Specific Surface, cm^2/gr	4300	3220
Residue on 45 m sieve,%	4.63	11.6
Compressive Strength (2 days), MPa	26.9	16.9
Compressive Strength (28 days), MPa	50.6	44.1

3.1.1. Portland Cement

Portland cement type CEM I with a strength class of 42.5 R according to EN 197-1 is supplied from Bolu Cement Plant. CEM I is manufactured with approximately 95 percent clinker and 5 percent limestone as minor additive with a few percent of gypsum. In relation to its highest clinker ratio among the types of Portland cement, it possesses highest reactivity with rapid hydration rate. Therefore, CEM I has the advantage of compensating the slow hydration rate of GGBFS in the blends of slag and Portland cement.

3.1.2. API Class G Cement

SRC, equivalent of Class G cement, with a strength class of 32.5 R according to TS 10157 is supplied from Bolu Cement plant. Class G cement is most widely used one among API cement types in various well conditions. It consists of mainly clinker with small amounts of gypsum. According to API, manufacturers are prohibited to use chemical admixtures, such as glycols or acetates to aid grinding. The clinker of this type of cement is coarsely ground to benefit from durability, lower porosity, increased pumpability, superior resistance against chemical attacks, low hydration rate and decreased setting time in well conditions.

API Class G cement is available in moderate sulfate resistant grade (MSR) and high sulfate resistant grade (HSR). The cement sample, used in this study as API Class G cement, possesses HSR grade according to chemical requirements of API Spec. 10A as clarified in Table 2-3. The chemical analysis, mineralogical composition and physical properties of SRC are equivalent to API Class G cement according to TS 10157. The chemical requirements for Class G cement with HSR grade is presented in Table 3-4.

Table 3-4 Requirements for API Class G cement with HSR grade (API Spec. 10A)

Chemical Anaysis	Limits	Actual value
MgO, %	max. 6.00	1.43
SO_3, %	max. 3.00	2.94
LOI, %	max. 3.00	2.6
IR, %	max. 0.75	0.58
C_3S	48 - 65	64.23
C_3A	max. 3.00	2.75
$2C_3A + C_4AF$	max. 24	21.29
Total alkali cont. (Na_2O equivalent)	max. 0.75	0.67

3.1.3. Ground Granulated Blast Furnace Slag

Ground granulated blast furnace slag (GGBFS) is supplied from Ereğli Iron and Steel Plant and manufactured according to the standard of EN 15167-1. The chemical analysis and physical properties of the GGBFS are presented in the following tables respectively, Table 3-1 and Table 3-5.

Table 3-5 Physical properties of GGBFS

Physical properties	Limits	GGBFS
Specific Gravity	-	2.82
Moisture, %	max. 1.0	0.05
Specific Surface, cm^2/gr	min. 2750	5360
Slag activity index (7 days), %	45	53.1
Slag activity index (28 days), %	70	73.4

3.1.4. Water

Tap water connected to the network in the Research Center of TPAO is used in this study for preparing cement slurries.

3.1.5. Cement Slurry Compositions

Five cement slurry compositions are prepared. First composition is prepared with neat G Class cement (G). The remaining compositions are prepared with the blends of CEM I and GGBFG. The ratios of CEM I and GGBFS in the blends by mass are (80:20), (60:40), (40:60) and (20:80), and named respectively as; S20, S40, S60 and S80 as illustrated in Table 3-6. The total amount of solid constituents (Class G cement, CEM I and GGBFS) used for preparing cement slurries is 800 gr. The w/c ratio required for Class G cement is 0.44 as specified in the API Spec. 10A, and thus all cement slurries are prepared with the same w/c ratio.

Table 3-6 Material proportion of cement slurries

	Cement blends				
Constituents	G	S20	S40	S60	S80
Class G, %	100	-	-	-	-
CEM I, %	-	80	60	40	20
GGBFS, %	-	20	40	60	80
Water, %	44	44	44	44	44

3.2. Experimental Procedures

3.2.1. Slurry Preparation

Cement slurries are prepared in the TPAO according to the specifications in API Spec. 10A. The mixing device is a 1 liter size, bottom-drive and blade-type as shown in Figure 3-1. It is a two speed mixer, operated at 4000 and 12000 RPM. The solid constituents (cement and other blends) are added to water in the mixer at 4000 RPM and followed by mixing at 12000 RPM for 35 seconds.

Figure 3-1 Cement slurry preparation with multi-speed mixer

3.2.2. Free Fluid

The free fluid is similar to the property of bleeding in fresh cement pastes. When cement slurry is allowed to stand for a period of time prior to setting, water may separate from slurry and accumulate at the top of the column (Nelson, 1997). Similarly, bleeding is the term used to describe the movement of water to the surface of the freshly placed concrete. Therefore they can be evaluated in the same manner. All cement pastes bleed to some extent. Bleeding ends when either the movement of water is blocked by the growth of hydration products or by the solids effectively coming into contact with each other.

In the free fluid test procedure, cement slurry is prepared according to API Specification 10A in TPAO. Then it is conditioned at atmospheric pressure and temperature (27 ºC) in the atmospheric pressure consistometer for 20 minutes. The atmospheric pressure consistometer, as shown in Figure 3-2, consists of a rotating cylindrical slurry container at a speed of 150 RPM with a temperature-controlled liquid bath.

Figure 3-2 Cement slurry conditioning in the atmospheric consistometer

After conditioning of the cement slurry, 400 ml equivalent of cement slurry by mass is taken to a 500 ml conical flask type I, class 2 in accordance with ASTM E 1404-94 shown in Figure 3-3. The flask is then sealed to prevent evaporation and left undisturbed for 2 hours.

Figure 3-3 Measuring free fluid content

At the end of the 2 hours, the supernatant fluid developed at the top of the flask is collected. The free fluid content of the slurry is calculated by volume fraction and expressed as percentage shown in Equation 3.1 as described by API Spec. 10A.

$$Ø = V_{FF} \cdot \rho / m_s \times 100 \quad (3.1)$$

where;

Ø	Free fluid content, percentage by volume;
V_{FF}	is the volume of free fluid collected, expressed in milliliters;
ρ	is the specific gravity of slurry;
m_s	is the initially recorded mass of the slurry, expressed in grams.

3.2.3. Compressive Strength

The cement slurries that are prepared as described in Section 3.2.1 are placed into 50 mm cubic moulds according to API Specification 10A. The moulds are then cured in a temperature-controlled water bath at 80 ºC for 22 hours. Later, they are cooled gradually in temperature-controlled water bath at 38 ºC for an hour and then at 27 ºC for the next hour. After the cooling period, cubic specimens are removed from their moulds. If the specimens are used for testing the compressive strength of 1-day, then they are ready to be tested. The remaining specimens are cured at 80 ºC in the same water bath until the end of the curing period. The compressive strengths of the specimens are tested at a loading rate of 2.4 kN/s by UTEST in the Materials of Construction laboratory of METU Civil Engineering Department.

3.2.4. Porosity

In the test procedure of porosity, cement slurries are mixed as specified in Section 3.2.1. Then, they are placed in to cubic moulds (50 mm size) to form specimens as mentioned in Section 3.2.3. After that, core samples are drilled from each cubic specimen to be tested by a coring bit with an internal diameter of 38 mm. After taking core, trim saw machine is used to smooth away both two edges of cylindrical cores, shown in Figure 3-4.

Figure 3-4 Coring and smoothing the edges of specimens

The core specimens as shown in Figure 3-5 are put into temperature-controlled oven to remove moisture and stop further hydration of hardened cement pastes. The core samples are conditioned in the oven at 80 ºC for 2 days as shown in Figure 3-5. After dehydration of core specimens, dimension and mass of each core are measured with digital compass and precision balance, as shown in Figure 3-6.

Figure 3-5 Dehydration of core specimens at temperature-controlled oven

Figure 3-6 Measuring dimensions and mass of each core specimen

Helium porosimeter from Vinci Technologies in TPAO is used to determine porosity of the hardened cement pastes as shown in Figure 3-7. Helium has the advantage over other gases because: (a) its molecules are small and can rapidly penetrate into the small pores, (b) it is inert and is not adsorbed on rock surfaces as air may do, (c) helium can be considered as an ideal gas (i.e., z = 1.0) when pressure and

temperature usually employed on the specimen, (d) helium has high diffusivity and therefore affords a useful mean for determining porosity of low permeability rocks.

Figure 3-7 Helium porosimeter

Helium porosimeter automatically measures solid volume and pore volume of samples by input of characteristic of samples (ID, diameter, length and weight). The measure is based on Boyle-Mariotte's law theory. Cores are tested with helium under the pressure of 0.7 MPa. The test method is performed according to the specifications described in API RP 40. After measuring solid and pore volume, porosity is calculated with the following equations.

$$\text{Porosity} = \text{Pore Volume} / \text{Bulk Volume} \tag{3.2}$$

$$\text{Pore Volume} = \text{Bulk Volume} - \text{Solid Volume} \tag{3.3}$$

$$\text{Porosity} = (\text{Bulk Volume} - \text{Solid Volume}) / \text{Bulk Volume} \tag{3.4}$$

3.2.5. Permeability

After measuring porosity, same specimens are used for permeability analyses. Steady State Gas Permeameter (GasPerm) in TPAO is used from Vinci Technologies for determining air permeability of hardened cement pastes as shown in Figure 3-8. Due to the low permeability of hardened cement pastes, air permeameter is preferred rather than water to measure the permeability.

Figure 3-8 Steady state gas permeameter

This instrument is designed for determination of permeability at steady state (constant pressure and flow through the sample) conditions. The calculation of permeability is derived from Darcy's law which is for liquids. Under steady state conditions of viscous or laminar flow may be expressed as;

$$k = \frac{\mu Q L}{A \triangle P} \tag{3.5}$$

where;

k: liquid permeability (Darcy)

μ: viscosity of saturating liquid (Cp)

Q: liquid flow rate (ml/s)

A: cross sectional area of cylinder (cm^2)

ΔP: pressure differential across cylinder (atm)

3.2.6. Mercury Intrusion

The remaining parts after coring of cubic specimens at 28-days are used for mercury intrusion analysis. The samples are dehydrated in the temperature-controlled oven at 80 ºC for 2 days. The aim of mercury intrusion analysis in this study is primarily to estimate permeability and secondarily to determine pore size distribution of hardened cement pastes. AutoPore IV 9520 from Micromeritics in TPAO is used for mercury intrusion analysis as shown in Figure 3-9. The pressure required to intrude mercury into the sample's pores is inversely proportional to the size of the pores. This is called mercury porosimetry, or often, "mercury intrusion." In addition, adsorption, permeability, total pore volume, total surface area and median pore diameter can be estimated. The AutoPore IV 9520 can determine the pore size diameters from 0.003 to 360 μm.

Figure 3-9 Micromeritics Autopore IV 9520

Washburn derived an equation for describing the equilibrium of the internal and external forces on the liquid-solid-vapor system. He states that the pressure required to force a non-wetting liquid to enter a capillary of circular cross-section is inversely proportional to the diameter of the capillary and directly proportional to the surface tension of the liquid and the angle of contact with the solid surface. Washburn's equation (Equation 3.6) assumes that the pore or capillary is cylindrical and the opening is circular in cross-section. The net force tends to resist entry of the mercury into the pore and this force is applied along the line of contact of the mercury, solid, and (mercury) vapor. The component of force is pushing the mercury out of the capillary acts in the direction cosθ (see Figure 3-10) and balancing the intrusion and extrusion forces results in the Washburn equation, i.e. Equation 3.6.

$$D = -4\gamma \cos\theta / P \qquad (3.6)$$

where;

D: diameter of pore
γ : the surface tension
θ: liquid-solid contact angle
P: external pressure

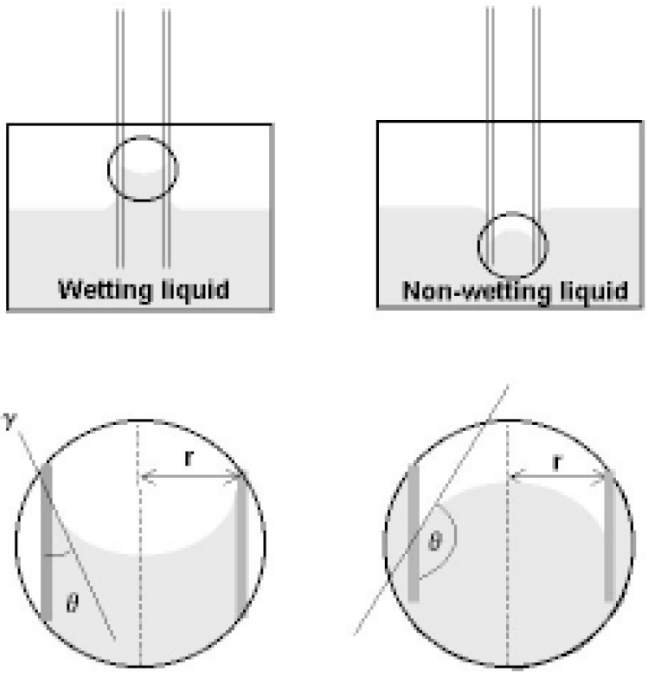

Figure 3-10 Capillary action of a wetting and non-wetting liquid relative to the walls of a capillary (Webb, 2001)

Katz and Thompson introduced two expressions for calculating absolute permeability (k) using data from a single mercury injection capillary pressure curve. Equations for calculating permeability are: (Katz and Thompson, 1986; Katz and Thompson, 1987).

$$k = 1/226\ (L_c)^2\ \sigma/\sigma_o \tag{3.7}$$

$$k = (1/89)(L_{max})^2(L_{max}/L_c)\text{Ø}S(L_{max}) \tag{3.8}$$

where;

k	is permeability (mD)
L_c	is characteristic length
σ/σ_o	is conductivity formation factor (conductance ratio)
L_{max}	is length (pore size) at which hydraulic conductance is maximum
Ø	is total porosity

The first provided rigorous results by incorporating the measured conductivity formation factor (conductance ratio) σ/σ_o as a parameter. Mercury porosimetry data are used to determine the characteristic length L_c of the pore space. The second equation provides an estimation of σ/σ_o to be obtained from the same mercury intrusion data as were used to determine k. This equation, in addition to L_c, requires the value of the length (pore size) at which hydraulic conductance is maximum (L_{max}), and the fraction of total porosity Ø filled at L_{max} (Webb, 2001).

3.2.7. Ultrasonic Cement Analyzer

Ultrasonic cement analyzer (UCA) from Chandler Engineering with model 4262 in TPAO is used for testing specimens, shown in Figure 3-11. UCA measures the transit time (second/meter) of ultrasonic waves through the cement slurry sample. It is a non-destructive test method and simulates the wellbore conditions of temperature and pressure.

Figure 3-11 Ultrasonic cement analyzer

The UCA indeed measures directly compressibility of samples, but estimation is developed and correlated with compressive strength (Nelson, 1990). The freshly mixed cement slurries are put into slurry cup and investigated for 24 hours at 20.7 MPa. The curing temperature gradually reaches to 80 ºC at 240 minutes. The transit time of the ultrasonic waves through the cement pastes is used to calculate the velocity of the ultrasonic waves. Knowing the velocity of the ultrasonic waves, approximate elastic modulus can be calculated by using following equation (Krautkramer and Krautkramer, 1983)

$$E = V^2 \cdot \rho \tag{3.9}$$

where;

E: elastic modulus, GPa

V: velocity, meter/sec,

P: density, kg/m^3

3.2.8. Ultrasonic Velocity

After measuring permeability of the core specimens, they are used for ultrasonic velocity measurements. Further, ultrasonic velocity measurements are used for calculating elastic module and shear module of the hardened cement pastes. The core specimens that are cured at 28-days cannot be measured due to the unavailability. The Sonicviewer SX from OYO is TPAO as shown in Figure 3-12 is used for velocity measurements of hardened cement pastes. Pulse velocity (V_p) and shear velocity (V_s) can be determined by P and S wave propagation.

Figure 3-12 Sonicviewer SX

The primary and shear wave velocity (V_p and V_s) are used to calculate dynamic elastic constants with the standard equations specified in ASTM D2845 are presented in 3.10, 3.11 and 3.12.

$$E = \frac{[\rho \cdot V_s^2 \cdot (3V_p^2 - 4V_s^2)]}{(V_p^2 - V_s^2)} \tag{3.10}$$

$$G = \rho \cdot V_s^2 \tag{3.11}$$

$$V = \frac{(V_p^2 - 2V_s^2)}{2(V_p^2 - V_s^2)} \tag{3.12}$$

where;

E: elastic modulus, GPa

G: shear modulus, GPa

V: Poisson's ratio

ρ: density, kg/m^3

V_p: pulse wave velocity, m/s

V_s: shear wave velocity, m/s

3.2.9. Core Scanner

Core plug images are taken by DMT CoreScan II from Vindum engineering from TPAO as shown in Figure 3-13. Highly accurate core images and quantitative fracture analysis are investigated with this instrument. It is based on a high resolution (up to 40 pixel/mm) digital acquisition system with the orientation of various bedding features. 20 pixel/mm resolution is supplied enough details of images for investigating the micro fractures of core plugs.

Figure 3-13 DMT Corescan II

3.2.10. XRD Analysis

X-Ray Diffraction (XRD) system from Rigaku D/Max-2200 Ultimate^{+}/PC in TPAO (see in Figure 3-14) is used to reveal the crystal structure and mineral composition of hardened cement pastes. Copper spectrum (with a wavelength of 1.54 angstrom) is used to make diffraction pattern. The remaining parts of the 28-day aged specimens are dehydrated in temperature-controlled oven at 80 ºC for XRD analysis. The samples used in the analysis are powdered to become representative sample. Powdered sample is then sieved with 0.062 mm mesh having the ASTM number of 230. X-ray diffractograms are evaluated in Jade-7.0 software with control of PC directly linked to diffractometer by using the Inorganic Crystal Structure Database (ICSD) of International Center for Diffraction Data (ICDD).

3.2.11. SEM Analysis

The specimens that cured at 80 ºC for 28-days are dehydrated in temperature-controlled oven at 80 ºC for SEM analysis. Scanning Electron Microscope (SEM) system from Jeol with Model JSM-6490LV in TPAO (see in Figure 3-14) is used in high vacuum mode to investigate micro morphology of hardened cement paste. The samples first dried (2 hours at 60 ºC) prior to analysis and coated with gold using Polaran E5100 Serie-II.

Figure 3-14 Left to right SEM and XRD instrument

3.3. Determination of Outliers

In a set of measurements, one or more of the values may differ considerably from the majority. In this situation, rejecting the suspected values, also characterized as outliers, recovers the overall precision of results. The Dixon's Q-Test is a simple method used for eliminating outliers even with three values with the formula is shown in the following equation.

$$Q = \frac{\text{gap}}{\text{range}} \tag{3.13}$$

where;

gap: absolute difference between outlier and the closest number to it

range: difference between maximum and minimum values

As seen in Table 3-7, there are three Q_{crit} values with different confidence levels (CL). Commonly CL taken as 95% for eliminating outliers and Q_{crit} will be 0.970 for CL 95%. If the calculated Q for suspected value is greater than 0.970, the value will be rejected (Fajgelj and Ambrus, 2000).

Table 3-7 Critical values for Dixon (Q) Test (Dixon and Massey, 1957)

N	Q_{crit} (CL:90%)	Q_{crit} (CL:95%)	Q_{crit} (CL:99%)
3	0.941	0.97	0.994
4	0.765	0.829	0.926
5	0.642	0.71	0.821
6	0.56	0.615	0.74
7	0.507	0.568	0.68
8	0.468	0.526	0.634
9	0.437	0.493	0.598
10	0.412	0.466	0.568

CHAPTER 4

RESULTS AND DISCUSSION

4.1. Characterization of Materials

CEM I type cement used in this study has a clinker with a high C_3S content (65.64 %) and a low C_2S content (3.71 %). In general C_3S promotes early hydration while C_2S later hydration (Bogue, 1949). Therefore, early strength of cement pastes expected to be higher as a result of improved early hydration. The specific surface area (fineness) of CEM I is 4300 cm^2/gr. An increase in the fineness of cement commonly increases hydration rate and also improves strength development of cement pastes with same w/c ratio. Another important factor that influences hydration is C_3A amount. The C_3A content of the CEM I is 6.05 % which can be considered as low for OPC. The amount of C_3A for medium sulfate resistant (MSR) cement type is limited to 8 percent according to ASTM C150.

The API Class G cement used in this study has a clinker with a high C_3S content (64.23 %) and a low C_2S content (5.15 %) similar to CEM I. The fineness of the sample is 3220 cm^2/gr which is lower than that of CEM I. The coarsely ground API Class G cement allows reducing hydration rate and delays setting time. The C_3A content of the Class G cement is 2.75% and considered in HSR grade. The limited amount C_3A also promotes to slow down the hydration rate of cement.

The GGBFS used in this study has an activity index of 73, even lower than that of Grade 80 according to ASTM C989. At ambient temperatures, early compressive strength of hardened cement pastes containing any grades of GGBFS (Grade-80, Grade-100 and Grade-120) is expected to be lower than that of reference hardened cement paste. On the other hand, at later ages, grade 120 increases strength, while grade 80 decreases and grade-100 shows equal or greater in strength (Hogan and Meusel, 1981; ACI 233). Therefore, the manufacturer increased fineness of the GGBFS to improve reactivity of slag and compensate for the strength losses. However, Olorunsogo (1998) introduces another idea that particle size distribution of GGBFS has little or negligible effect on strength development of cement pastes (Olorunsogo, 1998).

CEM I is more reactive than API Class G cement due to its chemical composition and fineness. On the other hand, hydration rate of GGBFS is slower than both cement types. The resulting hydration rate of GGBFS and CEM I blends will be mean of them according to their ratios in the blend. Investigations show that in the GGBFS blended cement pastes by using the clinkers with low C_3A content, strength contribution of the GGBFS clearly increases with an increasing alite content of the clinker (Muller, 2007). From the point of view of oil well cementing, rapid hydration rate is not desirable for oil well cements to provide chemical and physical stability of both fresh and hardened cement paste at high temperatures.

4.2. Free Fluid Content

The maximum allowed amount of free fluid designated in API Specification 10A is 5.9 percent by volume. All slurry compositions are appropriate for oil well cement as shown in Table 4-1. However, lower amount of free water content is desirable for various operations in oil well cementing.

Table 4-1 Free Fluid content of cement pastes

Cement Slurries	G	S20	S40	S60	S80
Specific Gravity	1.92	1.89	1.87	1.85	1.83
Recorded mass, g	766.2	756.3	750.3	740.1	733.4
Volume of measured FF, cc	3.7	5.9	7.0	4.5	2.5
Free fluid content, %	**0.94**	**1.48**	**1.75**	**1.13**	**0.62**

According to the report of ACI 233, bleeding capacity of cement slurry is mostly affected by the ratio of the specific surface area of solids to the unit volume of water. Therefore the average specific surface area and amount of residue on 45 μ sieve of cement blends are presented in the Table 4-2.

Table 4-2 Fineness and residue on 45μ sieves of cement blends

Cement blends	G	S20	S40	S60	S80
Residue 45 μ, %	11.6	3.8	3.0	2.1	1.3
Specific surface, cm^2/g	3215	4510	4720	4935	5150

According to Table 4.2, it is clear that free water amount decreases by increasing GGBFS amount in GGBFS blended cement pastes. However, various studies showed that bleeding amount of the cement slurries increases with the intrusion of GGBFS with similar specific surface areas (Wainwright and Ait-Aider, 1995). Little water absorbed during early hydration period due to its smooth and dense surface in structure (Wood, 1981). On the other hand, an increase in the specific surface area (fineness) of GGBFS increases water absorption and tends to reduce bleeding. Therefore, the reduction of free fluid content can be explained by specific surface area of the blends. The fineness of the GGBFS used in the experiments was higher than thought to be in general and thus water adsorption is increased. The fineness of GGBFS used in the experiments is 536 m^2/kg, some other GGBFS from different

countries are; United Kingdom in the range of 375-425 m^2/kg; United States in the range of 450-550 m^2/kg and in Canada about 450 m^2/kg (Pal et al, 2003).

As the GGBFS amount increases in the blend average fineness increases and thus results in a reduction of free fluid content as shown in Figure 4-1. For comparison, API Class G cement is removed on that figure to observe the influence of GGBFS on the free fluid content of cement pastes. S40 has higher free fluid content than S20, in addition, G has unreasonably low free fluid regarding to its low specific surface area. This may be explained by chemical composition or particle size distribution (PSD) of solid particles in slurry which remains out of this study. Best fitting of PSD of cement blends increases the settlement potential of the particles (Olorunsogo and Wainwright, 1998). Another idea introduced by Siddique and Khan that the bleeding property of GGBFS is generally affected by its physical properties (fineness and particle morphology) and chemical properties of GGBFS have negligible or little effect on bleeding (Siddique and Khan, 2011).

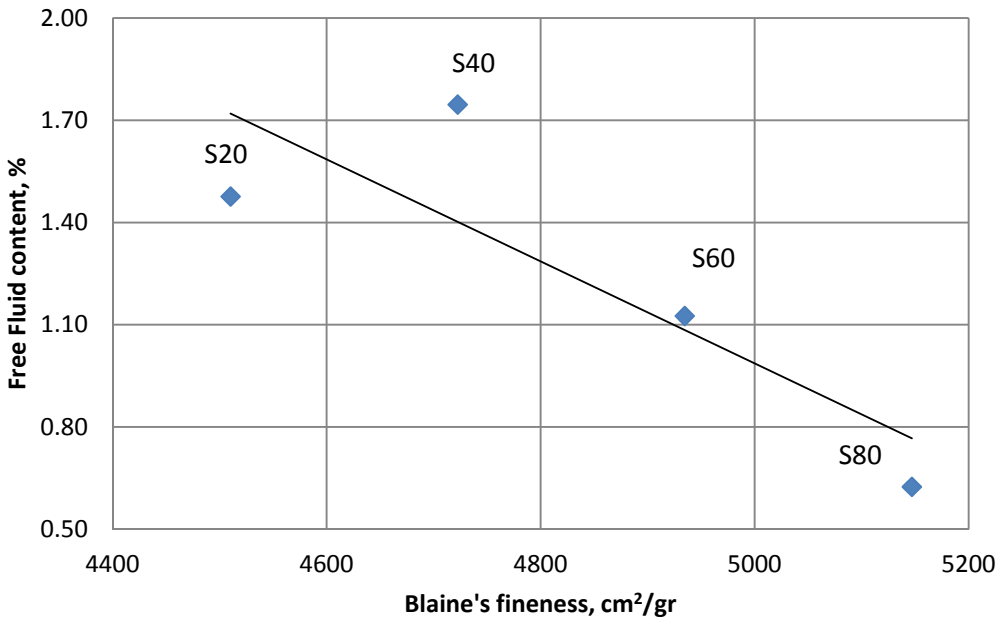

Figure 4-1 Free fluid content vs. fineness of the GGBFS blended cement pastes

The influence of GGBFS on bleeding of cement pastes is also investigated by Wainwright and Rey (2000). According to his studies, addition of 55 percent of GGBFS to the plain OPC increases bleeding of the cement paste while 85 percent of GGBFS addition has no significant effect on bleeding. Another study showed that there is not an exact relationship between PSD with bleeding of cement paste at the same w/c (Wainwright and Ait-Aider, 1995).

The reduced bleeding potential of GGBFS in cement paste is also explained by hydration mechanism of slag blended cement. The early hydration products of cement slurry help to block upward water passage to the surface. The GGBFS desires alkaline rich environment for hydration and reduces early hydration products and thus allows passage of free fluid (Hwang and Lin, 1986).

4.3. Compressive Strength

Compressive strength of GGBFS included hardened cement pastes can vary over a wide range. It is highly dependent on temperature; even 10° C increase in curing temperature accelerates strength development especially at early periods. It is more significant at higher levels of GGBFS replacement in the paste (Barnett et al, 2006). In most of the oil wells, cement slurries are exposed to high temperatures and in this study temperature is kept as 80 °C for curing cement pastes to represent “medium” range oil wells.

Table 4-3 shows the results of the compressive strength analysis of hardened cement pastes at ages of 1-day, 7-days and 28-days cured at 80 °C. In order to draw a more meaningful conclusion from the experimental data, the outliers are eliminated by using Dixon Q test with a confidence level of 95%.

Table 4-3 Compressive strength of the hardened cement pastes

Cement pastes	G	S20	S40	S60	S80
Compressive strength at 1-day					
#1	42.2	38.5	42.0	37.1*	22.9
#2	42.3	42.6	42.2	39.6	22.9
#3	44.8	44.0	48.1*	39.6	22.9
Mean	**43.1**	**41.7**	**42.1**	**39.6**	**22.9**
Compressive strength at 7-days					
#1	39.6	39.3	40.6	32.2*	23.8
#2	42.7	42.0	41.7	41.4	25.6
#3	50.6	43.5	42.1	41.6	27.5
Mean	**44.3**	**41.6**	**41.5**	**41.5**	**25.6**
Compressive strength at 28-days					
#1	43.4	45.5	42.5*	42.9	33.6
#2	48.5	47.3	51.9	43.2	33.6
#3	50.9	51.7	52.1	46.1	38.6*
Mean	**47.6**	**48.2**	**52.0**	**44.1**	**33.6**

*Shows the outliers

According to Table 4-3, most of the hydration of G has been achieved in the first day and relatively lower strength gain is observed at later ages. This can be explained by its high C_3S and low C_2S content. C_3S completes most of its hydration at 1-day and limited amount of C_2S hydrates further (Hooton and Bhadkamkar, 2005). The compressive strength of S20 is lower than G at 1-day whereas it is higher at 28-days. S40 with GGBFS content of 40 percent shows better compressive strength than other pastes at 28-days. Similar to these results, highest compressive strength is obtained with pastes containing 40-50 percent of GGBFS at 28-days (Fulton, 1974; Hogan and Meusel, 1981; Meusel and Rose, 1983).

The amount of GGBFS in S60 is 60 percent and shows relatively comparable results with G at all ages. However, expected compressive strength of S60 will be higher than G at longer ages. S80 contains highest amount of GGBFS and shows the lowest compressive strength at all ages. Its compressive strength at 1-day is even incomparable, nearly less than 50 percent of other cement pastes. This can be

explained by insufficient alkalinity provided by the hydration of limited amount of cement in the paste.

The vast majority of hydration of the pastes prepared with OPC without any supplementary material commonly achieved in 28-days at ambient temperatures; however GGBFS continues to gain strength at later ages. The increase of compressive strength in concretes made with GGBFS has been reported even after 20 years (Wood, 1992). Therefore, an increase of GGBFS content in the blend may result in an increase of the strength at later ages (28-days) as seen in Figure 4-2.

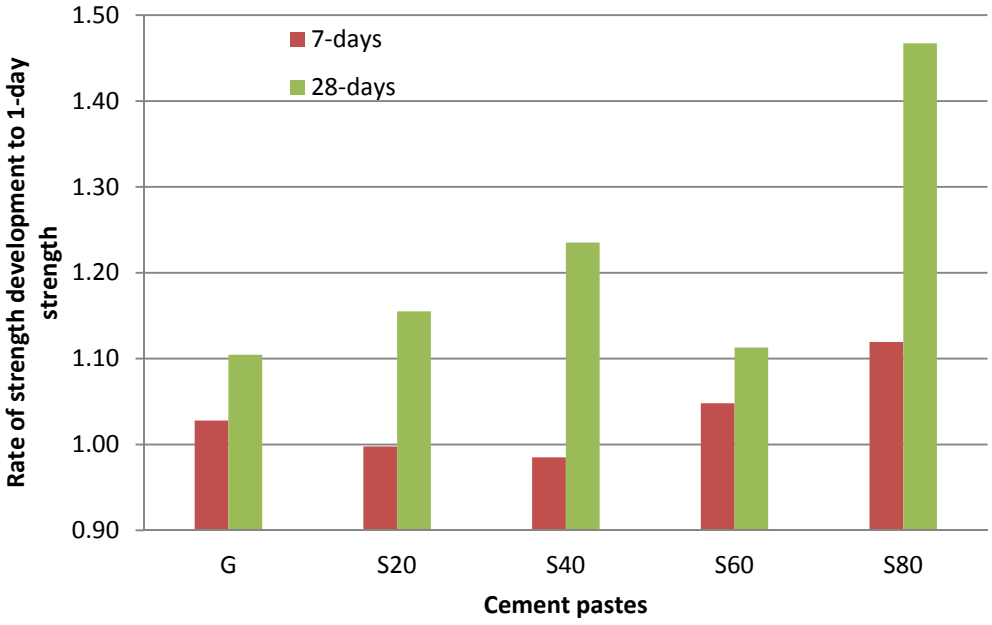

Figure 4-2 Rate of strength development of the hardened cement pastes

C/S molar ratio can be used to evaluate the compressive strength of cement pastes. The C/S molar ratio of C-S-H gel varies between 1.5 and 2.0 (Mehta, 2006) and generally acceptable values are 1.7 and 1.8 (Odler, 2004; Taylor, 1997). Moreover, Mg^{2+} can also be treated in the same manner with Ca^{2+}, and therefore ratio of C/S and (C+M)/S ratios of cement blends are illustrated in Table 4-4.

Table 4-4 C/S molar ratio of cement blends

Cement pastes	G	S20	S40	S60	S80
C/S	3.49	2.64	1.97	1.49	1.12
(C+M)/S	3.57	2.79	2.15	1.68	1.32

According to Table 4-4, C/S ratio of S40 is 1.97, closest to the molar ratio of C-S-H gel, and has the highest compressive strength among all pastes at 28-days. In S40 optimum amount of lime is provided by hydration of CEM I while Si is available in the GGBFS to form secondary C-S-H. Relatively low compressive strength of S80 can also be explained with this manner. The insufficient alkalinity released from the hydration of limited amount of CEM I slowdown further hydration.

Ultrasonic cement analyzer (UCA) is a relatively recent development used for estimating compressive strength of the cement pastes through a period of time. The UCA indeed measures the compressibility of samples, but estimation was developed and correlated with compressive strength (Nelson, 1990). The cement pastes are investigated for 24 hours at a temperature of 80 ˚C and illustrated in Figure 4-3.

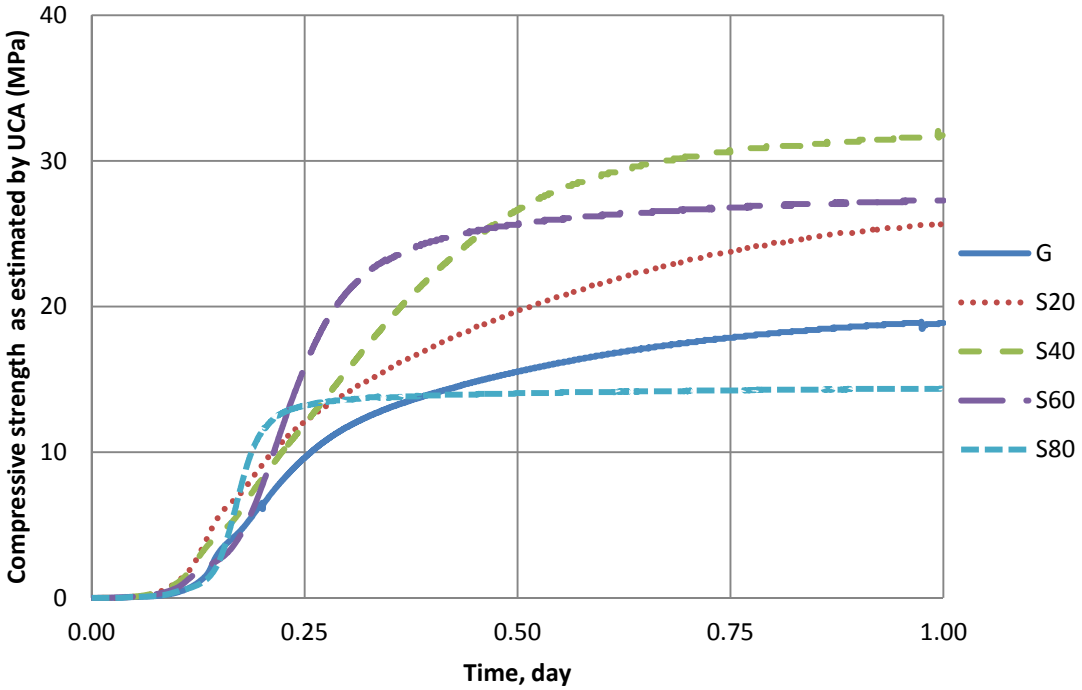

Figure 4-3 Time dependant compressive strength of the hardened cement pastes measured by UCA

According to Figure 4-3, compressive strength of the pastes obtained from UCA shows relatively low values when compared with the destructive method. On the other hand, the order of the compressive strength of the slag blended cements show relatively comparable outcomes among themselves. For example, the compressive strength of S40 possesses the highest value while S80 has the lowest in both methods of measurements. All graphs of UCA are presented in Appendix A.

The presence of GBBFS in the blend contributes to the compressive strength of hardened cement pastes. Mueller gets similar outcomes at 24-hours with GGBFS-OPC ratio of 40:60. The compressive strength of GGBFS blended cement pastes are higher than reference cement paste at temperatures of 77 ˚C and 93 ˚C at 24-hours, the differences are even higher at 72 hours (Mueller et al, 1995).

4.4. Ultrasonic Analysis

The UCA is used for measuring transit time of ultrasonic wave through freshly mixed cement pastes for 24-hours. The transit time of the ultrasonic waves through cement pastes is used for calculation of ultrasonic velocity and presented in Figure 4-4. The transit time of the ultrasonic waves decreases during setting and hardening of cement paste. Time dependent curves of ultrasonic velocity can be evaluated into three parts. The first part is the dormant period and characterized by a constant low velocity. In the second part, velocity increases rapidly which characterizes C_3S hydration and then it gradually turn to asymptotic curve in the third part (Robeyst et al, 2008). As seen in Figure 4-4, G, S60 and S80 are more asymptotic, while S20 and S40 still continue to increase in the third stage with the hydration of GGBFS.

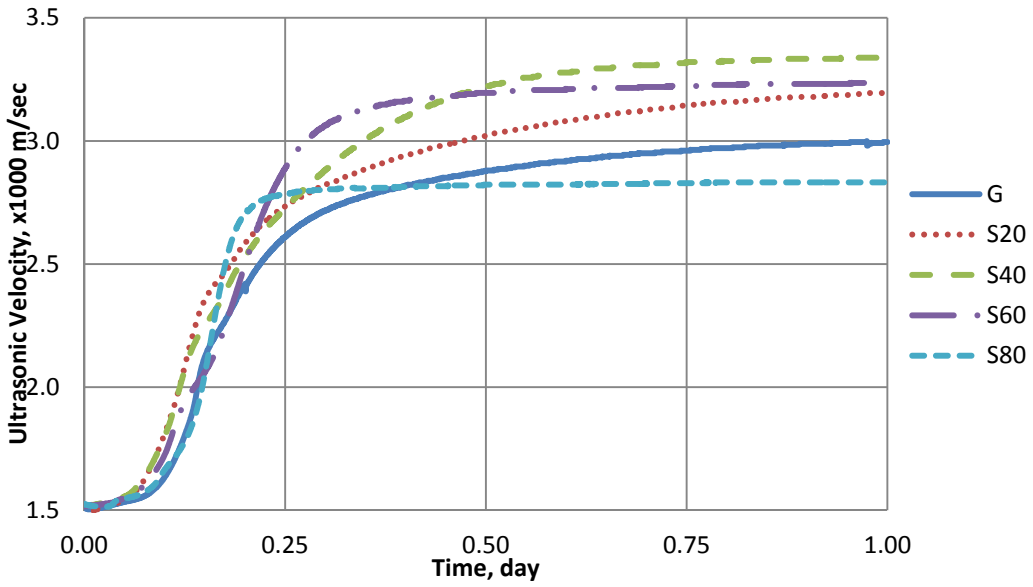

Figure 4-4 Ultrasonic velocity of the cement pastes

Elastic modulus of the cement pastes are calculated by using ultrasonic velocity by using Equation 3.9. The elastic modulus of GGBFS blended cement pastes except for S80 show higher values than G as shown in Figure 4-5. Enhanced hydration of GGBFS at elevated temperatures increases elastic modulus of the pastes. Studies

show that concretes containing slag blended cement has similar outcomes with concretes prepared with neat OPC (Kliger and Isberne, 1967).

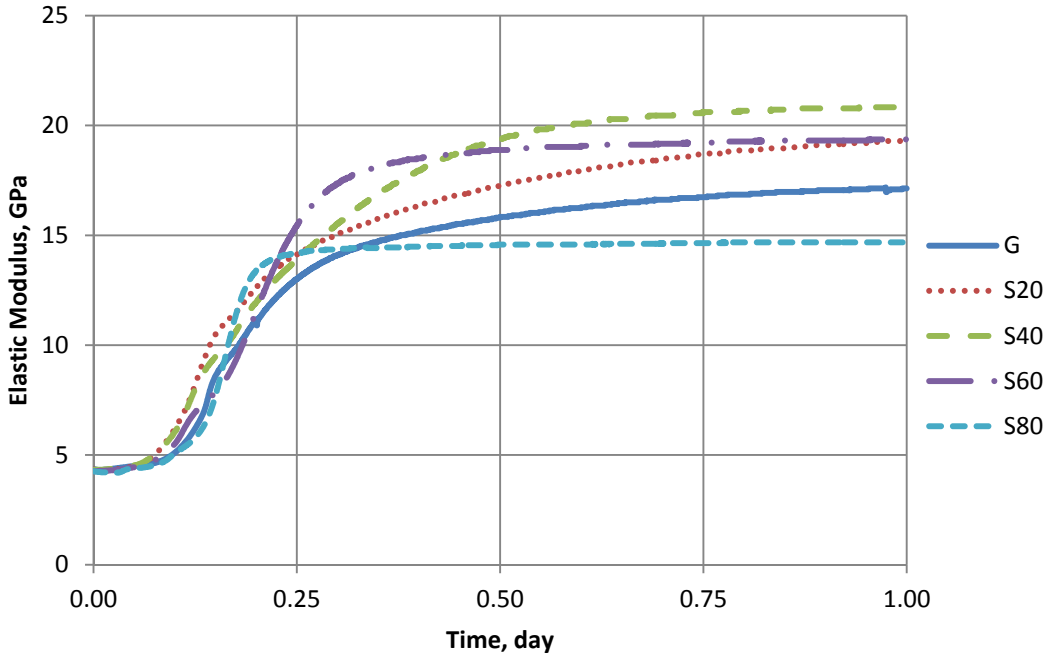

Figure 4-5 Modulus of elasticity of the cement pastes

Sonicviewer SX is used for measuring pulse velocity (V_p) and shear velocity (V_s) of hardened cement pastes on 1-day and 7-days specimens. The experimental data is presented in Table 4-5.

Table 4-5 Primary wave (longitudinal) velocity (V_p) and shear wave velocity (V_s) of hardened cement pastes

	Cement Pastes				
	G	S20	S40	S60	S80
1-day					
V_p	3140	3306	3241	3047	2616
V_s	2494	2249	2166	2337	1700
7-days					
V_p	3239	3483	3473	2809	2188
V_s	2089	2489	2370	1580	1619

The elastic modulus and shear modulus of the core specimens are calculated by using Equations 3.10 and 3.11. The results are presented in Figure 4-6. The amount of GGBFS in the pastes influences elastic modulus and shear modulus of hardened cement pastes as can be seen in Figure 4-6. Lower amounts of GGBFS presence in the paste (S20 and S40) increases elastic modulus while higher amounts of GGBFS (S60 and S80) adversely affects.

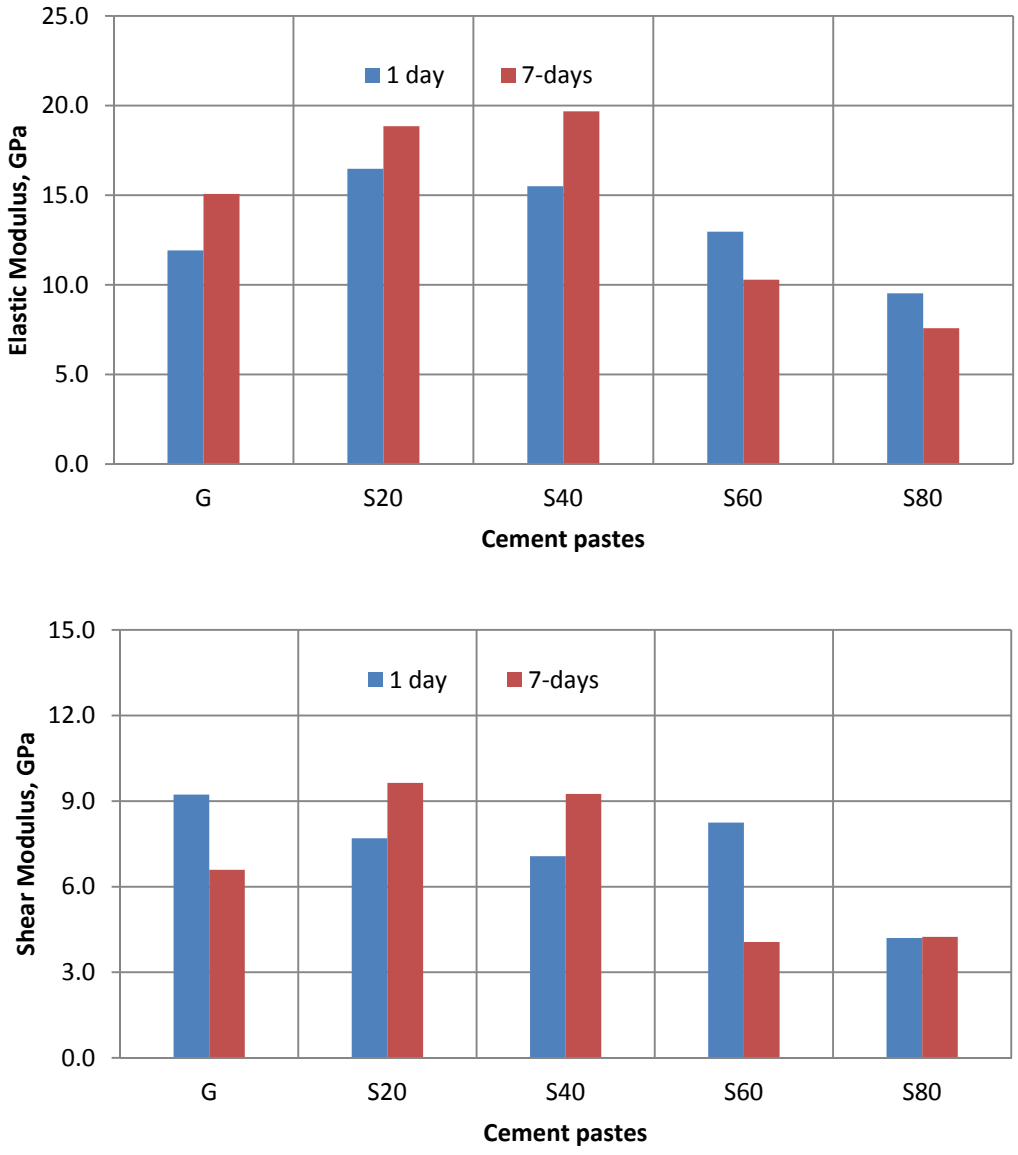

Figure 4-6 Elastic and Shear modulus of the hardened cement pastes

4.5. Porosity and Pore Size Distribution

Porosity of the hardened cement pastes as measured by helium porosimetry is listed in Table 4-6. For each composition of pastes three specimens are prepared to be tested, but during coring some of the specimens cracked and cannot be tested.

Table 4-6 Porosity of the hardened cement pastes

Cement pastes	G	S20	S40	S60	S80
Porosity at 1-day (%)					
#1	38.5	34.5	30.4	21.4	25.5
#2	38.6	34.6	30.4	21.6	27.2
#3	38.3	34.8	30.4	19.8	25.8
Avg	**38.5**	**34.6**	**30.4**	**20.9**	**26.2**
Porosity at 7-days (%)					
#1	37.7	33.7	23.8	13.6	22.0
#2	37.0	-	22.7	13.7	19.4
#3	37.1	33.5	23.7	15.4	19.8
Avg	**37.3**	**33.6**	**23.4**	**14.2**	**20.4**
Porosity at 28-days (%)					
#1	35.0	32.8	16.2	8.1	16.0
#2	35.0	33.7	16.8	-	15.7
#3	34.9	-	-	8.4	15.9
Avg	**35.0**	**33.3**	**16.5**	**8.3**	**15.9**

According to Table 4-6, porosity decreases while hydration advances in all pastes. The porosity of cement pastes at 1-day has comparable outcomes; however, G has highest porosity at all ages. Even, S20 with least GGBFS amount showed lower porosity than G at all ages, however the difference is reasonably comparable. At later ages, GGBFS blended cement pastes show indisputably low porosity than G. It is stated that when slag hydrates in the cement paste the pore sizes become finer and porosity decreases (Uchikawa, 1986).

After an extent amount of CEM I substitution with GGBFS in the paste, porosity decreases considerably. For example, the porosity of S40 at 28-days is less than half of G. The amount of GGBFS content is more than CEM I in the S60 and possesses lowest porosity at all ages. Its porosity is nearly quarter of G and S20, and nearly half of S40 and S80 at 28-days. S80 contains highest GGBFS amount and possesses highest pozzolanic potential; however limited amount of calcium and alkalinity provided by hydration of cement slows down further hydration. Therefore, increase in the porosity of S80 is due to the inadequate hydration of the paste. It is stated that GGBFS inclusion in the cement paste not only reduces porosity but also the pore become finer (Siddique and Khan, 2011). Furthermore, pores in the slag blended cement pastes are more discontinuous and thin-walled (Feldman, 1986). The percentage of porosity reduction of cement pastes at 7-days and 28-days are presented in Figure 4-7.

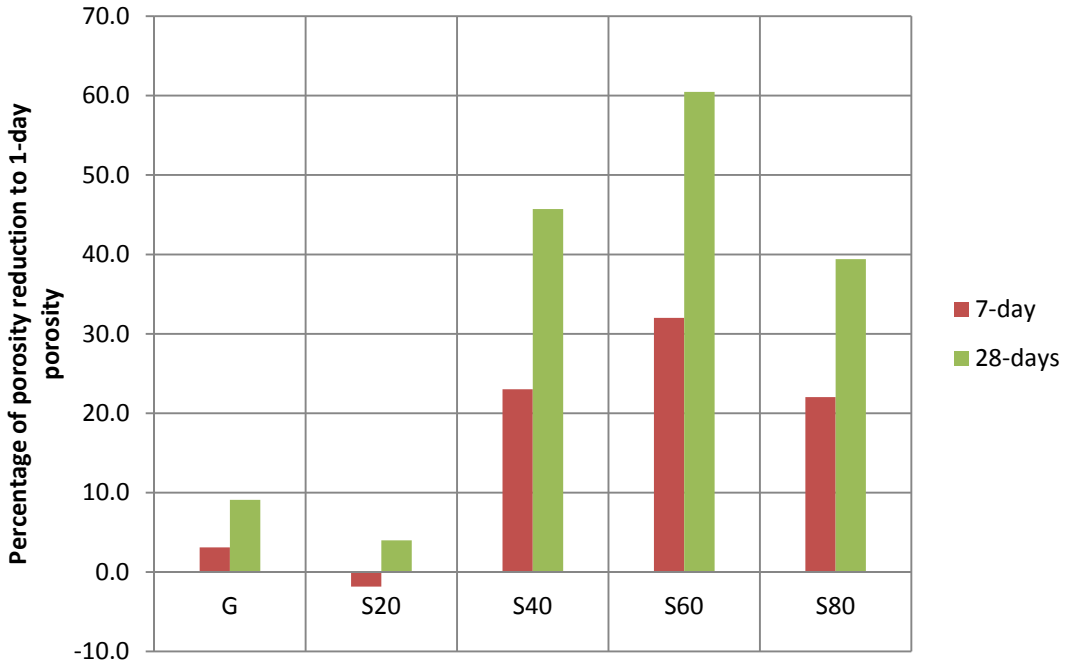

Figure 4-7 Ratio of porosity reduction of the hardened cement pastes

As can be seen in Figure 4-7, the ratio of porosity reduction of G and S20 are least at 7-days and 28-days. Most of the hydration of G is achieved in the first day and limited hydration contributes later. More than 40 % of GGBFS substitution in the paste reduces porosity at 7-days and 28-days. Relatively low hydration rate of GGBFS in the cement paste contributes porosity especially in long-term. The formation of the secondary C-S-H gel in the paste reduces porosity because of pozzolanic reaction between cement and GGBFS. S60 with a GGBFS content of 60 percent distinctively improves porosity. The reduction in porosity is more than 30 percent at 7-days and 60 percent at 28-days. An increase in the replacement of OPC with GGBFS in the pastes decreases porosity to an extent, after an amount of replacement porosity tend to increase as seen in S80.

Studies also show that, as the hydration advances, pores are gradually filled with hydration products of cement such as ettringite, portlandite, fine crystalline C-S-H and others (Pandey and Sharma, 1999). Also limited amount of C_3A and unavailability of ettringite at elevated temperatures adversely affect the porosity in the cement pastes prepared with OPC (Day, 1992). On the other hand, increased hydration rate of GGBFS at elevated temperatures with the contribution of pozzolanic reaction favors reduction of porosity in the matrix of hardened cement paste. Also inhomogeneous distribution of C-S-H at high temperatures results in coarser pore structure in cement pastes prepared with OPC (Lothenbach et al, 2008).

In order to determine pore size distribution of cement pastes mercury porosimeter is used. The pressure required to intrude mercury into sample's pores is inversely proportional to the size of the pores. Therefore pore size distribution can be estimated by knowing the intrusion amount of mercury with pressure. Pore size distribution of the hardened cement pastes and porosity vs. pore sizes are presented in the Figure 4-8 and Figure 4-9 respectively.

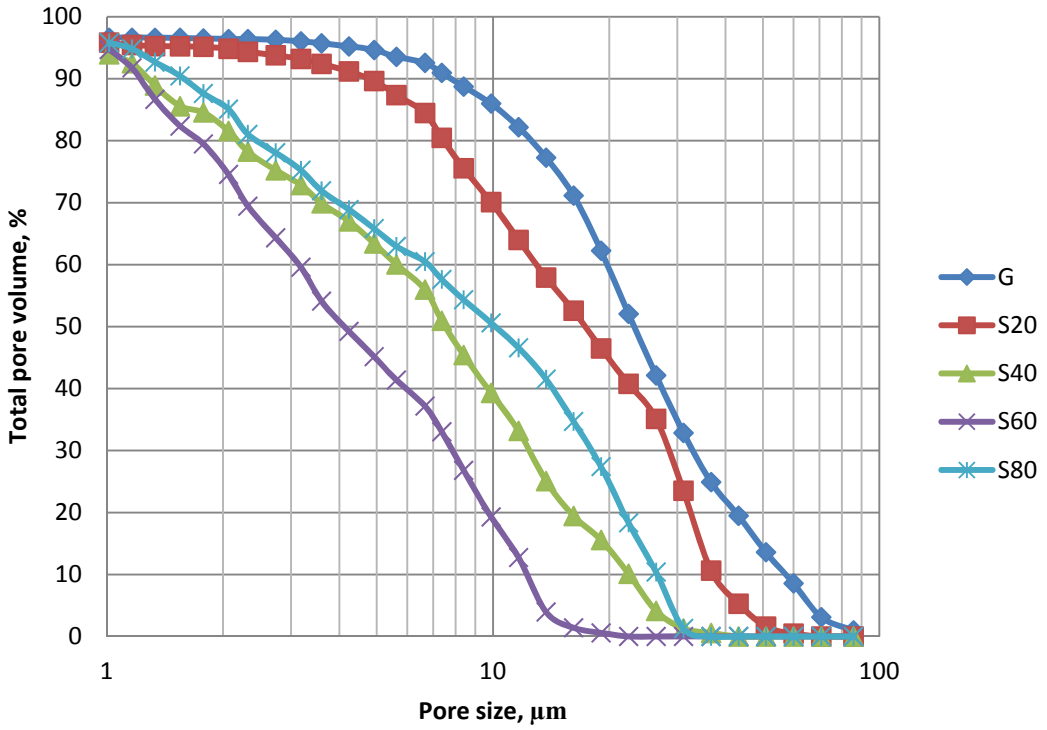

Figure 4-8 Pore size distribution of the cement pastes

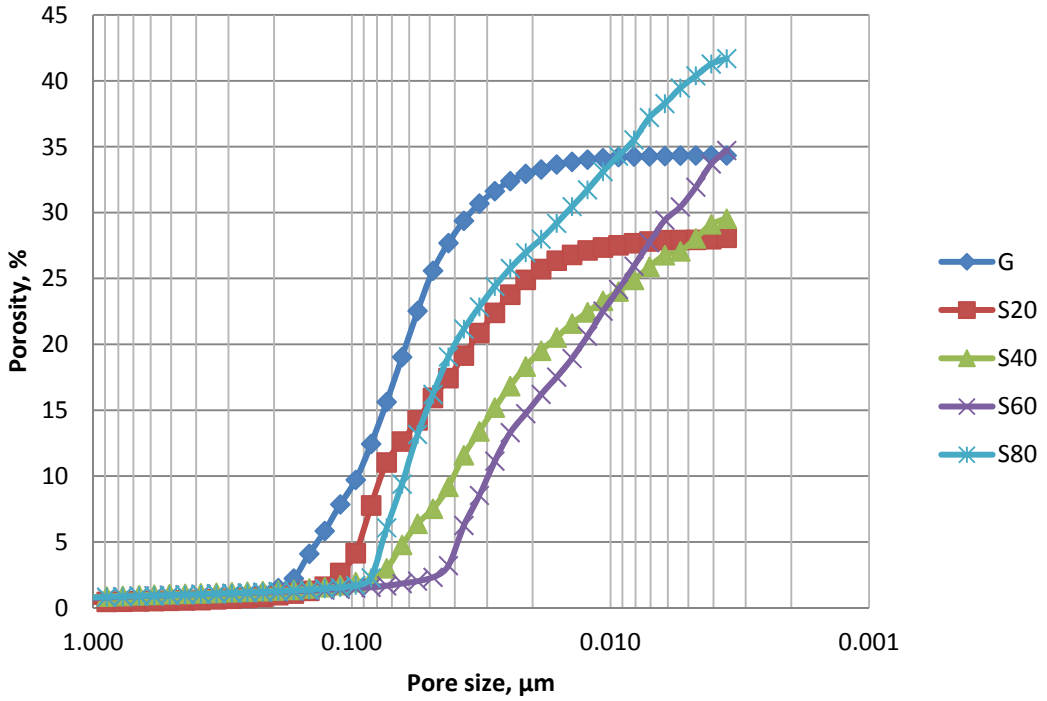

Figure 4-9 Total pore volume of the cement pastes at specified pore sizes

According to Figure 4-8 and Figure 4-9, presence of GGBFS in the cement paste not only reduces porosity but also the pores become finer as mentioned in Section 4.6. The pore sizes of both hardened cement pastes are in the range of 1 μm to 100 μm. More than 50 percent of the total pores of S40 and S60 are smaller than 10 μm, while G and S20 have pore sizes higher than 10 μm. In addition, more than 80 percent of total pores of S60 are lower than 10 μm which contributes to the reduction of permeability in the hardened cement pastes. The graphs of mercury saturation vs. pressure of cement pastes are given in Appendix C.

4.6. Density

Solid density and bulk density of the hardened cement pastes are measured by helium porosimeter and results are listed in Table 4-7.

Table 4-7 Solid and bulk density of the hardened cement pastes

Cement pastes	G	S20	S40	S60	S80
Solid Density, g/cm^2					
1 day	2.41	2.32	2.16	1.88	1.97
7 day	2.41	2.35	2.15	1.89	2.02
28 day	2.39	2.33	2.00	1.83	1.93
Bulk Density, g/cm^2					
1 day	1.49	1.52	1.51	1.51	1.45
7 day	1.51	1.56	1.65	1.62	1.61
28 day	1.55	1.56	1.69	1.68	1.62

According to Table 4-7, little or negligible changes are observed on G both in bulk and solid density while hydration advances. On the other hand, results show that GGBFS inclusion in the blends reduces solid density while increases bulk density. The decrease in the solid density is due to the decreased pore volume in the pastes.

The pores in the matrix of cement paste are filled with products of pozzolanic reaction between GGBFS and alkalis or calcium hydroxide released from hydration of cement (ACI 233). An increase in the pore volume increases solid density and conversely decreases bulk density. The more GGBFS used in the blends, the more bulk density and the less solid density is. However, after an amount of GGBFS in the paste, pore volume increases as can be seen in S80.

4.7. Permeability

Steady State Gas Permeameter is used for measuring air permeability of hardened cement pastes. The specimens that are used in helium porosimeter are also used in this analysis and results are listed in Table 4-8. The permeability of some specimens cannot be measured due to the cracks and remained blank in the table.

Table 4-8 Air permeability of the hardened cement pastes

Cement pastes	G	S20	S40	S60	S80
Permeability at 1-day (mD)					
#1	0.058	0.061	0.179	0.412	0.381
#2	0.059	0.050	0.310	0.611	0.559
#3	0.054	0.051	0.495	0.762	0.622
Avg	**0.057**	**0.054**	**0.328**	**0.595**	**0.521**
Permeability at 7-days (mD)					
#1	0.043	0.050	2.078	3.625	-
#2	0.041	0.051	2.005	1.964	1.302
#3	0.044	0.057	1.849	-	1.870
Avg	**0.043**	**0.053**	**1.977**	**2.795**	**1.586**
Permeability at 28-days (mD)					
#1	0.057	0.143	2.770	6.900	0.625
#2	0.057	0.093	2.310	-	0.455
#3	0.051	0.120	-	2.800	0.824
Avg	**0.055**	**0.119**	**2.540**	**4.850**	**0.635**

According to Table 4-8, G has the lowest permeability at all ages. Its permeability is steady, little or negligible changes observed while hydration advances. S20 has the lowest permeability among GGBFS blended cement pastes and shows reasonably comparable outcomes with G up to 28-days. The remaining GGBFS blended cement pastes; S40, S60 and S80 have quite higher permeability than G in spite of their lower porosity values. On the contrary, various studies show that permeability of the hardened cement pastes containing GGBFS noticeably reduce permeability compared with hardened cement pastes not containing GGBFS (Hooton and Emery, 1990; Rose, 1987). Pores in hardened cement pastes containing CH turn to C-S-H and fill the pores with pozzolanic reaction (Bakker, 1980; Mehta, 1980; Roy and Idorn, 1983).

To sum up, all slag-blended hardened cement pastes seem to have greater permeability than cement paste that does not contain GGBFS. The unreasonably high permeability of pastes is caused by cracks formed within the hardened cement pastes. The more GGBFS used in the blend makes the hardened cement paste becomes more brittle. Hardened cement pastes are exposed to mechanical stresses during sample preparation before testing, primarily during coring and secondarily thermal changes on the cement pastes or both of them. These stresses may probably cause mechanical deformation on the hardened cement paste and thus cracks are formed. These cracks are inversely proportional to the porosity of the pastes. For example, G and S20 have the highest porosity and almost no cracks observed while S40 and S60 have lower porosity and exposed to more severe cracks.

Core scanner used for investigation of cracks in the core samples. One of the specimens used for measuring porosity and permeability analysis is examined for core scanning. The images of the core specimens analyzed by a high resolution (20 pixel/mm) digital acquisition system in order to investigate fractures. Figure 4-10 shows core images of the samples cured at 80 ˚C for 1 day, 7 days, and 28 days. More detailed images are illustrated in Figure 4-11 to reveal the fractures in the cement pastes. They were signed in red color to be shown more clearly.

a) 1-day of cured specimens

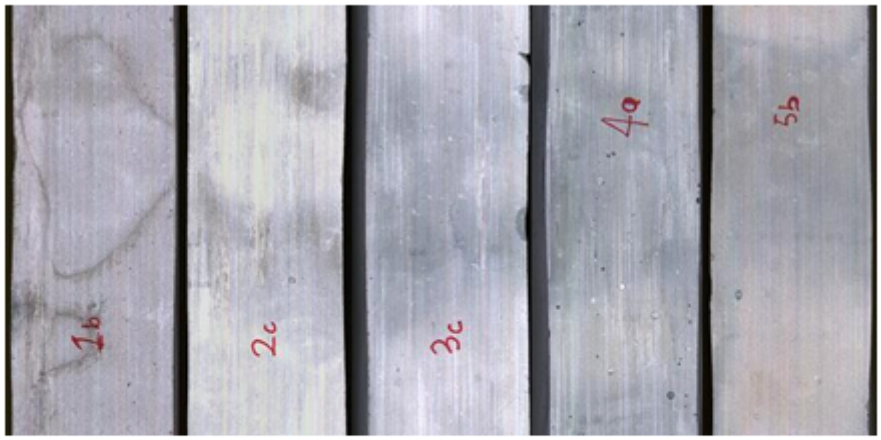

b) 7-days of cured specimens

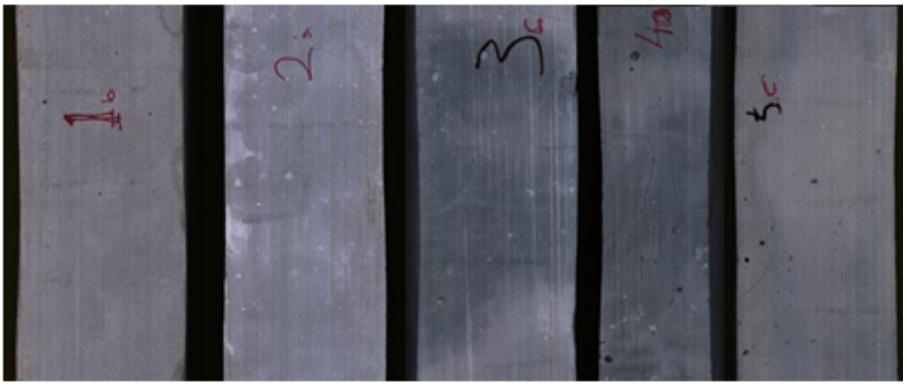

c) 28-days of specimens

Figure 4-10 Images of 1-day, 7-days and 28-days aged core samples, left to right order of the cement pastes are G, S20, S40, S60 and S80.

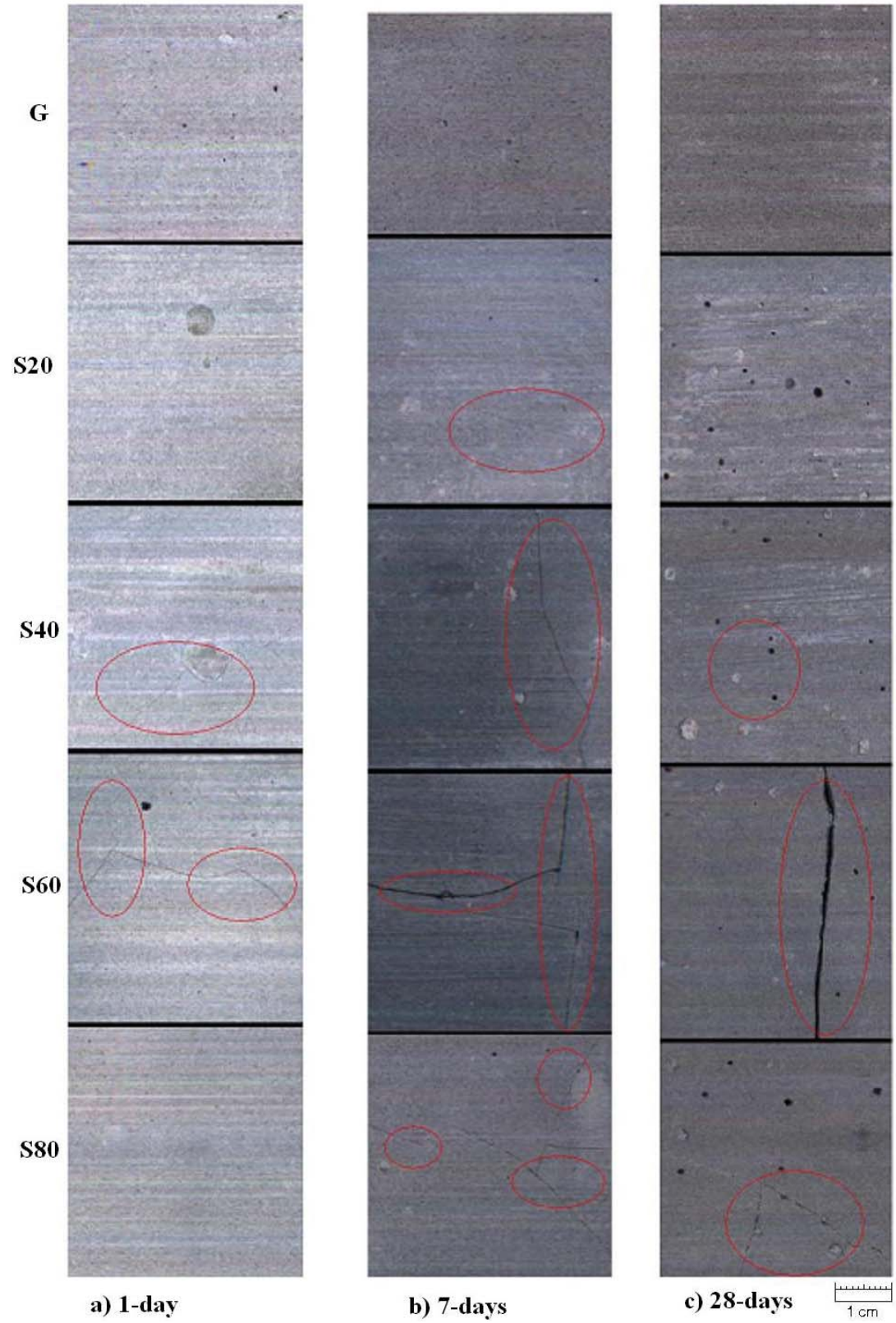

Figure 4-11 Magnified view of the hardened cement pastes, from up to bottom the order of cement pastes are G, S20, S40, S60 and S80.

Mercury intrusion analyzer is also used for measuring permeability of cement pastes. By using mercury intrusion analyzer the effects of cracks on the permeability of the hardened cement pastes is prevented. Permeability is estimated by Katz and Thompson (1986) method as mentioned in Chapter 3 by using the experimental data obtained from the analysis. Estimated permeability and measured threshold pressure of the hardened cement pastes are presented in Figure 4-12.

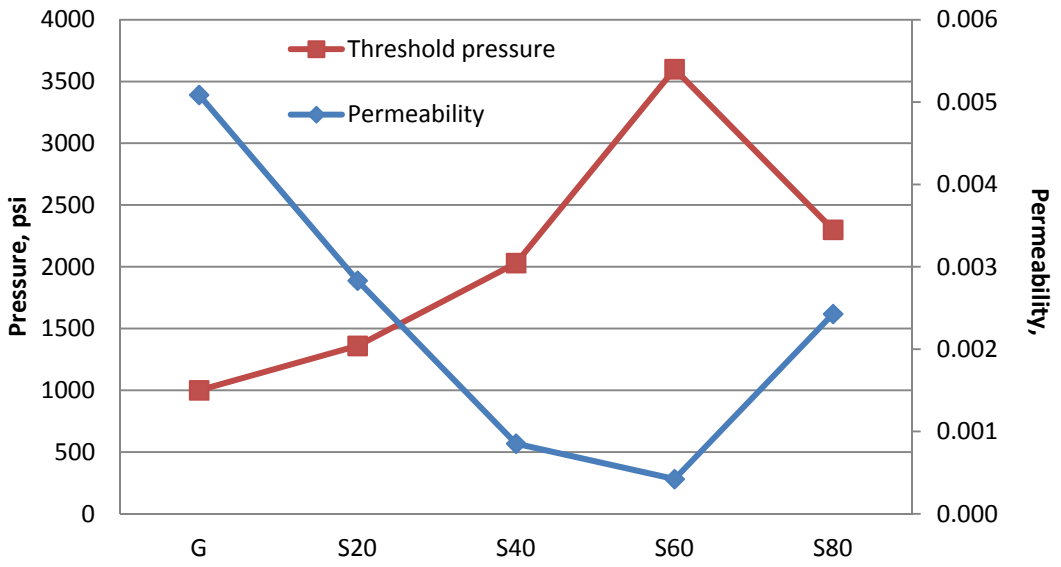

Figure 4-12 Permeability and threshold pressure of the hardened cement pastes

Threshold pressure is the pressure that is required for initial intrusion of mercury into the sample (Webb, 2001). It is inversely proportional to the permeability of cement pastes as shown in Figure 4-12. Both GGBFS blended hardened cement pastes have a threshold pressure higher than G. The permeability of G is nearly more than twice of slag blended cement pastes, even it is more than 10 times of S60 and 5 times of S40. It is also stated that the structure of GGBFS blended cement pastes have different morphology than that of pastes prepared with OPC (Mueller et al, 1995). The structure becomes denser and yields a lower permeability in the paste. The permeability values of cement pastes are also supporting the results of porosity obtained from helium porosimeter. The existence of GGBFS in the hardened cement

paste makes the pore sizes smaller and thus capillary pore pressures become higher. Therefore, permeability of the hardened cement pastes are in the same order with the porosity obtained from helium porosimeter.

4.8. XRD

Figure 4-13 shows XRD patterns of the cement pastes and can be seen in seperately Appendix B. Portlandite crystals can be easily recognized from the figure; however C-S-H phases have incoherent peaks to be understood. Katoite, a hydrogarnet type mineral, is suggested in the analysis. It is a hydration product of C_3A and C_4AF, that is formed directly at hydrothermal conditions (Negro and Stafferi, 1979). Another mineral presented in the graph is brownmillerite, which isa type of anhydrous calcium aluminoferrite. GGBFS blended cement pastes are more amorphous in structure and has more complicated peaks when compared to G. The peak of portlandite crystals decreases with an increasing proportion of GGBFS in the paste.

It is not clear enough to bring out the minerals containing Mg^{2+} and Al^{3+} like brucite and gibbsite. These elements are probably incorporated to C-S-H or hydrotalcite like poorly crystalline structures that could not be observed clearly in the figures. Another mineral group that cannot be observed from the XRD analysis is sulfoaluminates. This may be caused due to the limited amount of gypsum in the blend and also instability of these phases at elevated temperatures. Therefore, gypsum remains uncombined or incorporated into the C-S-H structure in the hardened cement pastes.

To sum up XRD analysis, except for the portlandite, the peaks cannot refer to a specific crystalline mineral because of the poorly crystalline structure of hardened cement pastes. Even an increase in the proportion of GGBFS in the blend makes it more amorphous and diminishes crystalline structures as can be seen in Figure 4-13. For example, S80 has weakest peaks and it is difficult to reveal the mineral structures to be understood. Therefore, SEM analysis is used to give more experimental data for amorphous structures in the cement pastes.

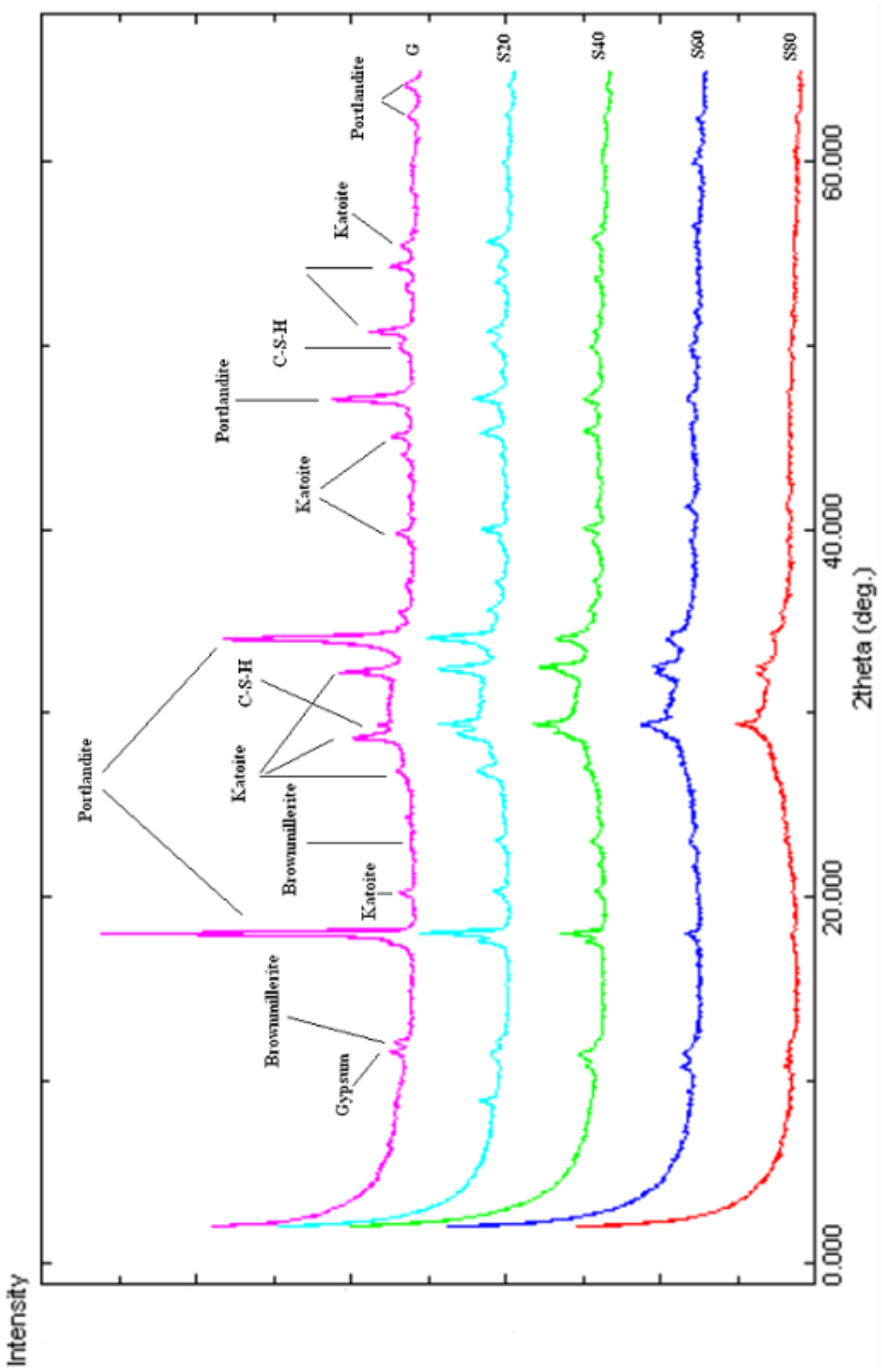

Figure 4-13 XRD patterns of the hardened cement pastes at 28-days

4.9. SEM

The specimens cured at 28-days are used for SEM observations combined with EDX microanalysis. As seen in Figure 4-14, G mainly consists of C-S-H and portlandite minerals. The C-S-H phases are commonly fibrillar (Type I) and honeycomb-like (Type II) in structure.

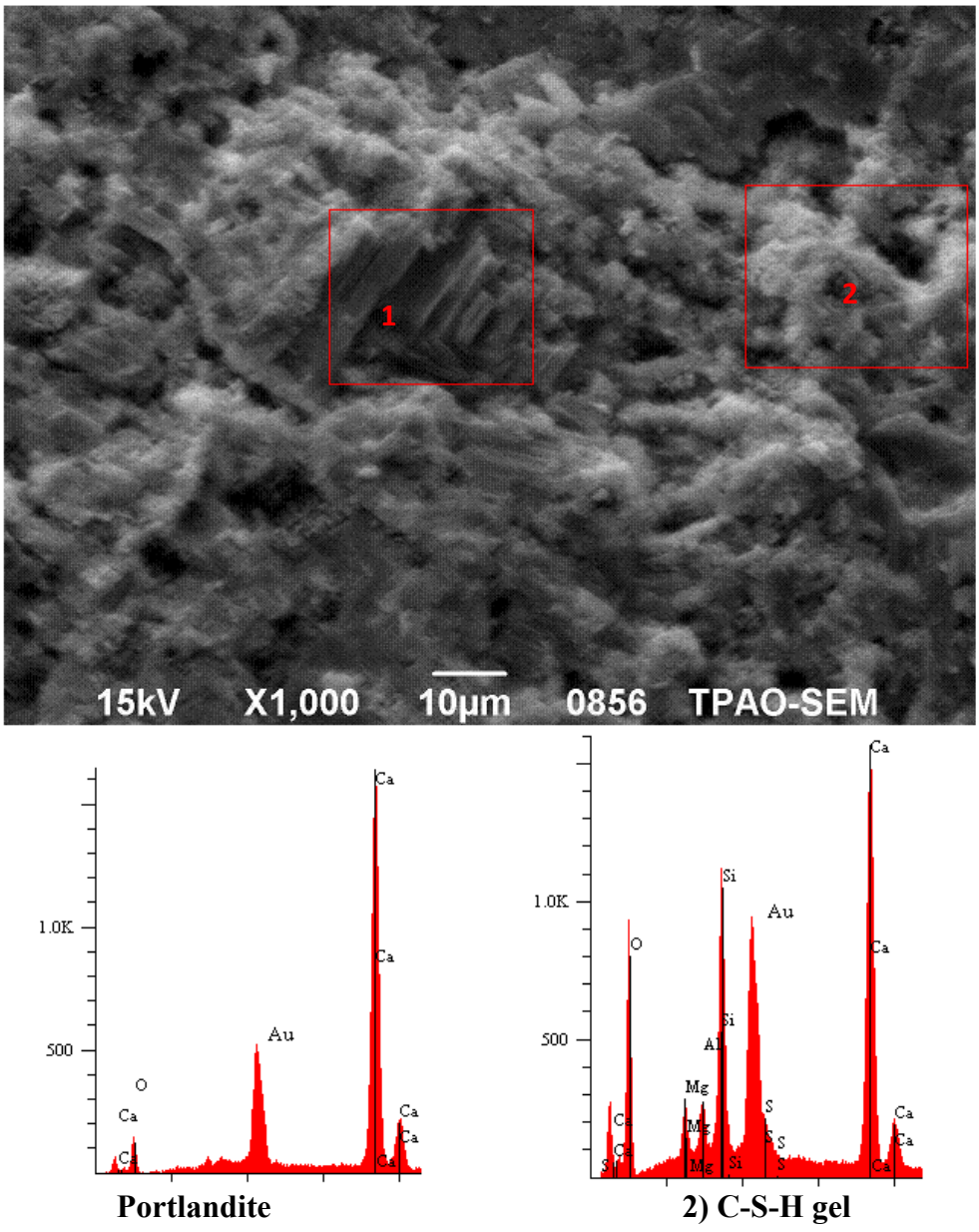

Figure 4-14 SEM micrograph of G

S20 has lower amounts of portlandite crystals and also C-S-H phases are more honeycomb-like and less-fibrillar in structure compared to G as seen in Figure 4-15. Mg^{2+} and Al^{3+} are incorporated to the structure of C-S-H phases.

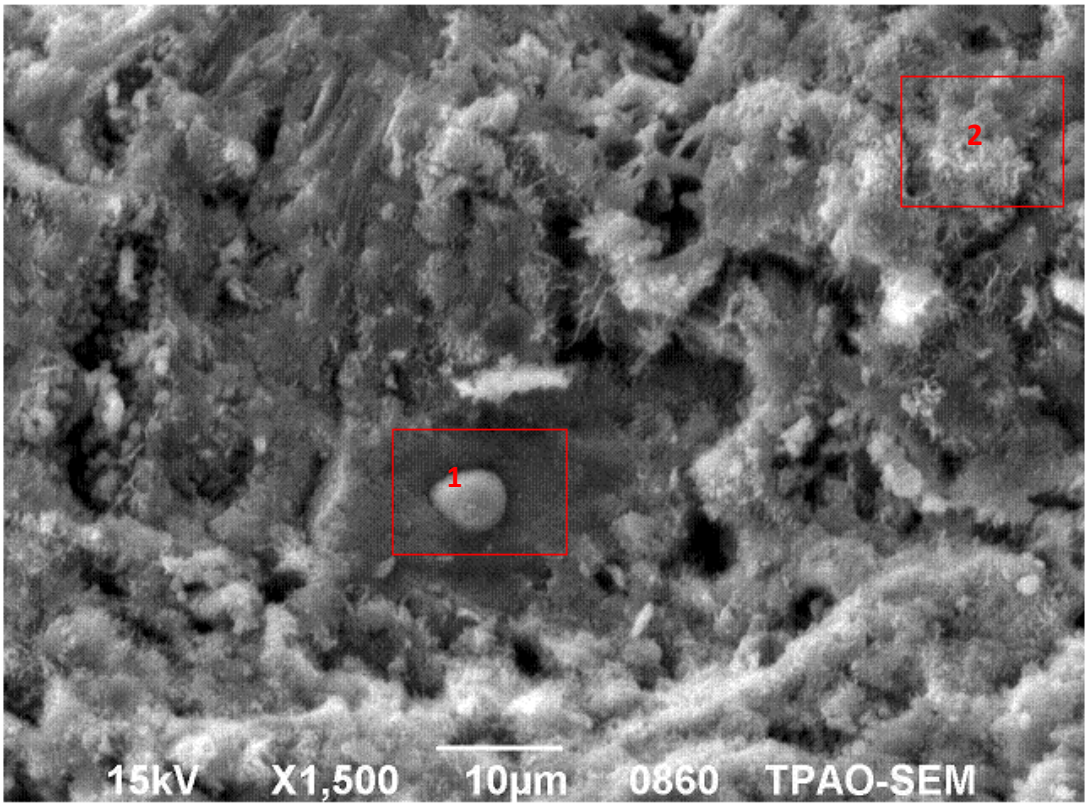

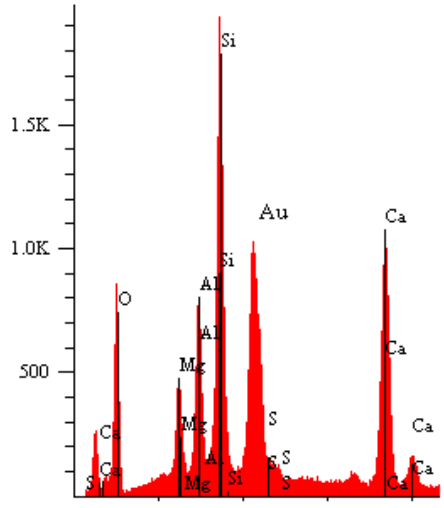

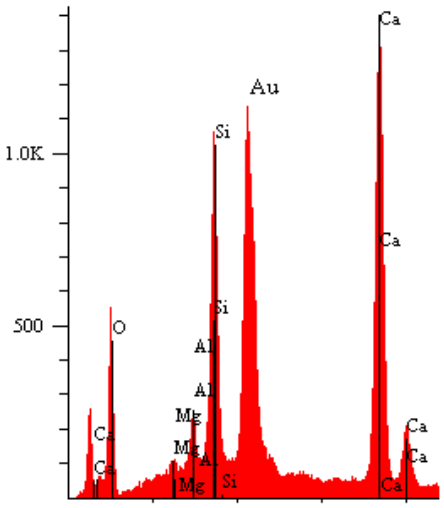

1) Hydrotalcite-like structure **2) C-S-H gel**

Figure 4-15 SEM micrograph of S20

S40 has flake-like C-S-H structures with low Ca/Si ratio and more Al^{2+} and Mg^{3+} incorporated in structure as shown in Figure 4-16. Also, there are structures similar to anhydrous slag grains observed in SEM micrographs.

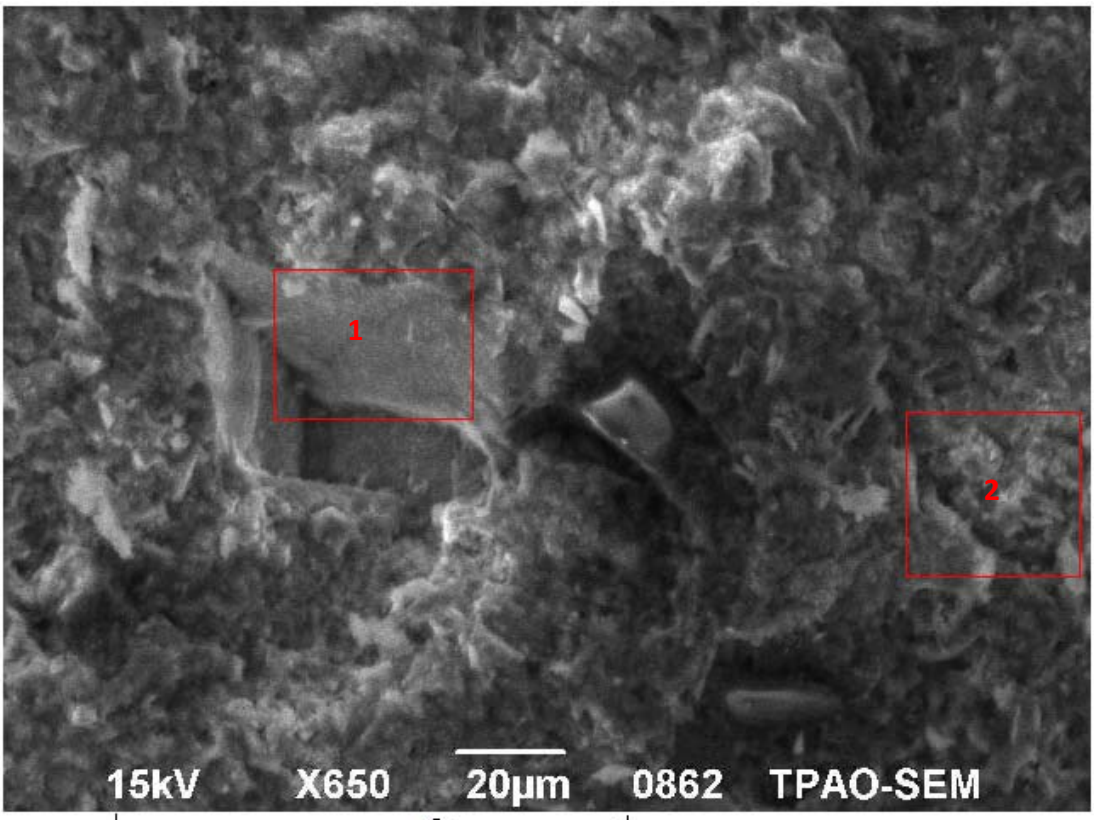

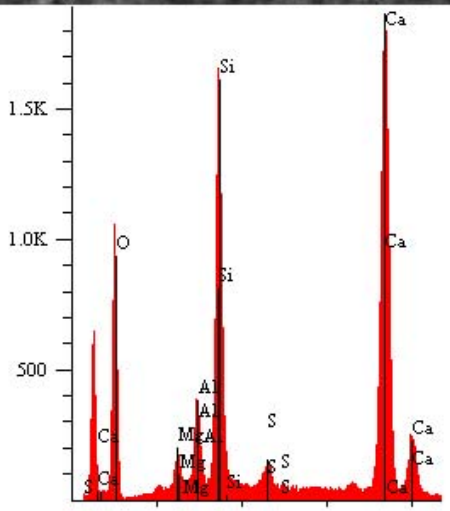

1) C-S-H

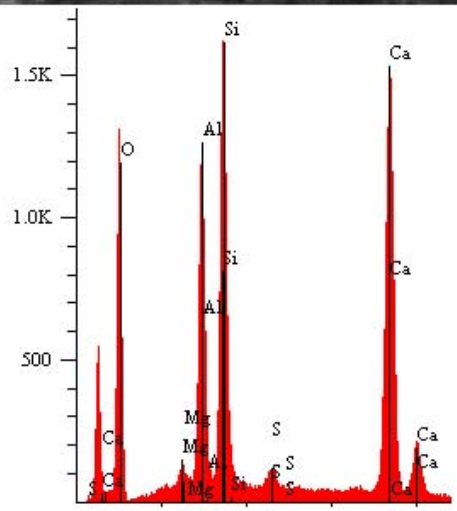

2) Flakes-like C-S-H

Figure 4-16 SEM micrograph of S40

According to Figure 4-17, S60 seems to be relatively more amorphous and less porous compared to G, S20 and S40. C-S-H phases are more flakes-like and foil-like in structure and more amounts of Mg^{2+} and Al^{3+} incorporated.

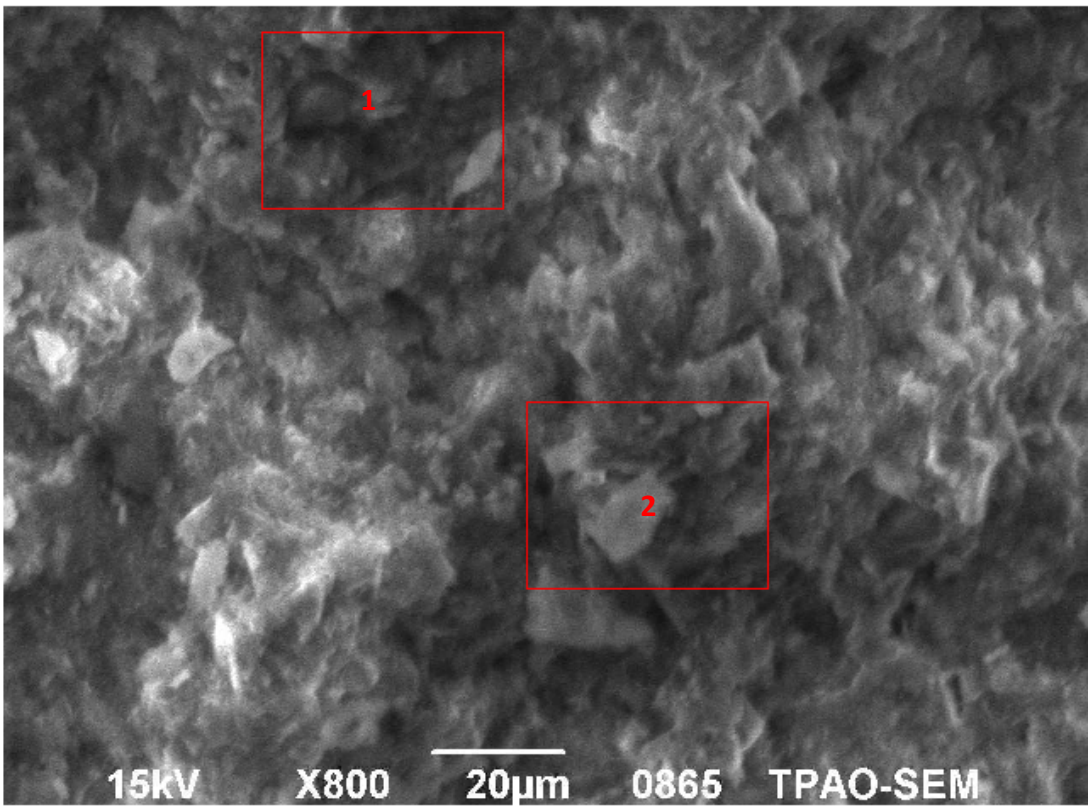

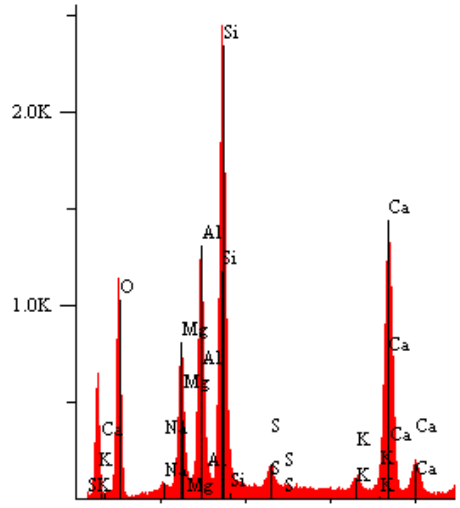

1) Flakes like C-S-H

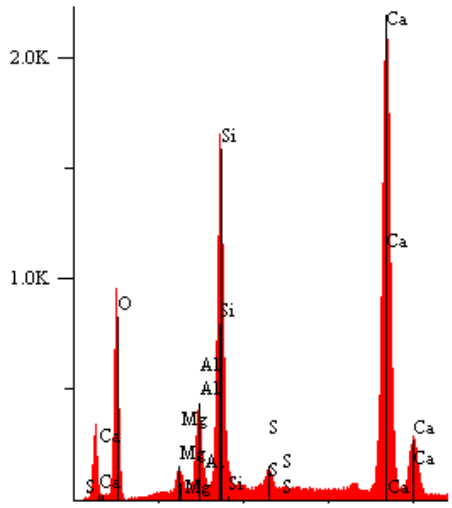

2) Flakes like C-S-H

Figure 4-17 SEM micrograph of S60

S80 is totally amorphous in structure with more smooth and foil-like C-S-H structures as shown in Figure 4-18. They are featureless and massive in structure and no specific structures observed. It possesses highest amount of Mg^{2+}, Al^{3+} and Si in structure among all cement pastes.

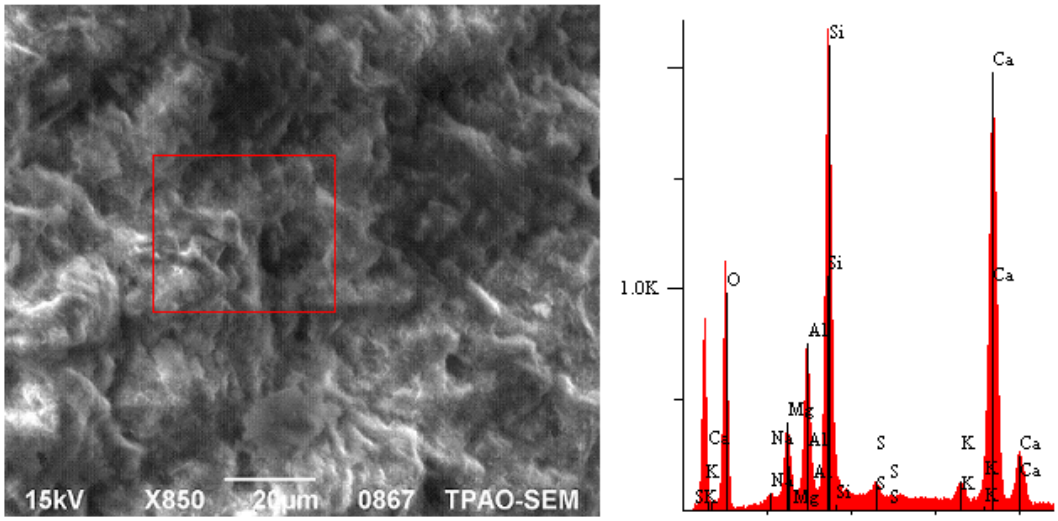

Figure 4-18 SEM micrograph of S80

To conclude the SEM analysis, an increase in GGBFS amount changed the microstructure and mineralogy of the hardened cement pastes. C-S-H phases become progressively less fibrillar and more foil-like in structure with increasing proportion of GGBFS in the blend. Mg^{2+} and Al^{2+} in the pastes generally come from GGBFS and enter into hydrotalcite-like C-S-H structures. This is also concluded by Mueller et al (1995) that the C-S-H produced during the hydration of a slag is lower in calcium and higher in aluminum and magnesium than the C-S-H formed during the hydration of Portland cement (Mueller et al, 1995). AFm and AFt phases could not be observed in the SEM analysis. AFt phases are thermally metastable above 70 °C and decompose to AFm phases. It is also possible that, AFm phases in the presence of C-S-H become dispersed. In fact, negatively charged main layers of C-S-H gel produce strong mutual attractions on the positively charged main layer of AFm phases. Thus the crystalline structure of the AFm phases are destroyed and incorporated to the C-S-H structure (Taylor, 1989).

CHAPTER 5

CONCLUSIONS

In the free fluid analysis all cement slurries are in the range of required specifications according to API Specifications 10A. However, GGBFS-CEM I blended cement slurries expected to be lower than that of neat Class G cement slurry due to their high Blaine's fineness value. An increase of GGBFS amount in the blend increases the fineness of blend and resulting in a reduction of free fluid content among the GGBFS blended cement slurries. Both particle morphology and chemical composition of cement and GGBFS has an effect on the free fluid content of cement slurry.

Relatively comparable compressive strength of neat class G cement paste can be provided by the GGBFS blended cement pastes with same w/c ratio. Intrusion of GGBFS in the cement paste especially increases the compressive strength at 28-days. In addition, curing at elevated temperatures favors the compressive strength of GGBFS blended cement pastes. 20 and 40 percent of GGBFS amount in the paste shows better compressive strength than neat Class G cement paste at 28-days, while 60 and 80 percent of GGBFS has lower compressive strength at all ages. Among the GGBFS blended cement pastes, S40 has the optimum compressive strength development over G.

Compressive strength of the cement pastes at 1-day is also estimated by ultrasonic cement analyzer (UCA). However, it is far different from destructive test method (DTM). The differences of compressive strength between cement pastes are exaggerated. However, the compressive strength of the pastes obtained from UCA is relatively in the same order with DTM.

GGBFS existence in the blend clearly reduces porosity of hardened cement pastes with the same w/c ratio. All GGBFS blended cement pastes have porosity lower than neat Class G cement paste at all ages. Hydration products of cement and GGBFS in the cement paste as a result of pozzolanic reaction filling up the pores and thus porosity decreases. The decrease of porosity in the cement pastes is more significant at 28-days due to the slow hydration rate of GGBFS. After an extent amount of CEM I substitution with GGBFS in the paste, porosity decreases considerably. For example, the porosity of S40 with 40 percent GGBFS at 28-days is less than half of G and S60 with 60 percent of GGBFS is less than quarter of G.

The results of air permeability analysis are unconformable with the results obtained from the helium porosimeter. A reduction in porosity is expected to decrease permeability of the hardened cement paste. However, GGBFS blended cement pastes have unacceptably high permeability values in spite of their low porosity. This is caused due to the uncontrolled fractures on the hardened cement pastes. The fractures are formed by mechanical stresses on the hardened cement pastes that are thought to occur primarily during core extraction and secondarily temperature changes on the specimens during cooling. Generally, the more amounts of GGBFS used in the blend, the more hardened cement pastes subjected to fractures.

Mercury intrusion analyzer is used for estimating permeability of cement pastes to prevent from the effects of cracks on the permeability of the hardened cement pastes. These results of permeability do not conflict with porosity in contrast to the results of air permeameter. The permeability of G is nearly more than twice of all slag blended cement pastes, even it is more than 10 times of S60 and 5 times of S40.

The pore sizes of all hardened cement pastes are in the range of 1 μm to 100 μm. The existence of GGBFS in the paste reduces not only porosity but also the pore sizes. More than 50 percent of the total pore volume of S40 and S60 are smaller than pore diameter of 10 μm whereas G and S20 have pore sizes higher than 10 μm.

Microstructure of the hardened cement pastes change significantly with the inclusion of GGBFS in the blend. An increment of GGBFS amount in the blend make the paste progressively more amorphous in structure and amount of portlandite crystals decreases. In addition, microstructure of C-S-H becomes less fibrillar and honeycomb-like but more dense and foil-like in structure.

In order to get adequate hydration for cement paste, the amount of CEM I must be kept more than GGBFS in the blend to provide sufficient alkalinity. Optimum amount of GGBFS in the blend is 40 percent to get C/S ratio close to C-S-H structure. Even small amounts of GGBFS presence in the blend indicates better C/S ratio compared to the neat Class G cement paste.

GGBFS existence in the blend favors hydration especially at long-term and at elevated temperatures. However, excessive amounts of utilization of GGBFS in the blend do not contribute enough to the properties of cement paste. The contribution of GGBFS hydration improves the physical properties of hardened cement pastes like compressive strength, porosity and permeability. They are comparable to and under some conditions more favorable than neat Class G cement paste.

To conclude, 20, 40 and 60 percent of GGBFS replacement in the cement paste has comparable outcomes against neat Class G cement paste. The cement paste with 20 percent of GGBFS has physical and chemical properties closest to neat Class G cement paste. However, S60 with 60 percent of GGBFS amount sometimes shows better and under some conditions worse results compared to G. In the S40 with 40 percent of GGBFS, properties of cement paste are considerably different than G. Its compressive strength, porosity, permeability, microstructure and chemical properties are more favorable compared to G.

CHAPTER 6

RECOMMENDATIONS AND FUTURE STUDIES

6.1. Recommendations

The following recommendations could be made for researchers for future studies.

- The specimens that are used for porosity and permeability analysis are subjected to fractures. Therefore, cooling and heating rate of the specimens could be done gradually to prevent fracturing.

- Increased fineness of the CEM I and GGBFS result in difficulties on preparing cement slurries. Therefore, during slurry preparation dispersants could be used to get more accurate results.

- In the air permeability analysis, specimens need to be dehydrated to remove the moisture. However, cement pastes in the oil wells are commonly subjected to hydrothermal conditions. Therefore, permeability test could be done with water instead of air to prevent from dehydration of the specimens.

6.2. Future Studies

The following topics could be studied to develop better comprehension of the future studies on the similar subjects.

- In well cementing operations, chemical additives used for designing properties of fresh and hardened cement pastes. The performance and compatibility of the chemical additives could be observed on GGBFS blended cement pastes.

- Salts commonly KCl or NaCl are used as an additive in well cementing to design the properties of fresh and hardened cement pastes or directly come from sea water used for slurry preperation. The effect of chloride on the properties of GGBFS blended cement pastes could be investigated.

- The behavior of the cement pastes could be investigated at more elevated temperatures.

- GGBFS used in this study has an activity grade of 73, even lower than grade 80. Therefore different type of GGBFS with different chemical composition can be used as experimental material.

- CEM I and GGBFS used in this study have both high fineness and rheological properties of the GGBFS blended cement pastes are higher than pastes prepared with neat API class G cement. Therefore, the fineness of the CEM I and GGBFS could be kept lower for superior rheological properties.

- In addition to GGBFS, fly ash and/or silica fume can be used for preparing ternary mixes.

- Investigating performance of API Class G and GGBFS blended cement pastes on sulfate resistance.

- The GGBFS used in this study has a broad range in the blends. As a result of this study, the range can be taken narrower to discover more accurate amount of GGBFS in the blend.

- The performance of silica flour and GGBFS as a substitute for cement can be investigated at temperatures higher than 110 °C.

REFERENCES

1. ACI Committee 116R, “Cement and Concrete Terminology”, American Concrete Institute Committee, March, 2000.

2. ACI Committee 232, “Use of Raw or Processed Natural Pozzolans in Concrete”, American Concrete Institute Committee, December, 2000.

3. ACI Committee 233R, “Ground Granulated Blast-Furnace Slag as a Cementitious Constituent in Concrete”, American Concrete Institute Committee, October, 1995.

4. Advanced Cementing Seminar, Halliburton, Dubai, 2011.

5. API Specification 10, “Specification for Materials and Testing for Well Cements”, American Petroleum Institute, January, 1995.

6. API RP 40, “Recommended Practices for Core Analysis”, American Petroleum Institute, February, 1998.

7. Andrew, C. J., Wilkinson, A. P., Luke, K., Funkhouser, G. P., “Class H cement hydration at 180 ˚C and high pressure in the presence of added silica”, Cement and Concrete Research, Volume 38, pp. 660-666, 2008.

8. ANSI/API Specification 10A, “Petroleum and natural gas industries - Cements and materials for well cementing-Part 1: Specification”, American Petroleum Institute, December, 2010.

9. ASTM C125, “Standard Terminology Relating to Concrete and Concrete Aggregates”, American Society for Testing and Materials, December, 2011.

10. ASTM C150, “Specification for Portland cement”, American Society for Testing and Materials, November, 1999.

11. ASTM C204, “Standard Test Methods for Fineness of Hydraulic Cement by Air-Permeability Apparatus”, American Society for Testing and Materials, June, 2011.

12. ASTM C219, “Standard Terminology Relating to Hydraulic Cement”, December, American Society for Testing and Materials, 2007.

13. ASTM C595, “Standard Specification for Blended Hydraulic Cements”, January, American Society for Testing and Materials, 2008.

14. ASTM C989, “Specification for Ground Iron Blast-Furnace Slag for Use in Concrete and Mortars”, American Society for Testing and Materials, November, 1999.

15. ASTM D2845, “Standard test method for laboratory determination of pulse velocities and ultrasonic elastic constants of rocks”, American Society for Testing and Materials, 1995.

16. ASTM E 1404-94, “Standard Specification for Laboratory Glass Conical Flasks”, American Society for Testing and Materials, 1994.

17. Bakker, R. F. M., “On the Cause of Increased Resistance of Concrete Made from Blast-Furnace Cement to Alkali Reaction and to Sulfate Corrosion,” Thesis RWTH-Aachen, The Netherlands, 1980.

18. Bakker, R. F. M., “Permeability of Blended Cement Concrete, Fly Ash, Silica Fume, Slag, and Other Mineral By-Products in Concrete”, American Concrete Institute, Detroit, 1983.

19. Barnett, S.J., Soutsot, M. N., Millard, S. G., Bungey, J. H., “Strength development of mortars containing ground granulated blast-furnace slag: Effect of curing temperature and determination of apparent activation energies”, Cement and Concrete Research, Volume 36, pp 434 - 440, 2006.

20. Bensted, J., “Special Cements”, in Lea’s chemistry of cement and concrete, 4th edition, Arnold, London, U.K., 2004.

21. Bogue, R. H., Portland Cement, Portland Cement Association Fellowship Paper #53, National Bureau of Standards, Washington, 1949.

22. Brown, P.W., Journal of American Ceramic Society 70, p.487 1987.

23. Chatterji S., Jeffrey J. W., "Studies of Early Stages of Paste Hydration of Cement Compounds, I", Journal of the American Ceramic Society, Volume 45, pp. 536-543, 1962.

24. Chen, W., "Hydration of Slag Cement Theory, Modeling and Application", PrintPartners Ipskamp BV, Enschede, 2006.

25. Cheron, M., Lardinois, C., "Proceedings of the 5th International Congress on the Chemistry of Cement", Volume 4, pp 277–285, Tokyo, 1968.

26. Damidot, D., Nonat, A., "C3S hydration in diluted and stirred suspensions: (I) study of the two kinetic steps", Advances in Cement Research, Volume 6, Issue 21, 1994.

27. Day, R. L., The effect of secondary etringite formation on the durability of concrete: Literature analyses, Portland cement Association, Illinois, USA, 1992.

28. Diamond, S., in Hydraulic Cement Pastes: Their Structure and Properties, Cement Paste Microstructure – An Overview at Several Levels, Cement and Concrete Association, UK, 1976.

29. W. J. Dixon, F. J. Massey, Introduction to statistical analysis, Mcgraw-Hill, 1957

30. Domone, P, Illstone, J., Construction Materials: Their nature and behavior, 4th edition, Spon Press, New York, 2010.

31. EN 197-1, "Cement-Part 1: Compositions and conformity criteria for common cements", European Standards, June, 2000.

32. EN 15167-1, "Ground granulated blast furnace slag for use in concrete, mortar and grout. Definitions, specifications and conformity criteria.", European Standards, October, 2006.

33. Erdoğan T. Y., "Admixtures for Concrete", Middle East Technical University Press, Ankara, 1997.

34. Escalante, J. I., Gomez, L. Y., Johal, K. K., Mendoza, G., Mancha, H, Mendez, J., "Reactivity of blast-furnace slag in Portland cement blends hydrated under different conditions", Cement and Concrete Research, Volume 31, pp. 1403-1409, 2001.

35. Fajgelj A., Ambrus A., Principles and practices of method validation, The Royal Society of Chemistry, 2000.

36. Feldman, R., "Pore structure, permeability and diffusivity as related to durability", 8th International Congress on the Chemistry of Cement, pp. 336-356, Brazil, 1986.

37. Frigione G., " Manufacture and characteristics of portland blast furnace slag cements", ASTM STP 897, American Society for Testing and Materials, Philadelphia, pp. 15-28, 1986.

38. Fulton, F. S., "The Properties of Portland Cement Containing Milled Granulated Blast-Furnace Slag," Portland Cement Institute, pp. 4-46, Johannesburg, 1974.

39. Galibert, R., "Glass Content Influence upon Hydraulic Potential of Blast-Furnace Slag", National Slag Association Publications, 1984.

40. Gollop, R. S., Taylor, H. F. W., "Microstructural and Microanalytical studies of sulfate attack. IV. Reactions of a slag cement paste with sodium and magnesium sulfate solutions", Cement and Concrete Research, Volume 6, pp 1013-1029, 1996.

41. Harrison, A. M., Winter, N. B., Taylor, H. F. W., Microstructure and microchemistry of slag cement pastes, Materials Research Society Symposia Proceedings, 1987.

42. Hewlett P. C., Lea's Chemistry of Cement and Concrete, Elsevier Ltd., United Kingdom, 2004.

43. Hinrichs, W., Odler, I., "Investigations on the hydration of Portland blast furnace slag cement", Advances in Cement Research, Volume 2, pp. 9-13, 1989.

44. Hogan, F. J., Meusel, J. W., “Evaluation for Durability and Strength Development of a Ground Granulated Blast- Furnace Slag,” Cement, Concrete and Aggregates, Volume 3, pp. 40-52, 1981.

45. Hooton, R. D., Emery, J. J., “Sulfate Resistance of a Canadian Slag,” ACI Materials Journal, Volume 87, pp. 547-555, 1990.

46. Hooton, R. D., Boyd, A. J., Bhadkamkar, D., “Effect of Cement Fineness and C_3S Content on Properties of Concrete: A Literature Review”, Portland Cement Association, PCA R&D Serial No. 2871, 2005.

47. Hwang, C. L., Lin C.Y., Proceedings of 2nd International Conference on the Use of Fly Ash, Silica Fume, Slag, and Natural Pozzolans in Concrete, pp. 1323–1340, Madrid, 1986.

48. Jackson, P. J., Portland cement: Classification and Manufacture, in P. Hewlett (ed.), Lea’s chemistry of cement and concrete, 4th edition, London, 2004.

49. Jawed, I., Skalny, J.,”Alkalies in cement: A review: II. Effects of alkalies on hydration and performance of Portland cement”, Cement and Concrete Research, Volume 8, pp. 37-51, 1978.

50. Kalousek, G. L,, “Sulfoaluminates of calcium as stable and metastable phases”, PhD thesis, University of Maryland, 1941.

51. Kalousek, G.L., “Analyzing SO_3-bearing phases in hydrating cement”, Materials. Research and Standards, Volume 6, pp. 292-304,1965.

52. Katz, A.J. and Thompson A.H., “A Quantitative Prediction of Permeability in Porous rock”, Phys. Rev. B, 1986.

53. Katz A.J. and Thompson A.H., “Prediction of Rock Electrical Conductivity From Mercury Injection Measurements”, Journal of Geophysical Research, Vol. 92, No. B1, Pages 599-607, January, 1987.

54. Keil, F., Slag cements, Proceedings of the Third International Symposium on the Chemistry of Cements, Cement and Concrete Association, pp. 530–571, London, 1952.

55. Kelly, R., Solid-liquid reactions Part 2: Solid-liquid reactions amongst the calcium aluminates and sulphoaluminates, Canadian Journal of Chemistry, Volume 38, pp. 1209-1226, 1960.

56. Klemm, W.A., Adams, L.D., "Investigation of the formation of carboaluminates", ASTM Special Technical Publications, 1990.

57. Klieger, P. and Isberner, A. W., "Laboratory Studies of Blended Cement-Portland Blast-Furnace Slag Cements," PCA Research and Development Department Laboratories, Volume 9, No. 3, September, 1967.

58. Kondo. R., Oshawa S., "Studies on method to determine the amount of GGBF slag and rate of hydration in cements," Proceedings of the 5th International Symposium on the Chemistry of Cement, Tokyo, 1968.

59. Krautkramer, J., Krautkramer, H., Ultrasonic Testing of Materials, Springer-Verlag, 1983.

60. Labahn, O., Cement Engineers' Handbook, Bauverlag, Berlin, 1983.

61. Lawrence, C. D., The Constitution and Specification of Portland cements, in P. Hewlett (ed.), Lea's chemistry of cement and concrete, 4th edn, Arnold, London, U.K., 2004.

62. Lea, F. M., The Chemistry of Cement and Concrete, 3rd edition, Chemical Publishing Co., New York, 1971.

63. Lee, A. R., Blast Furnace and Steel Slag, Halsted Press, New York, 1974.

64. Lewis, D., "History of slag cements", Slag Cement Seminar, Alabama, 1981.

65. Locher, F. W., "The Problem of the Sulfate Resistance of Slag Cements", Zement-Kalk-Gips, Volume 19, pp. 395-401, Bauverlag, 1966.

66. Lottenbach, B., Matschei, T., Möshner, G., Glasser F. P., "Thermodynamic modeling of the effect of temperature on the hydration and porosity of Portland cement", Cement and Concrete Research, Volume 38, pp. 1-18, 2008.

67. Lumley, J. S., Gallop, R. S., Moir, G. K., Taylor, H. F. W., "Degrees of reaction of slag in some blends with Portland cements", Cement and Concrete Research, Volume 26, pp. 139-151, 1996.

68. McGarl, H. N., Eggleton, H. K., Barton, W. R., Aggregates – Slag, in Industrial Minerals and Rocks, 1994.

69. Mehta, P. Kumar, "Durability of Concrete in Marine Environment—A Review," Performance of Concrete in Marine Environment, SP-65, American Concrete Institute, pp. 1-20, Detroit, 1980.

70. Mehta, P. K., Monteiro, P. J. M., Concrete Microstructure, Properties, and Materials, McGraw-Hill Companies, USA, 2006.

71. Meusel, J. W., Rose, J. H., "Production of Granulated Blast Furnace Slag at Sparrows Point, and the Workability and Strength Potential of Concrete Incorporating the Slag," Fly Ash, Silica Fume, Slag and Other Mineral By-Products in Concrete, SP-79, American Concrete Institute, pp. 867-890, Detroit, 1983.

72. Mindess, S., Young, J. F., Concrete, Prentice-Hall Inc., Englewood Cliffs, NJ, U.S., 1981

73. Micheline M., Micheline, R., Cements Made from Blast Furnace Slag, in P. Hewlett (ed.), Lea's chemistry of cement and concrete, 4th edition, Arnold, London, U.K., 2004.

74. Mueller, D. T., Gino, D., Hibbeler, J., Kelly, P., BJ Services, "Portland Cement – Blast Furnace Slag Blends in Oilwell Cementing Applications", SPE Annual Technical Conference and Exhibition, Dallas, 1995.

75. Muller, C., "Ground Granulated Blast Furnace Slag (GGBFS) as a concrete additive", The Federal Association of the German Ready-Mixed Concrete Industry, Düsseldorf, 2007.

76. Negro, A., Stafferi, N., "The hydration of calcium ferrites and calcium aluminoferrites", Zement-Kalk-Gips, Volume 32, pp 83-88, 1979.

77. Nelson, E. B., “Portland Cements Characterized, Evaluated,” Oil and Gas Journal, pp 73-77. 1983.

78. Nelson, E. B., Well Cementing, Sclumberger Educational Services, Texas, 1990.

79. Nelson, E. B., Guillot, D., Well Cementing, Second Edition, Sclumberger, Texas, 2006.

80. Neville A. M., Properties of Concrete, Fourth Edition, Pearson Education Limited, England, 2003.

81. NSA, National Slag Association, http://www.nationalslag.org/blastfurnace.htm, last accessed date 09.03.2012.

82. Odler, I., Hydration, setting and hardening of portland cement, in P. Hewlett (ed.), Lea’s chemistry of cement and concrete, 4th edition, Arnold, London, U.K., 2004.

83. Odler, I., Special Inorganic Cements, Modern Concrete Technology Series, London, 2000.

84. Olorunsogo, F.T., “Particle size distribution of GGBS and bleeding characteristics of slag cement mortars”, Cement and Concrete Research, Volume 28, pp. 907 – 919, 1998.

85. Olorunsogo, F.T., Wainwright P. J., “Effect of GGBF Particle-size Distribution on Mortar Compressive Strength”, Journal of Materials in Civil Engineering, pp. 180 - 187, USA, 1998.

86. Pal, S. C., Mukherjee A., Pathak S. R., “Investigation of hydraulic activity of ground granulated blast furnace slag in concrete”, Cement and Concrete Research, Volume 33, pp 1481–1486, 2003.

87. Pandey S.P., Sharma R.L., “The influence of mineral additives on the strength and porosity of OPC mortar”, Cement and Concrete Research, Volume 30, pp. 19-23, 2000.

88. Powers, T.C., Brownyard, T.L. Studies of the Physical Properties of Hardened Portland Cement Paste, Portland Cement Association, Chicago, 1948.

89. Richardson, I. G., Groves, G. W., "Microstructure and microanalysis of hardened ordinary Portland cement pastes involving ground granulated blast-furnace slag", Journal of Material Science, Volume 27, pp. 6204-6212, 1992.

90. Richardson, J. M., Biernacki, J. J., Stutzman, P. E., Bentz, D. P., "Stoichiometry of Slag Hydration with Calcium Hydroxide", Journal of the American Ceramic Society, Volume 85, No. 4, pp 947-953, 2002.

91. Robeyst, N., Gruyaert, E., Grosse, C. U., Belie, N. D., "Monitoring the setting of concrete containing blast-furnace slag measuring the ultrasonic p-wave velocity" Cement and Concrete Research, Volume 38, pp. 1169-1176, 2008.

92. Rogers, M. J., Dillenbeck, R. L., Eid, R. N., BJ Services Company, "Transition Time of Cement Slurries, Definitions and Misconceptions, Related to Annular Fluid Migration", SPE Annual Technical Conference and Exhibition, Society of Petroleum Engineers, Houston, 2004.

93. Rose, J. H., "The Effects of Cementitious Blast-Furnace Slag on Chloride Permeability of Concrete," Corrosion, Concrete, and Chlorides, V. M. Malhotra, Ed., SP-102, American Concrete Institute, pp. 107-125, Detroit, 1987.

94. Roy, D. M., Idorn, G. M., "Hydration, Structure, and Properties of Blast Furnace Slag Cements, Mortars, and Concrete," Proceedings, ACI JOURNAL V. 79, No.6, pp. 445-457, 1983.

95. Satarin, V. I., "Slag Portland cement", Proceeding of the 6th International Congres on the Chemistry of Cement, Principal Paper, pp 1-55, Moscow, 1974.

96. Schröder, F., "Blastfurnace slag and slag cements", Proceedings of the 5th International Congress on the Chemistry of Cement, Tokyo, 1968.

97. Schwiete, H. E., Dolbor, F., "The effect of cooling conditions and the chemical composition on the hydraulic properties of the haematitic slags", Forschungsbericht des Landes, pp. 23– 29, 1963.

98. Siddique, R., Khan, M. I., Supplementary Cementing Materials, Springer-Verlag Berlin Heidelberg, 2011.

99. Smolczyk, H. G., "The effect of chemistry of slag on the strength of blast furnace cements", Zem.-Kalk-Gips, Volume 31, pp. 294-296, 1978.

100. Smolczyk, H. G., "Slag structure and identification of slags", 7th ICCC, Vol. I, pp. III-1/3 – III-1/17, Paris, 1980.

101. Swamy, R. N., Bouikni, "Some engineering properties of slag concrete as influenced by mix proportioning and curing", ACI Materials Journal, Volume 87, pp. 210–220, 1990.

102. Swamy, R. N., Design for Durability and Strength Through the Use of Fly Ash and Slag in Concrete, CANMET/ACI International Workshop on Supplemantary Cementing Materials, American Concrete Institute, pp. 1-72, Toronto, 1998.

103. Tanaka, H., Totani, Y., "Structure of hydrated glassy blastfurnace slag in concrete", in V. M. Malhotra (ed.), 1 International conference on the use of fly ash, silica fume, slag, and other mineral by-products in concrete, Vol. II, American Concrete Institute, Montebello, Canada, pp. 963–977, 1983.

104. Taylor, H.F.W., "Do Cement Pastes Contain Substituted C-S-H Gel?", in Advances in Cement Manufacture and Use (Ed. E. Gartner), pp. 295-302, Engineering Foundation, New York, 1989.

105. Taylor, H. F. W., Cement Chemistry, Thomas Telford, London, 1997.

106. TS 10157, "Cement – Composition, specifications and conformity criteria for sulfate-resisting cement", Turkish Standard, April, 2008.

107. Uchikawa, H., "Effect of blending components on hydration and structure formation", 8th ICCC, Volume 1, pp. 250–280, Rio de Janeiro, Brazil, 1986.

108. Verbeck, G. J., Foster, C. W., Longtime Study of Cement Performance in Concrete – The Heats of Hydration of the Cements" Chapter 6, Proceedings of American Society for Testing and Materials, Volume 50, pp. 1235-1262, 1950.

109. Wainwright, P.J., Ait-Aider, H., “The influence of cement source and slag additions on the bleeding of concrete”, Cement and Concrete Research, Volume 25, pp. 1445–1456, 1995.

110. Wainwright, P.J., Rey, N., “The influence of ground granulated blast furnace slag (GGBS) additions and time delay on the bleeding of concrete”, Cement and Concrete Composites, Volume 22, pp. 253–257, 2000.

111. Webb, P. A., An Introduction To The Physical Characterization of Materials by Mercury Intrusion Porosimetry with Emphasis On Reduction And Presentation of Experimental Data, Micromeritics Instrument Corp., Georgia, 2001.

112. Wood, K, “Twenty Years of Experience with Slag Cement”, Symposium on Slag Cement, University of Alabama, Birmingham, 1981.

113. Wood, S. L., “Evaluation of the Long-Term Properties of Concrete,” RD102, Portland Cement Association, pp. 14-15, 1992.

114. World Oil, Special Focus: Outlook 2007 Worldwide Drilling, in World Oil Magazine, Vol. 228, Houston, 2007.

APPENDIX A

ESTIMATED COMPRESSIVE STRENGTH OF CEMENT PASTES BY UCA

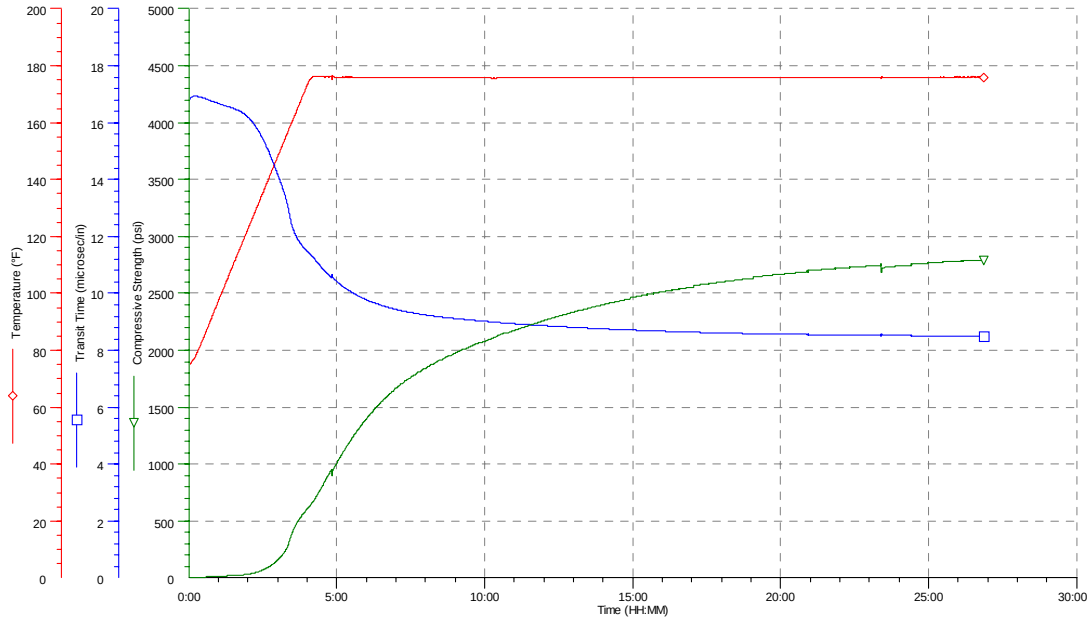

Figure A.1. Compressive strength of G

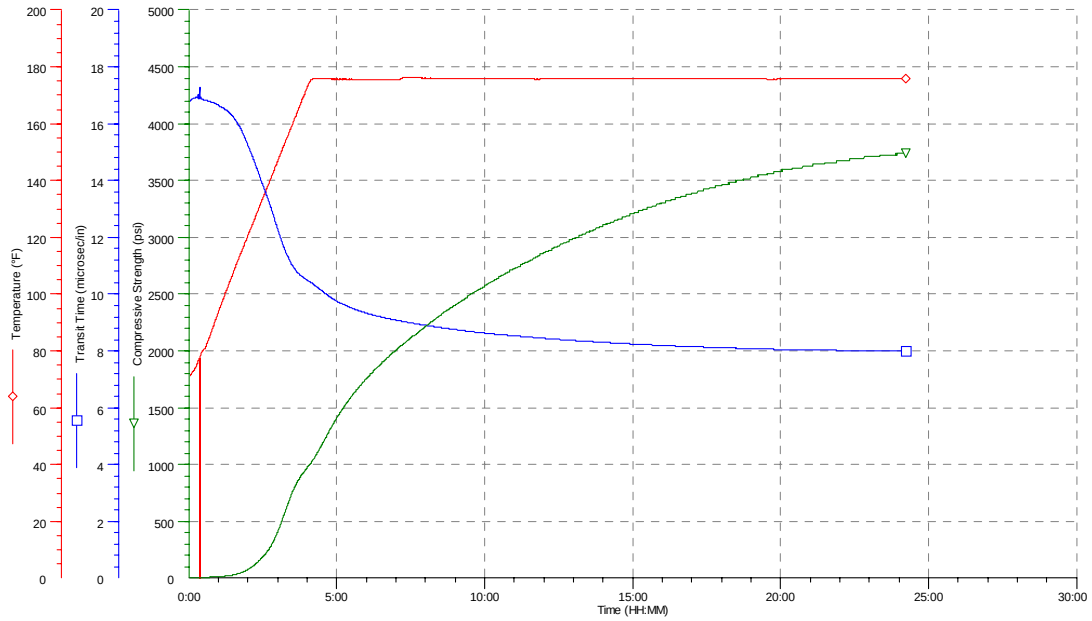

Figure A.2. Compressive strength of S20

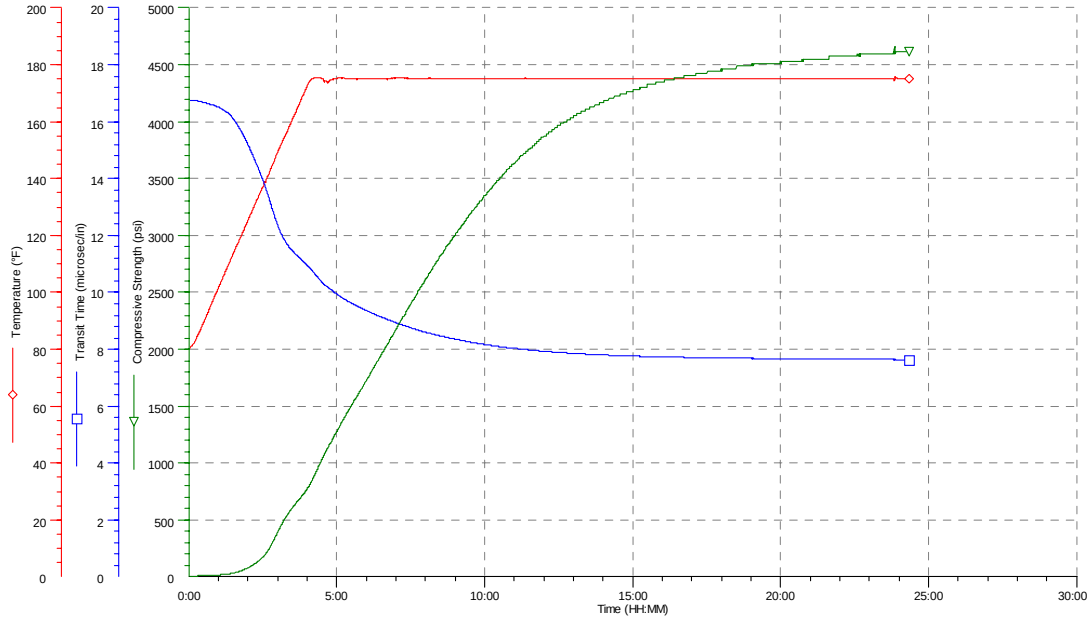

Figure A.3. Compressive strength of S40

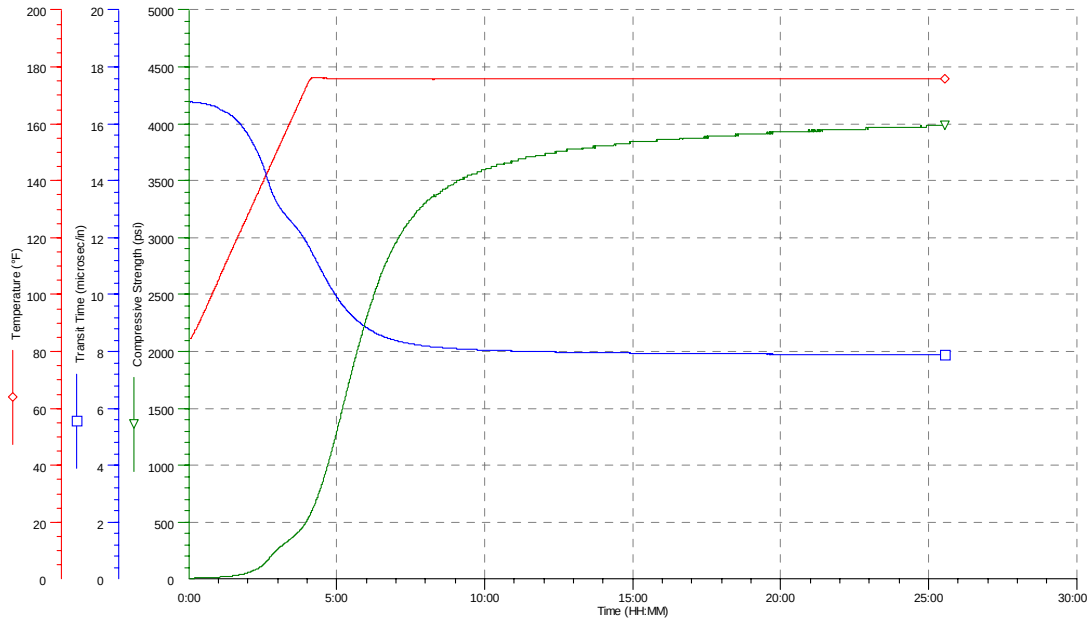

Figure A.4. Compressive strength of S60

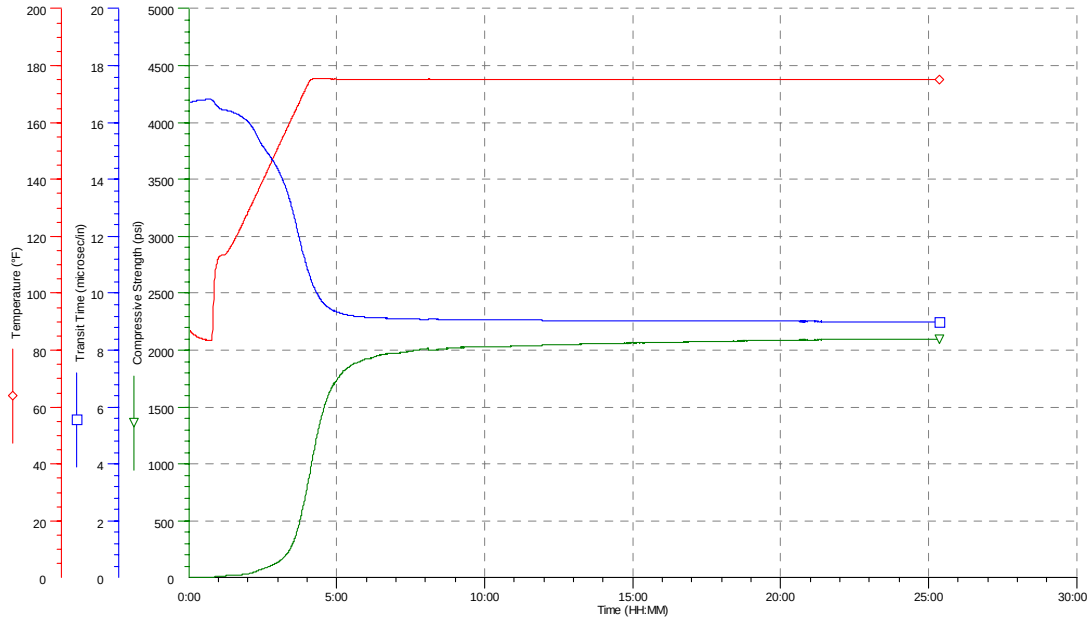

Figure A.5. Compressive strength of S80

APPENDIX B

XRD PATTERNS OF CEMENT PASTES

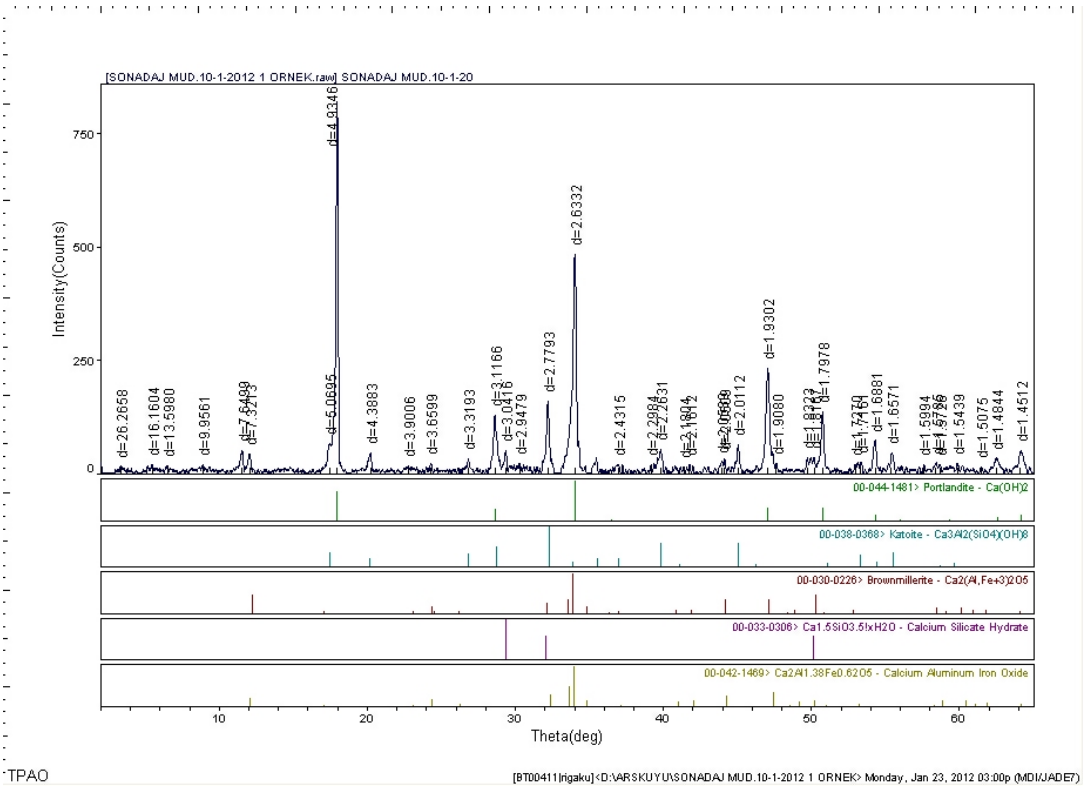

Figure B.1. XRD Patterns of G

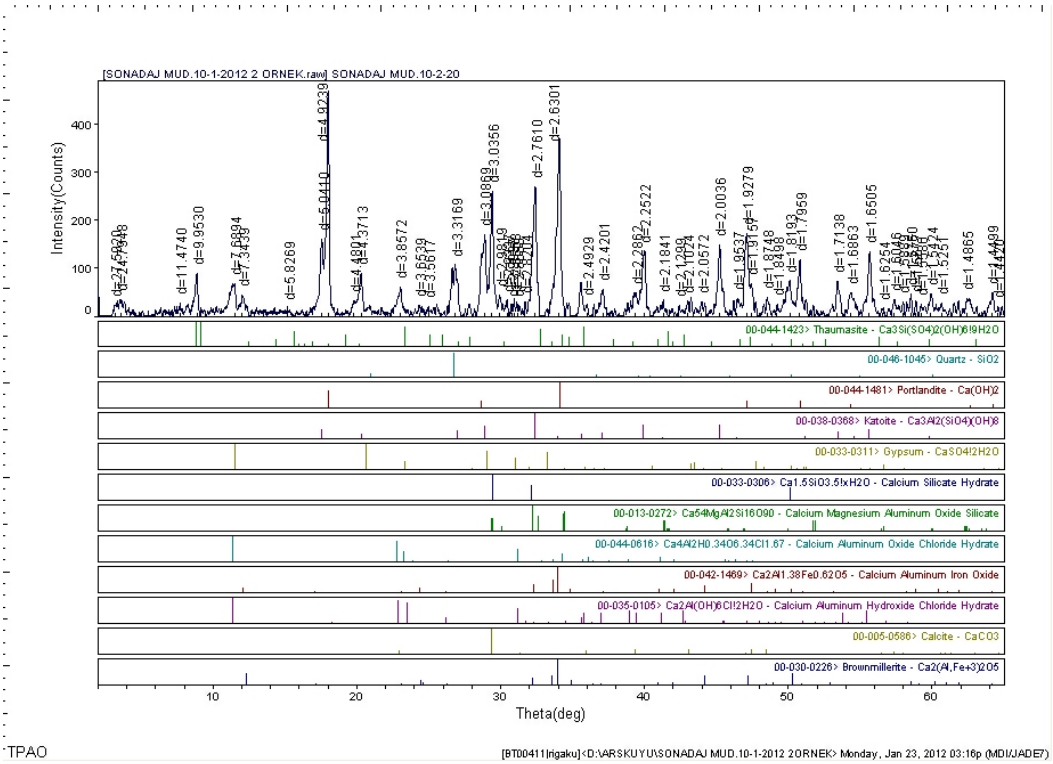

Figure B.2. XRD patterns of S20

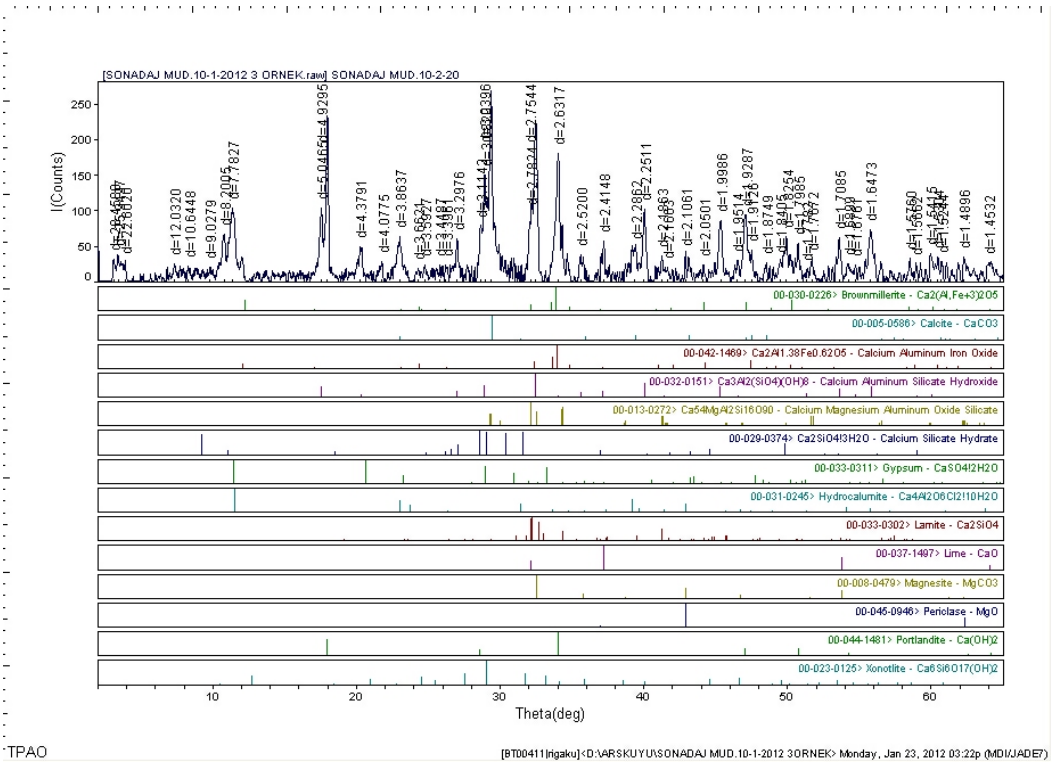

Figure B.3. XRD patterns of S40

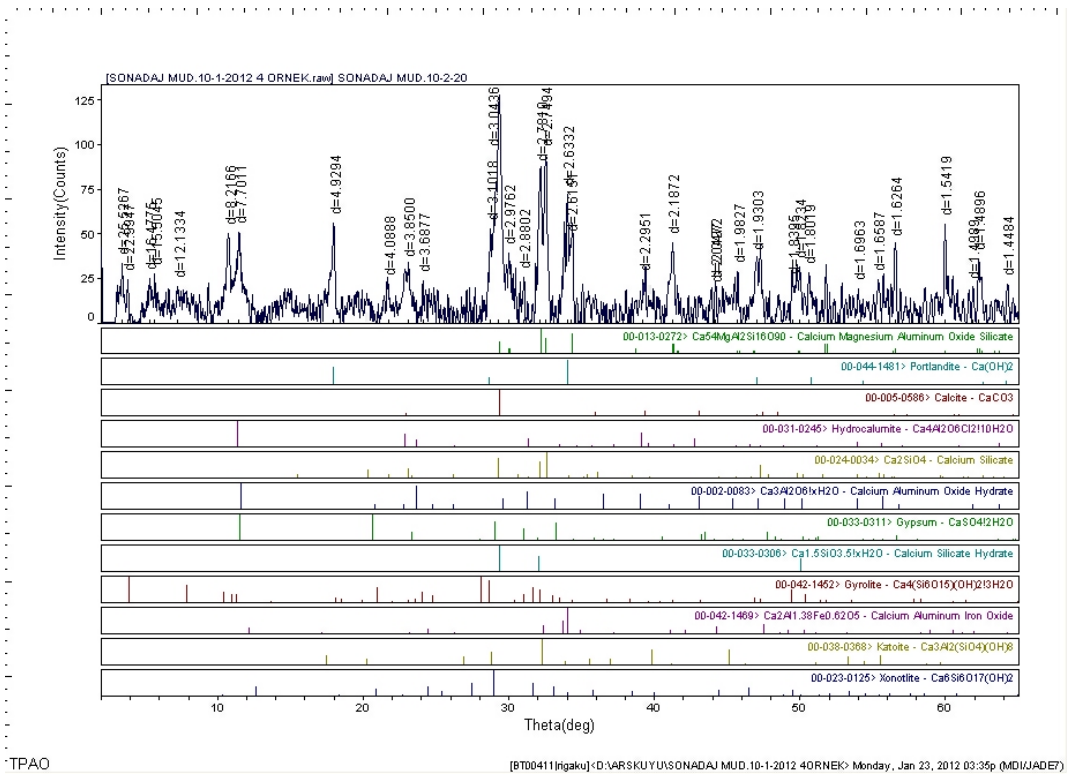

Figure B.4. XRD patterns of S60

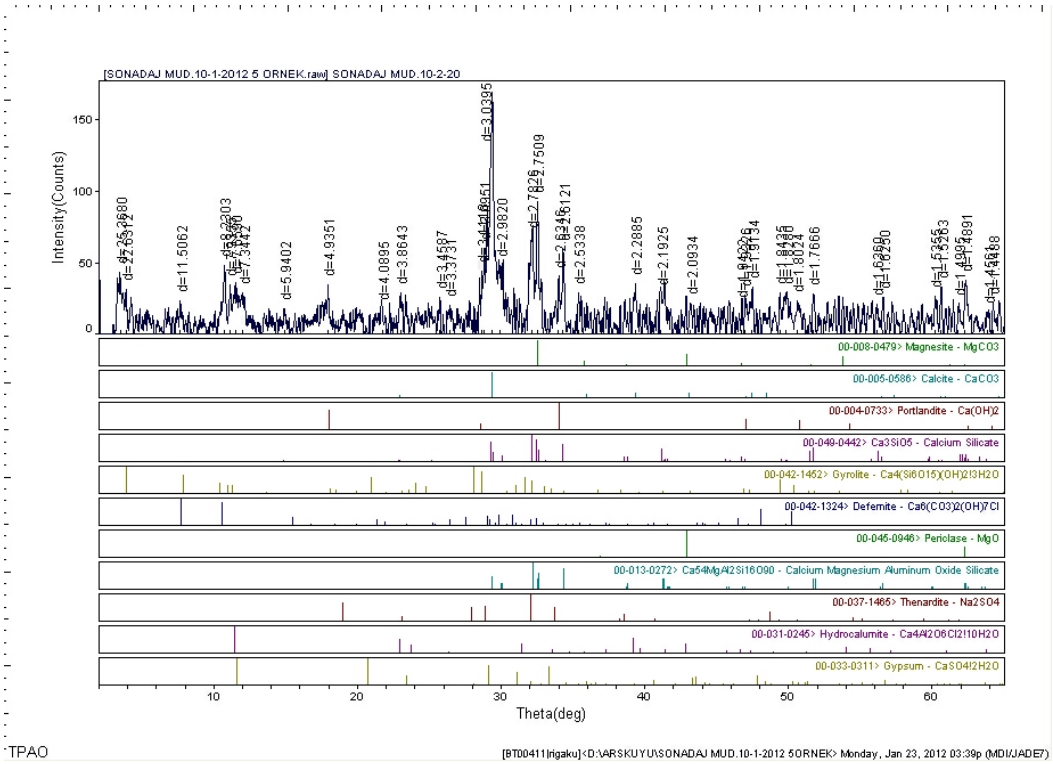

Figure B.5. XRD patterns of S80

APPENDIX C

MERCURY SATURATION OF CEMENT PASTES

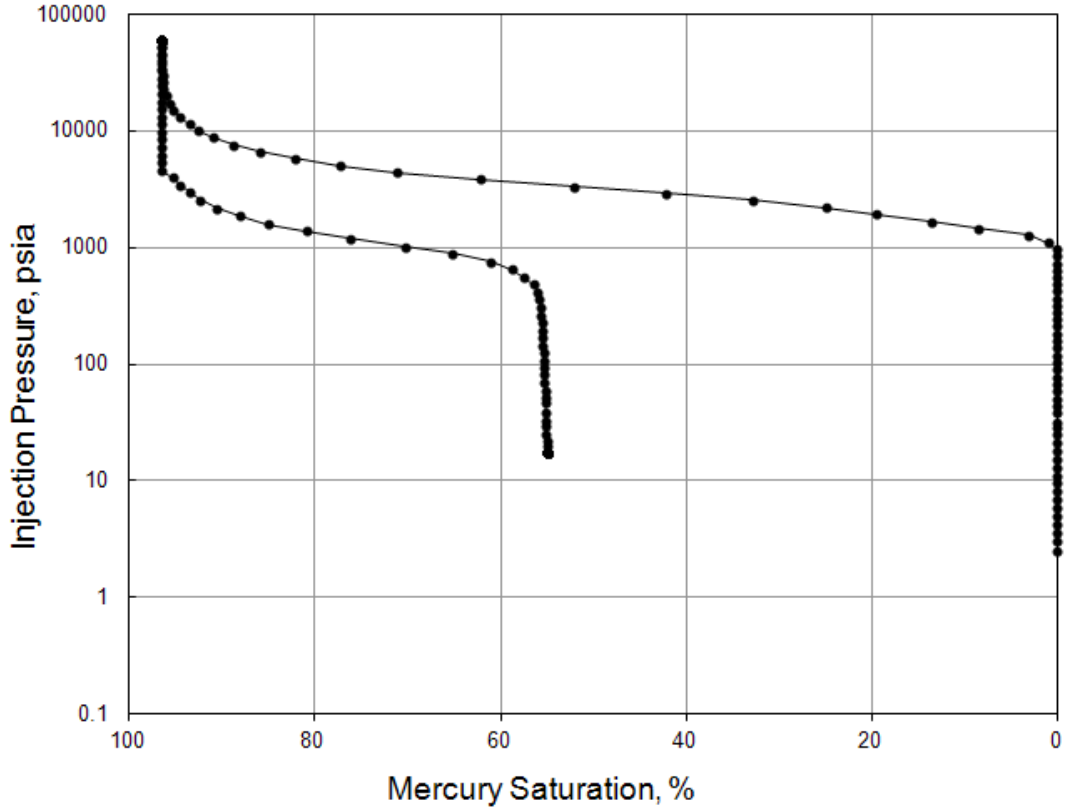

Figure C.1. Mercury saturation of G

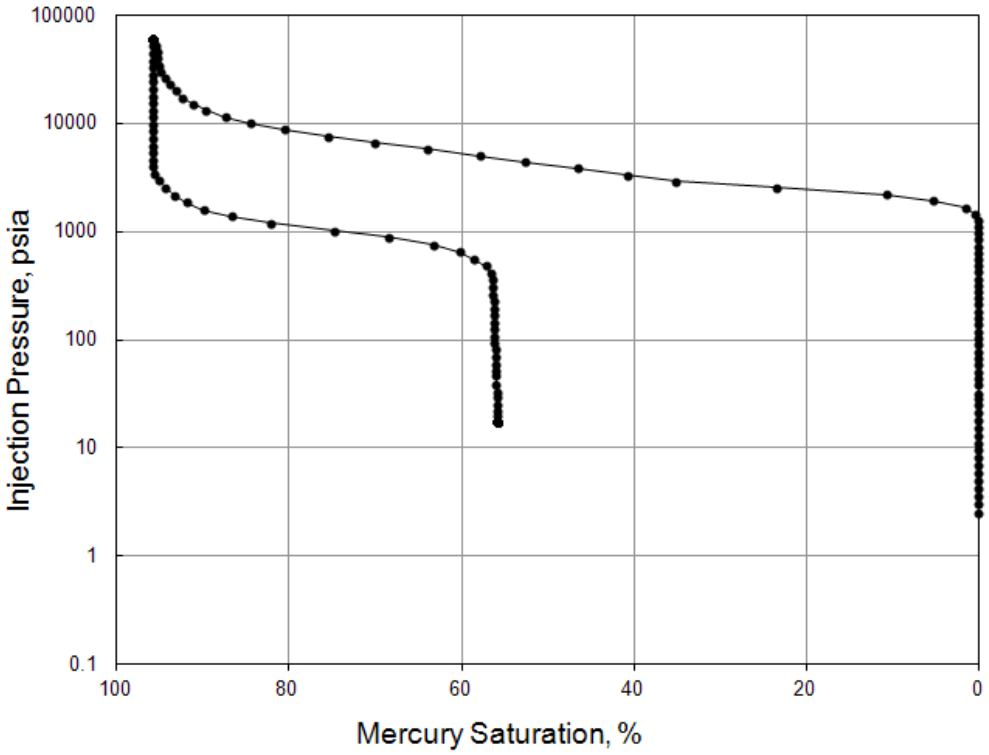

Figure C.2. Mercury saturation of S60

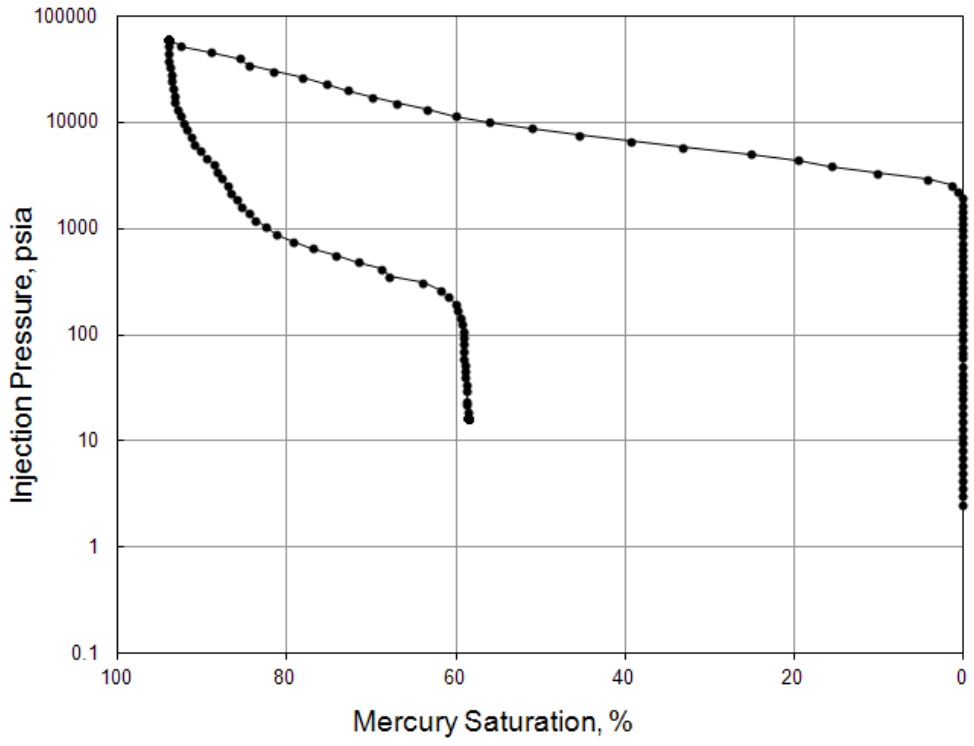

Figure C.3. Mercury saturation of S80

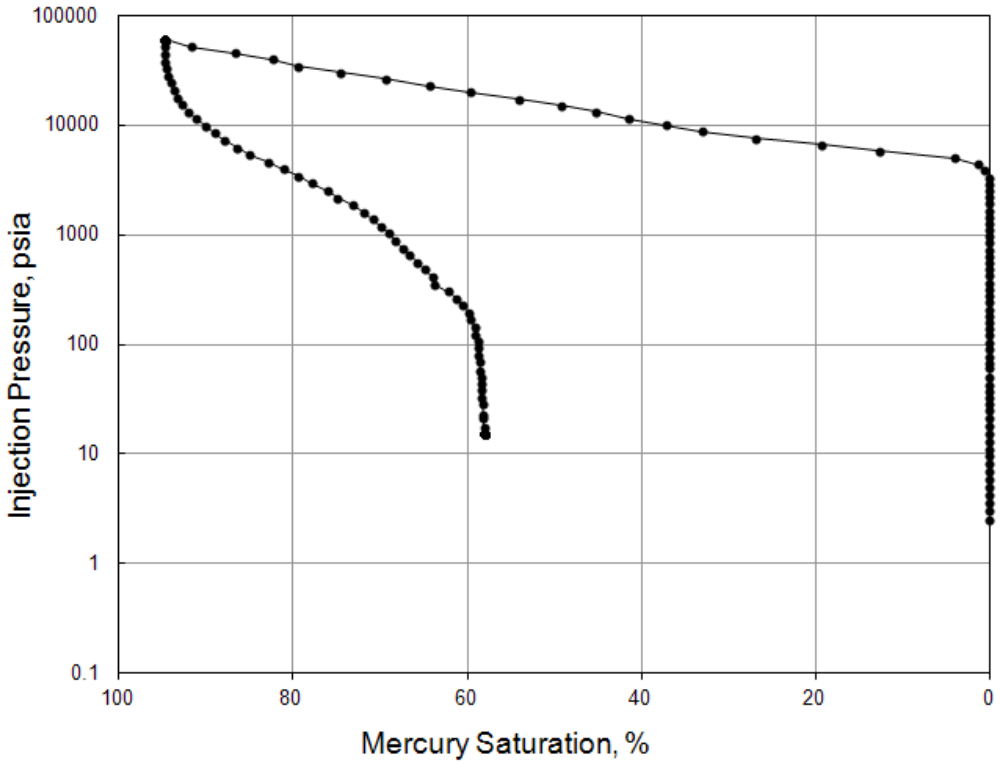

Figure C.4. Mercury saturation of S60

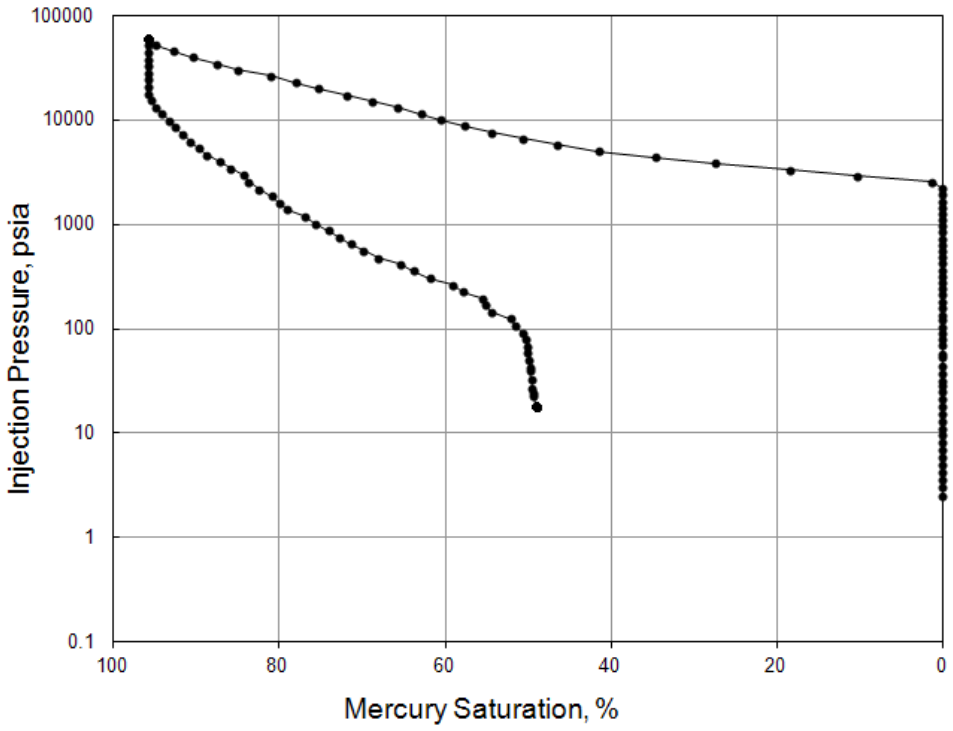

Figure C.5. Mercury saturation of S80